CELL BIOLOGY OF CORONAVIRUS REPLICATION

By

Megan Culler Freeman

Dissertation

Submitted to the Faculty of the

Graduate School of Vanderbilt University

in partial fulfillment of the requirements

for the degree of

DOCTOR OF PHILOSOPHY

in

Microbiology, and Immunology

December 2014

Nashville, Tennessee

Approved:

John Williams, M.D.

Earl Ruley, Ph.D.

Jim Goldenring, M.D., Ph.D.

Alissa Weaver, M.D., Ph.D.

Mark Denison, M.D.

To my family, both given and chosen, and my many teachers, both officially and informally, for believing in me always and inspiring me to learn.

ACKNOWLEDGEMENTS

Graduate school has been, in some ways, exactly what I expected, and in others, much more challenging or different than my expectation. It is at the same time incredibly collaborative, as you work as part of a lab team working each day to make new discoveries, and also very solitary, as your project very rapidly becomes, at least in my case, segregated from other studies of the lab. You're the one defending it and your ideas that you've created since the first day it crossed your desk. Some get to stay on your to-do list, and others rapidly get axed. You begin to learn how to better formulate questions, and how to decide which of those are most important for your project on any given day. You learn to seek advice in, perhaps unexpected places, finding collaborators at Vanderbilt and beyond from whom you can learn or borrow reagents.

For as long as I can remember, I have always loved learning and discovery. It's impossible to know if that was my genetic destiny, but I can absolutely, without one doubt say that it was fostered along the way by my many, many teachers, beginning of course with my earliest teachers, my parents, and some other really special people along the way. The least I can do is to thank them here, but I hope that my continued passion for discovery and ambition for making a difference in science and medicine will help demonstrate that their effort in my development continues to be very appreciated.

Glenn Collins, I'm not sure why, but you believed in me from the very beginning. You were one of the very first people to suggest that doing an MD/PhD would be a good path for me, and I'm so thankful for that.

Becky Dutch, thank you for taking a chance on a very new undergraduate student many years ago. Your lab is where I truly fell in love with science and discovered how incredibly interesting viruses can be. I'm so lucky to continue to count you as a mentor and one of the best parts of staying in the field is that I get to see you at least annually at meetings.

Mark Wurth, thanks so much for teaching me to love bench science. You taught me to pipet, how to work in cell cultures, and how to find the perfect level surface on which to pour my gels. Most importantly, you spent three entire years persuading and cajoling me to go for an MD/PhD just like you. You probably have no idea the amount of influence you had in my investigating that decision and believing that I might be good at it. Thank you very much. PS: I'm not anticipating doing a joint residency (at some point, a girl just has to pick one), but will promise to try to be a great doctor anyway.

To my mentor Mark Denison, your enthusiasm for science is truly infectious (I know you love a good pun). Thanks for being such an inspiration to me. I've so enjoyed our lab trips, particularly the one where you spent an entire day driving us around Yellowstone or to the top of the Rockies where you divvied up the warm clothing you'd brought along to all of us who were unprepared. I've also enjoyed our chats about science, life, Kentucky

or Kansas basketball, theatre, and the occasional singing of show tunes. I admire your fearlessness-whether break dancing in front of an entire class of medical students, putting cicadas on your face, or boldly asking the next great scientific question, you're never afraid to go there. And I hope as I move forward in my career that I can most emulate how much you care for your students, both as people and developing scientists, your wide-reaching scientific curiosity, and your enthusiasm for life in general.

To my committee, John, Earl, Jim, and Alissa, thank you for your patience. And thank you for pushing me to do my very best work. I'm so grateful to you for your ideas, time spent with me, reagents lent, careful questions, and helpful criticisms. I've grown so much during this process and I hope I've made you proud. Also, thanks to Earl for telling me to "discover my inner bitch." I think she's really quite effective.

To my Denison lab mates Xiaotao, Michelle, Dia, Clint, Nicole, and Brett - most of all thank you for making it fun to go to work everyday. Thanks for sharing your magical lab hands, your expertise, your stories, your good and bad days, hatred for the noise of "the beast", your baked goods and birthday parties, for being my traveling companions, and most of all for your friendship. Collaboration is one of the things I like most about science, and I thank you all for being the best of collaborators. I look forward to many more in the future.

ChrisP, it was an honor to mentor you, though we often learned things together more than me teaching you something new. I enjoyed working on many hours of protocol

optimization, experimental design, microscopy, and image processing with you. Thanks for sharing your enthusiasm for science with me-nothing has proven to be more motivating. I'm so proud to watch you apply for MD/PhD programs and I expect that nothing less than the best of things will happen for you.

To Reagan Cox, of the Williams lab, and Bernardo Mainou, of the Dermody lab, thank you for being my resident microscopists and cell biologists, and for taking so much time to help me when I had questions. It's a scary thing doing something without guidance, and I'm very grateful that I found you to help me.

I've always said that my favorite labs are the ones who take a break and have a social lunchtime with each other. Thanks for supporting this extrovert-scientist, members of the Peds ID lunchtime crew.

To the many kind scientists from Vanderbilt and beyond who have given me reagents, often after nothing more than an email describing my project, thank you very, very much for helping me do my work. An incomplete list, most likely, but thank you very much to Tom Gallagher, Susan Weiss, Paul Masters, Rebecca Dutch, Michael Whitt, John Fleming, Alissa Weaver, Ramya Chandrasekaran and Borden Lacy, Tanner Freeman and Dan Beauchamp, Larry Swift, Byron Knowles, Joe Roland, and Jim Goldenring, Barney Graham, Matt Frieman, Emily Poulin and Bob Coffey, Catherine Meador and William Pao, Reagan Cox and John Williams, Bernardo Mainou and Terry Dermody. Your willingness to share and collaborate represents one of the very best parts of science.

To Terry Dermody and the members of the MSTP leadership team, thank you for seeing my potential and accepting me into this wonderful program of yours. I feel like I've had a tremendous amount of opportunities here for learning, discovery, program design, and friendship, and I thank you for allowing me to be a part of that and also to help shape it in some small way.

To the entering Vanderbilt MSTP class of 2008, patrons of ladies' cocktail hour and trivia team members, thanks for taking this journey with me. It's been unbelievably helpful to have a cohort of people that understand how navigating this process feels. Not to mention it's also been incredibly fun. I've so enjoyed our adventures, late nights, and experiencing everyone's big-time-life-events. Thanks also to the class I married into, the entering Vanderbilt MSTP class of 2007, for adopting me as one of their own and becoming incredibly good friends of mine along the way.

To my friends that live far away (or in the hospital), Erin, Carolyn, Jenny, Katie, Carla, Kate, Chelsea, and Emily-sometimes a phone call away isn't that far at all. Thanks for continuing to make time for me years and years after our paths crossed and for being so grand at picking up right where we left off. You're all incredible people and I'm lucky to know you.

To Mama Kat, Mama Sue, Dad Dave, and the rest of the Chauvin and Freeman tribes, thank you so much for being so accepting of me into the family. I've enjoyed getting to know you and being introduced to all of your local traditions and delicious food items

(including but not limited to Andouille and chicken gumbo, Mr. Ronnie's doughnuts, crawfish boils, and red beans and rice). I'm looking forward to many shared celebrations to come!

To Memom, thank you so much for your unconditional love and support from the very beginning. Thanks for always greeting me with a smile and a hug, many, many dinners (and breakfasts!) at your home and away from home, and always sending me away with goodies from your oven or freezer. I hope that Gandy would be proud. I know I would have loved sharing my studies with him.

To Grandmama and Grandaddy- I'm sorry that you only got to see the very beginning of my journey, but I hope that you would be very proud. As I've gotten older, I've developed some common interests-mainly gardening, cooking, and food preservation, and I'm terribly sad that I didn't get the chance to talk to you about all of those things.

To Mom, thanks for the extra summer math workbooks (sorry, Alex, I know you blame me for you having to do them too), letting me sign up for all of the summer reading programs, always being endlessly supportive, checking my homework, reading my essays, helping with projects, having necessary discussions with several school officials to get classes or programs that I needed, and for carting me around to many, many extracurricular activities. Also, thanks very, very much for making me take the Math, Science, and Technology Center entrance exam for high school, despite that at the age of 13 I truly thought that being a "nerd" would be the end of my life. Luckily, by now, I've

accepted that it's really the best way to be. That program was one of the very best things that could have happened to me and was the first domino in a long line that led to my love for scientific research. Thank you also for the encouragement that I could be anything that I wanted to be and for helping me have the confidence to believe that too. Oh, and thank you for always picking up the phone when I have some sort of freak out about a test that I will fail. (You're always right, in approximately 22 years of education, save one, they've always gone well).

Daddy, thank you for always believing in me too, for attending countless dance and theatre productions and at least five performances of Hello, Dolly! in a row. I remember how excited you were when I went to "women in engineering" day at UK when I was in high school. I didn't quite follow in your footsteps, but I'm somewhat of a "gene engineer" every now and again, so perhaps that counts. In any case, thanks for sharing your sense of humor with me. I'm always happy to laugh at any and all jokes even if mom doesn't think that they're funny. Also, thank you for always holding me to the standard of doing my very best, regardless of the task.

Alex/ "Little Brother", Thank you for inspiring me to be as good at what I do as you are at what you do. I've so loved watching you find your style and love your work, and I'm incredibly impressed and in awe of what that has become. Thanks for being my occasional travel companion and constant memory keeper. I'm honored to be your oldest friend.

To my Tanner, what to say that you don't already know? I had no idea that when I decided to join an MD/PhD program that I would choose one that contained my future husband. Thank you for being so incredibly supportive, thoughtful, and inspiring, and for allowing me to make magnificent messes in our kitchen and frequently cleaning them up without a single complaint. I so admire how hard you work and I am in constant awe of how kind and thoughtful you are. You truly inspire me to be at my very best, because that's what you deserve. Who knows where we will go from here, but I look so forward to sharing all of that with you. Cheers to the next adventure and many more after that.

Thank you to the departments of Pathology, Microbiology, and Immunology and Pediatrics, the division of Pediatric Infectious Disease, the Elizabeth B. Lamb Center for Pediatric Research, Sean Schaffer and the Vanderbilt Cell Imaging Shared Resource (DK20593), and funding from the NIH T32 GM007347 (M.C.F.), R01 AI50083 (M.R.D.) and AI108197 (M.R.D.) for educational and financial support.

LIST OF TABLES

LIST OF FIGURES

TABLE OF CONTENTS

Chapter I: BACKGROUND AND LITERATURE REVIEW

Introduction

Coronaviruses are a family of positive stranded RNA viruses that are important pathogens of humans and animals. They cause up to 15% of common colds and have been implicated in more serious diseases including croup, asthma exacerbations, bronchiolitis, and pneumonia (Denison, 2011; Perlman and Netland, 2009). Evidence also suggests that coronaviruses may cause enteritis or colitis in neonates and infants and may be underappreciated as agents of meningitis or encephalitis (Denison, 2011). Four coronaviruses are endemic in humans: human coronaviruses (HCoV) 229E, OC43, NL63, and HKU1. In addition, two epidemics of previously unknown coronaviruses caused significant respiratory distress and high mortality rates among infected individuals. The discovery of SARS-associated coronavirus (SARS-CoV), the cause of severe acute respiratory syndrome (SARS) in 2003, and of Middle East respiratory syndrome coronavirus (MERS-CoV) in 2012 support the potential for coronaviruses to emerge from animal hosts to become human pathogens with great capacity for morbidity and mortality. In addition to being a burden on human health, coronaviruses are also important agricultural pathogens, as they can infect cows, pigs, birds, cats, dogs, rodents, and many more exotic species which contributes to their zoonotic potential (Masters, 2006).

Coronaviruses are enveloped viruses of large size (80-220 nm) (Figure 1) that possess the largest known single-stranded positive-sense RNA genome. Coronaviruses derive their

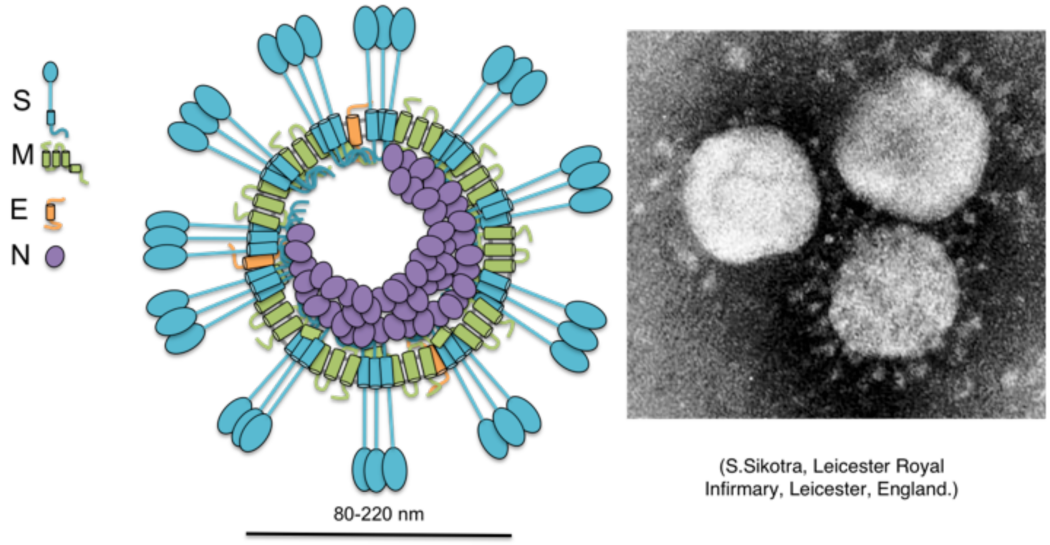

Figure 1. Coronavirus Virion

Coronaviruses derive their name from the spike proteins protruding from the surface, which resemble a corona, or sun. This can be seen in both the schematic and the electron micrograph. Virions are enveloped and pleomorphic, ranging in diameter from 80-220 nm. Viruses derive their envelope from the ERGIC of the host cell. The structural proteins Spike (S), Membrane (M), Envelope (E), and Nucleocapsid (N), are shown in the schematic.

name from the characteristic surface projections of spike protein, which give a corona or crown-like appearance on negative-stain electron microscopy (Masters, 2006). Coronaviruses are organized taxonomically by a lettering system based on genomic phylogenetic relationships (van Boheemen et al., 2012). Alphacoronaviruses include human coronavirus 229E (HCoV-229E) and HCoV-NL63. Betacoronaviruses include four human pathogens and the prototypical model virus, murine hepatitis virus (MHV). Betacoronaviruses are commonly divided into four lineages, without formal taxonomic recognition. HCoV-OC43 and the HCoV-HKU1 are in lineage A, while SARS-CoV falls in lineage B. Lineages C and D were exclusively comprised of bat coronaviruses until the discovery of MERS-CoV, which aligns with lineage C. Gammacoronaviruses and deltacoronaviruses presently include exclusively non-human pathogens (Perlman and Netland, 2009).

Our laboratory utilizes MHV, SARS-CoV, and MERS-CoV, to investigate viral replication, viral evolution, and viral-cellular interactions. MHV replicates in the mouse nasopharynx before dissemination to sites of secondary replication, and SARS-CoV replicates in the nasopharynx and respiratory tract in mouse models. MHV is a powerful model for studying replication, pathogenesis and virus-host interactions, and is primarily used in the studies of this dissertation since MHV can be studied at BSL2, shares many conserved replication and pathogenesis characteristics with human CoVs, including SARS-CoV, has a well-established reverse genetic system and reagents, and can infect cell lines from multiple species expressing the MHV receptor, including cells able to

support SARS-CoV replication. Results from MHV experiments are directly applicable to and testable in SARS-CoV.

The different strains of MHV vary in their pathogenesis. MHV-A59, the strain used as "WT" in the Denison lab and in this dissertation, has a dual tropism in mice with severe hepatitis and meningoencephalitis with chronic demyelination (Navas et al., 2001). Because of the demyelination phenotype, MHV-infected mice are also used as models for multiple sclerosis. MHV-2, however, causes hepatitis and meningitis but does not cause encephalitis or demyelination. MHV-2 and MHV-A59 have 91% genetic identity, but only 79% sequence identity within the spike protein. Differences in tropism and pathogenesis have been attributed to differences in the MHV spike protein, though the backbone of MHV-JHM has been shown to be able to impart pathogenicity in absence of MHV-JHM spike (Navas and Weiss, 2003). These differences in the spike proteins became valuable tools for much of the work in Chapter III of this dissertation.

In 2002-2003, coronaviruses received international attention during the SARS outbreak, which was responsible for over 800 deaths in 30 countries and greater than 8000 cases. SARS-CoV, a novel coronavirus at the time of the epidemic, was found to be the causative agent of SARS (Kuiken et al., 2003; Peiris et al., 2003). The detection of SARS-like coronaviruses in a live animal market in the Guangdong province in Southern China, along with serologic evidence of exposure in food handlers in the same market, suggest that these markets may have facilitated the spread of SARS-CoV to humans from an animal reservoir. Once passed to humans, SARS was an explosive disease, with very

high person-person transmission rates (Hui et al., 2014). Subsequent studies identified SARS-like coronaviruses in fecal specimens from asymptomatic Chinese horseshoe bats that are very closely related, but not direct precursors to, SARS-CoV (Lau et al., 2005; Li et al., 2005). Finally, in 2013, two whole-genome sequences of novel bat CoVs were reported that are able to use ACE2 from humans, civets and Chinese horseshoe bats for cell entry, the strongest evidence to date that bats act as the reservoir for SARS-CoV without requiring an additional animal reservoir before transitioning to humans (Ge et al., 2013).

In June 2012, another novel coronavirus, MERS-CoV was isolated from a man with acute pneumonia and renal failure in Saudi Arabia (Zaki et al., 2012). By publication, an additional 826 cases had been confirmed in Saudi Arabia, Qatar, Jordan, and UAE, as well as cases in Malaysia, the United Kingdom, Italy, Tunisia, France, the United States, and the Netherlands involving patients who had traveled to the Middle East (Zumla and Memish, 2014). Two hundred and eighty-seven of these patients died due to their infection. Compared with SARS-CoV, MERS-CoV to date has a higher mortality, but appears to be less communicable by human-to-human transmission. MERS-CoV uses dipeptidyl peptidase 4 (DPP4) as its cellular receptor, while SARS-CoV utilizes ACE-2, and is able to infect cells from several animal lineages, including human, pig, and bat, suggesting the possibility of movement between multiple species (Raj et al., 2013). In a survey of bats in Europe and Ghana for β-coronaviruses, 46 of 185 Nycteris bats and 40 of 272 Pipistrellus bats contained sequences from clade 2c betacoronaviruses phylogenetically related to MERS-CoV (Annan et al., 2013). In another study, one

Taphozous bat of 1100 samples from various species was found to have a small fragment of a CoV genome with sequence homology to MERS-CoV (Memish et al., 2013). Dromedary camels from the Canary Islands, Egypt, and Oman were shown to have neutralizing antibodies to MERS-CoV, but no viral genetic material was detected in sera or stool samples (Reusken et al., 2013). An investigation of virus sequences during an outbreak of MERS-CoV infection involving three camels and two humans on a Qatari farm demonstrated that people and camels be infected by the same strains, although the direction of transmission is not known (Haagmans et al., 2014). Another study looking at sera from camels in the UAE from 2003 determined that 97.1% of 151 samples had antibodies to MERS-CoV, suggesting that MERS-CoV has been a virus of camels long before its recent recognition in humans (Meyer et al., 2014). There is serological evidence that MERS-CoV has existed in the camel population since at least 1992, but it is unknown if the spillover event occurred before the first documented human case, or if it was stable in the camel population until recently (Alagaili et al., 2014).

Coronaviruses pose a significant zoonotic threat to human health. This has been demonstrated by the emergence of two novel and dangerous coronaviruses within a decade, the capacity of coronaviruses to infect diverse animal species, and the prevalence of coronaviruses endemic to bat populations throughout the world. These characteristics suggest that future emergence of novel zoonotic coronaviruses is likely.

Coronavirus life cycle and replication

The replication cycles of CoVs range from 6-24 hours. CoV infection is initiated by binding of the viral spike (S) glycoprotein to cellular receptors. Virus entry into cells occurs via direct fusion at the plasma membrane or by endocytosis (Figure 2). CoVs have 27-32 kb positive-strand RNA genomes containing 7-9 genes (Figure 3) (Perlman and Netland, 2009). The 5' most replicase gene comprises 2/3 of the genome and is composed of two open reading frames, ORFs 1a and 1b. Translation of genome RNA is initiated following entry into a host cell, first of ORF 1a and then of the longer ORF 1ab following a -1 ribosomal frameshift. The ORF1a and ORF1ab polyproteins are proteolytically processed by the papain-like proteases 1 and 2 (PLP1 and 2) in nsp3, and by the nsp5 protease (3CLpro) to generate 16 nonstructural proteins (nsps1-16). Functions of nsp 1-16 include RNA-dependent RNA polymerase (nsp12), helicase (nsp13), primase (nsp8), cap methylation (nsp14/16) and a novel proofreading exonuclease (nsp14). The exonuclease was identified by our lab and others and is the first known viral RNA proofreading enzyme, likely responsible for the evolution of the large and complex coronavirus genome (Eckerle et al., 2007; Perlman and Netland, 2009). Upon cleavage, nsp domains yield mature proteins that initiate viral genome transcription and replication on modified ER membranes in the cytoplasm, known as replication complexes, induced by replicase proteins nsps 3, 4, and 6 (Angelini et al., 2013).

The downstream genes vary in number and organization, but encode structural proteins, including spike (S), envelope (E), membrane (M), and nucleocapsid (N), as well as several "accessory" proteins which may be dispensable for replication but serve roles in

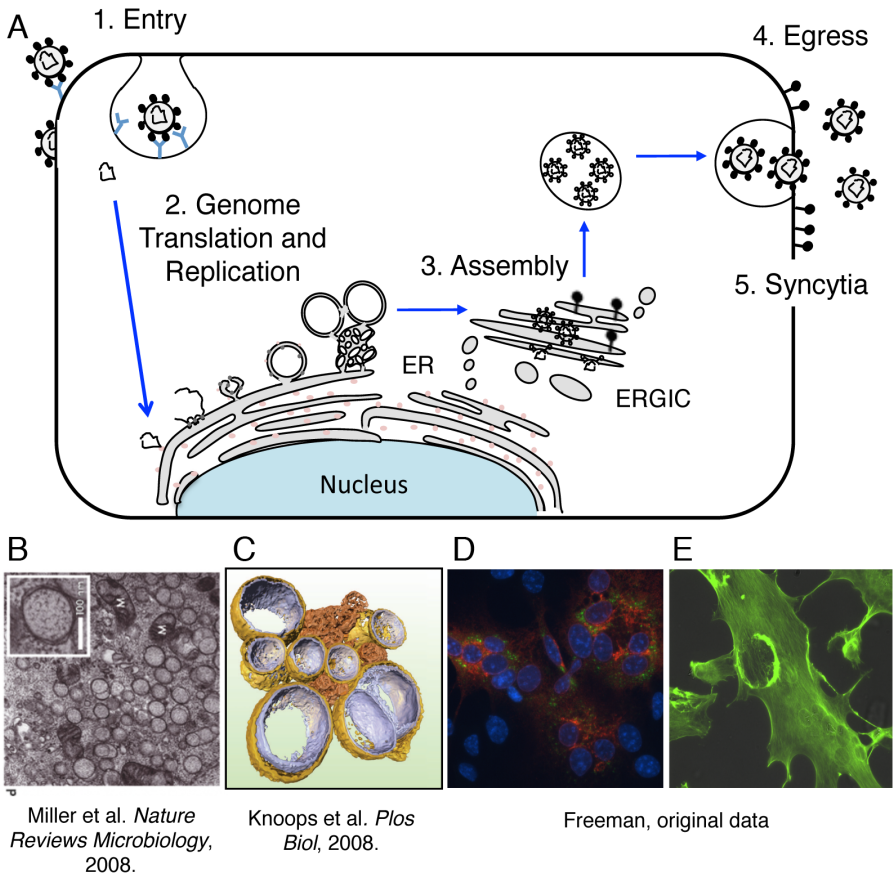

Figure 2. Positive-stranded RNA viruses induce membrane rearrangements

A-E. CoV infection is initiated by binding of the viral spike (S) glycoprotein to cellular receptors. Cellular entry occurs via direct fusion at the plasma membrane or endosomal uptake, depending on the virus strain. Nsp domains in the polyprotein are cleaved to yield mature proteins that initiate viral genome transcription and replication on modified cytoplasmic membranes, known as replication complexes, formed by replicase proteins nsps 3, 4, and 6. **(B-C)**. Double membrane vesicles (DMVs) and convoluted membranes (CMs) make up the replication complexes, and DMVs are visible in the EM image **(B)** and the tomography image **(C)**, where the DMVs are gold and purple and the CMs are orange. Following replication of genomic RNA, assembly of progeny virions occurs in the ER-Golgi intermediate compartment (ERGIC), with virion maturation and release via non-lytic secretory mechanisms. Cell surface expression of proteolytically mature S protein mediates interactions with receptors on adjacent cells resulting in fusion and syncytia formation. The fluorescent microscopy image in **(D)** demonstrates MHV-infected cells forming syncytia, where spike is red, nsp8, a replication protein, is green, and nuclei are blue. Expression of S alone may be sufficient for syncytia formation. The fluorescent microscopy image in **(E)** demonstrates an MHV-infected syncytium forming a large plasma membrane ruffle. Green-F-actin.

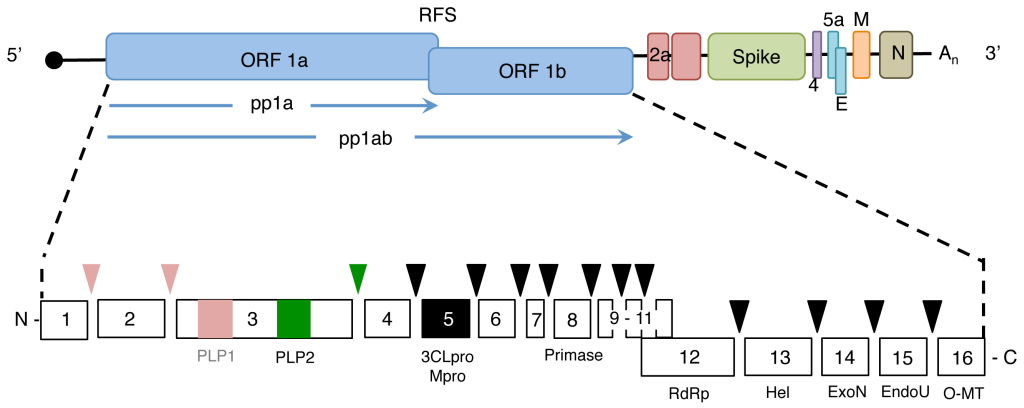

Figure 3. Murine Hepatitis Virus Genome

CoVs have 26-32 kb positive-strand RNA genomes containing 7-9 genes. The genome contains both a 5' cap and a 3' poly-A tail. The 5' most replicase gene makes up 2/3 of the genome and is composed of two open reading frames, ORFs 1a/b. Translation into a single large polyprotein begins upon entry into a host cell, first of replicase ORF 1a and then ORF 1ab following a -1 ribosomal frameshift (RFS). The replicase polyproteins are proteolytically processed by the papain-like proteases 1 and 2 (PLP1 (pink) and 2 (green)) in nsp3, and by the nsp5 protease (3CLpro/Mpro (black)) to generate 16 nonstructural proteins (nsps1-16); functions include RNA-dependent RNA polymerase, helicase, primase, cap methylation and a novel proofreading exonuclease. Cleavage events are represented by the caret of the color corresponding to the protease. The remaining genes encode structural proteins and accessory proteins.

virus host interactions and immune evasion. Following replication of genomic RNA, assembly of progeny virions occurs in the ER-Golgi intermediate compartment (ERGIC), with virion maturation and release via non-lytic secretory mechanisms. For several CoVs, including MHV, cell surface expression of proteolytically mature S protein mediates interactions with receptors on adjacent cells, resulting in fusion and syncytia formation (Figure 2). For these viruses, expression of S alone is sufficient to cause cell fusion (Belouzard et al., 2009; Bertram et al., 2011).

Coronavirus spike and fusion

The coronavirus spike protein is a large, class I fusion protein that exists as a trimer on the surface of the virion. Class one fusion proteins form alpha-helical coiled-coil structures, with the prototype being the influenza HA (Belouzard et al., 2012). Spike is comprised of S1 and S2 subunits of approximately equal size, with S1 at the N terminus responsible for binding the receptor and S2 at the C terminus responsible for fusion (Figure 4). Spike contains two heptad repeats in S2 (HR1 and HR2), as typical of class I fusion proteins. For both MHV and SARS-CoV, the post-fusion form of the protein has been solved and is known to form a six-helix bundle. In most alphacoronaviruses and some betacoronaviruses, the S1 and S2 subunits exist in an uncleaved state. For other betacoronaviruses, including MHV A59, and all gammacoronaviruses, the subunits are cleaved apart from each other, usually by the enzyme furin in the trans-Golgi, to activate the fusion function of the protein (Masters, 2006). Cleavage differences between MHV-A59 and MHV-2, which is cleaved in the early endosome by cathepsins after entry via clathrin-dependent endocytosis (Pu and Zhang, 2008), are thought to be responsible for

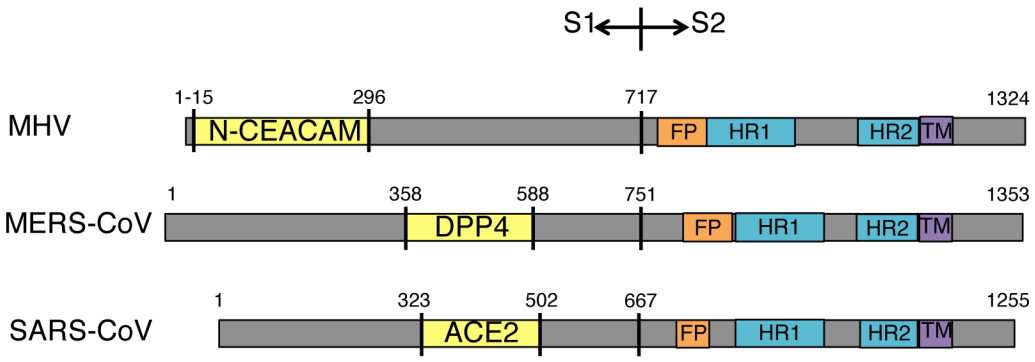

Figure 4. Linear spike protein schematic

Linear schematic of the spike proteins from MHV, MERS-CoV, and SARS-CoV. The cleavage site divides spike into S1 and S2, designated with the arrow logo. The receptor binding domain (RBD) is represented in yellow, and the receptor bound by each virus is indicated (CEACAM, Carcinoembryonic antigen-related cell adhesion molecule, DPP4, Dipeptidyl peptidase-4, ACE2, Angiotensin-converting enzyme 2). The fusion peptide inserts into the host membrane after triggering of fusion, and is represented in orange. Heptad repeats (HR) 1 and 2 are denoted in turquoise. The transmembrane domain (TM) exists within the viral membrane.

the phenotypic differences of these viruses discussed in Chapter III (Figure 5). After cleavage of spike proteins between S1 and S2, they are able to mediate membrane fusion. This generally occurs after binding the cellular receptor, but some spike proteins also have certain pH or additional proteolytic activation requirements (Figure 6). Once fusion is triggered, the fusion peptide (FP) inserts into the cell host membrane and the protein refolds into its energetically favorable six-helix bundle formation. During this refolding event, the membranes of the virus and the cell are brought in proximity and fuse to one another. The viral genome is then able to enter the cell through the created fusion pore. In addition to initiating fusion between the virus and the cell, spike is also responsible for receptor binding, which influences tissue tropism, as virus will only bind to tissues expressing the necessary cellular receptor or receptors. Tissue tropism has been intensively studied, particularly for MHV (Belouzard et al., 2012).

When spike is expressed on a cell surface in cleaved and fusogenic form, it can initiate cell-cell fusion and form giant, multinucleated cells termed syncytia (Figure 2). This has generally been thought to be a surrogate for fusion protein functionality; however, differences in membrane curvatures and viral envelope glycoprotein density are now thought to create differences between virus-cell fusion and the cell-cell fusion surrogate (Belouzard et al., 2012). The relationship between spike protein cleavage and cell-cell fusion capacities for coronaviruses, however, has been well established. MHV-A59 is able to generate large syncytia during infection. MHV-JHM has a more basic cleavage site than MHV-A59 such that it is more efficiently cleaved than MHV-A59. Interestingly, MHV-JHM replicates to a lower titer in cell culture

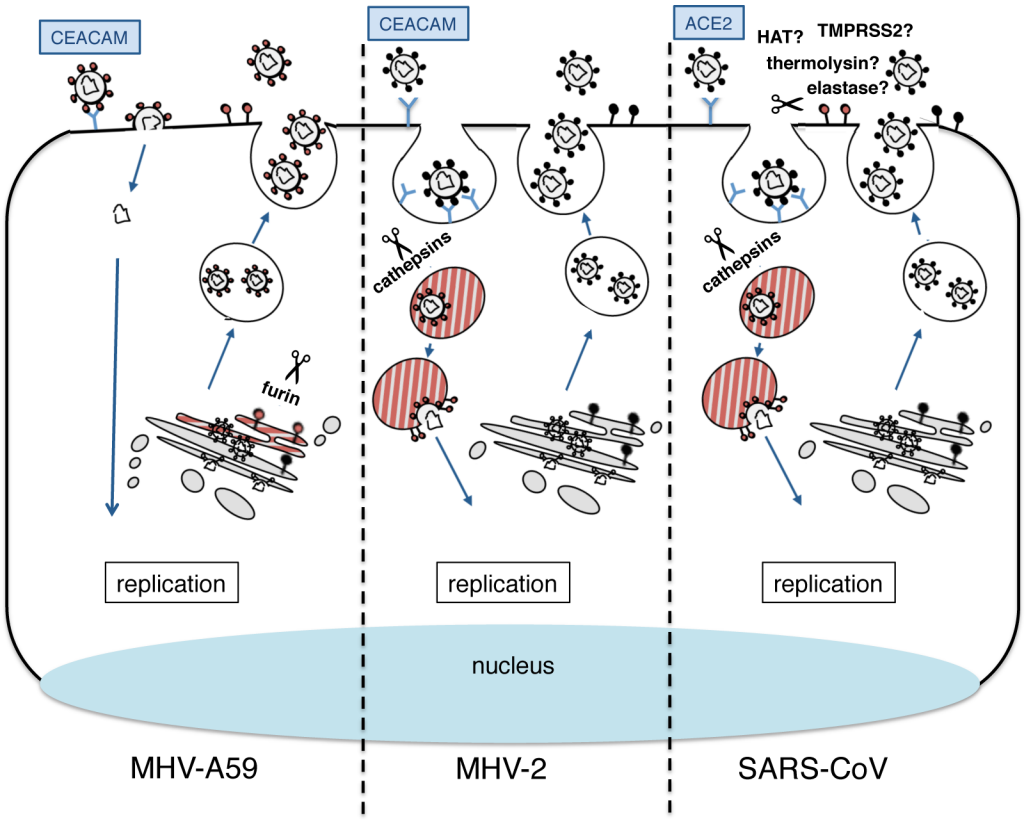

Figure 5. Spike is cleaved by different proteases in different CoVs

For MHV-A59, spike is cleaved post assembly in the trans-Golgi by furin. Spike on the surface of the virion is fusogenic, as well as any excess spike on the cell surface. This virus can enter cells via direct fusion, and causes syncytia. For MHV-2, after entry via endocytosis, spike on the virion surface is cleaved by cathepsins. Spike on the exiting virions is not cleaved, and syncytia do not form. For SARS-CoV, it is thought that after entry via endocytosis, spike on the virion is cleaved by cathepsins. If this was the only protease capable of cleaving spike, then no syncytia would be evident, however, syncytia are sometimes reported *in vivo* and *in vitro*. HAT, TMPRSS2, elastase, and thermolysin have been reported to cleave surface spike, and may be responsible for syncytia formation or for allowing virions to enter cells directly at the plasma membrane.

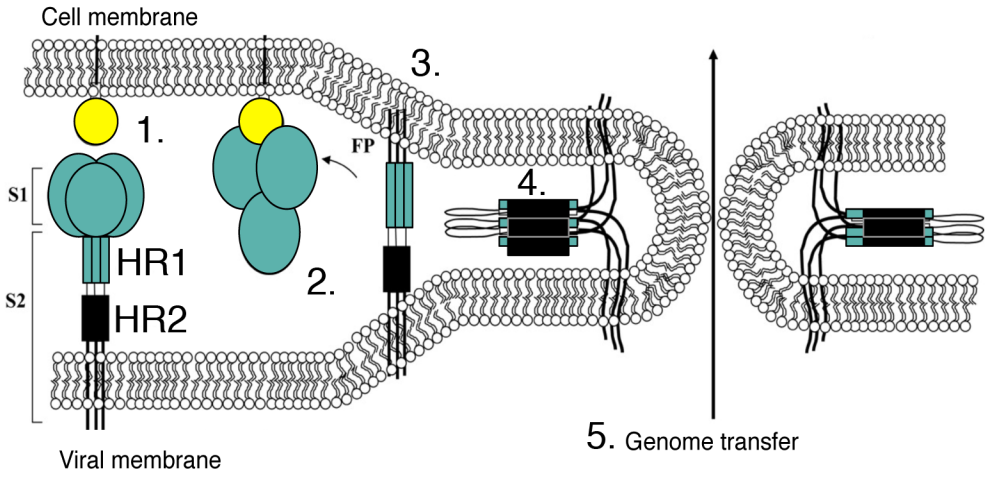

adapted from: Tripet B et al. J. Biol. Chem. 2004

Figure 6. Coronavirus spike induces membrane fusion

The spike fusion protein exists as a trimer at the surface of the virion. Upon interaction with the host cellular receptor **(1)**, the S1 domain separates from S2 **(2)**, allowing the fusion peptide (FP) to insert into the host cell membrane **(3)**. The peptide then folds into a lower energy state, the six-helix bundle **(4)**, while fusing the membranes of the virus and cell together to form a fusion pore to allow viral genome entry **(5)**.

(Navas and Weiss, 2003). Ablation of the furin cleavage site by introduction of an H716D mutation in spike of MHV-A59 impairs protein cleavage and significantly delays cell-cell fusion (Leparc-Goffart et al., 1997). Changes in fusion capacity as measured by cell-cell fusion have unclear effects on viral pathogenesis (Gombold et al., 1993). MHV-A59 infected cells treated with furin inhibitor are unable to form syncytia, but can still infect new cells, likely through the same entry mechanism natively used by MHV-2 (de Haan et al., 2004).

SARS-CoV spike (Figure 5) has been shown in culture to be dependent on the cathepsins for entry (Qiu et al., 2006; Simmons et al., 2005), though treatment with exogenous trypsin can trigger more efficient entry (Matsuyama et al., 2005; Simmons et al., 2004). Spike has been shown to be able to be cleaved *in vitro* by thermolysin and elastase (Matsuyama et al., 2005) and by the TMPRSS2 and HAT (TMPRSS11d) proteins, which associates with ACE2 on the surface of the cell (Bertram et al., 2011; Glowacka et al., 2011; Kam et al., 2009; Shulla et al., 2011). SARS-CoV has been reported to form syncytia in cell culture, in animal models, and in human infections, but the syncytia are less frequent than during MHV infection (Ksiazek et al., 2003).

Coronaviruses induce extensive rearrangement of cellular membranes

Positive-strand RNA viruses induce extensive rearrangement of intracellular membranes to form replication complexes that are thought to recruit and concentrate critical viral replication materials, and provide protection from host immune surveillance (Figure 2). During infection with CoVs, cytoplasmic membranes reorganize into a complex network

of interconnected convoluted membranes and double-membrane vesicles contiguous with the ER that are critical for viral replication (Knoops et al., 2008). The CoV proteins nsp 3, 4 and 6 contain defined transmembrane domains, and have been demonstrated to nucleate ER membrane alterations to form double-membrane vesicles (Denison and Perlman, 1986; Graham and Denison, 2006; Kanjanahaluethai and Baker, 2000; Lu et al., 1995; Salonen et al., 2005). All nsps studied have been shown to localize to these complexes, but the exact method of their formation is yet to be determined. While several cellular proteins and pathways, including small GTPases and autophagy components (Prentice et al., 2004; Verheije et al., 2008), have been implicated in viral replication complex formation, little is known about the virus-host interactions required for cellular membrane reorganization.

While much has been learned about virus-induced host cell modifications, little is known of the process of replication complex formation and how replication complexes change over time. It is known that nucleocapsid is associated with new sites of RNA synthesis, but also at sites of virus assembly in the ER-Golgi intermediate compartment (ERGIC) and Golgi distinct from sites of replication (Bost et al., 2001). The mechanisms by which replication complexes form, RNA synthesis occurs, and structural proteins and genomes transit to sites of virion assembly, however, remain unknown.

The development of fluorescent reporter viruses, described in Chapter II, have allowed us to examine live, infected cells in real time to quantify the movement of the replication proteins thought to be responsible for these membrane changes. These reporter viruses

are fusions between firefly luciferase (FFL) or green fluorescent protein (GFP) and a replicase protein, either nsp2 or nsp3. These viruses are the first coronaviruses to express reporters from the replicase gene, and demonstrate the flexibility of the large coronavirus genome to tolerate extensive additions of foreign material. The fluorescent reporters can be used quantify the formation and evolution of replication complexes. The FFL versions of these viruses allow for quantification of the earliest stages of virus replication-specifically measurement of genome translation and amplification even early during the eclipse phase of replication.

Live-cell imaging of MHV-infected cells utilizing these fluorescent reporter viruses revealed additional membrane rearrangements that had not been previously described for coronaviruses: constitutive membrane ruffling at the plasma membrane and the formation of long filopodia. Ruffling events were frequent and dynamic, and included two conformations of ruffles: peripheral ruffles that extended laterally from the cell and circular dorsal ruffles (Figure 7), which extended toward the observer, and closed with a "beggar's purse formation" while retracting back into the cell. Cells ruffle for several different purposes, including immune surveillance, motility, to facilitate interactions with neighboring cells, and membrane ruffling is a hallmark of macropinocytosis (Swanson and Watts, 1995). Also, during these experiments, long filopodia extending from infected cells were first noticed. These, in addition to the previously described formation of syncytia during infection, make up a great amount of external surface membrane rearrangements that occur during infection in addition to the internal membrane rearrangements previously described during replication complex formation.

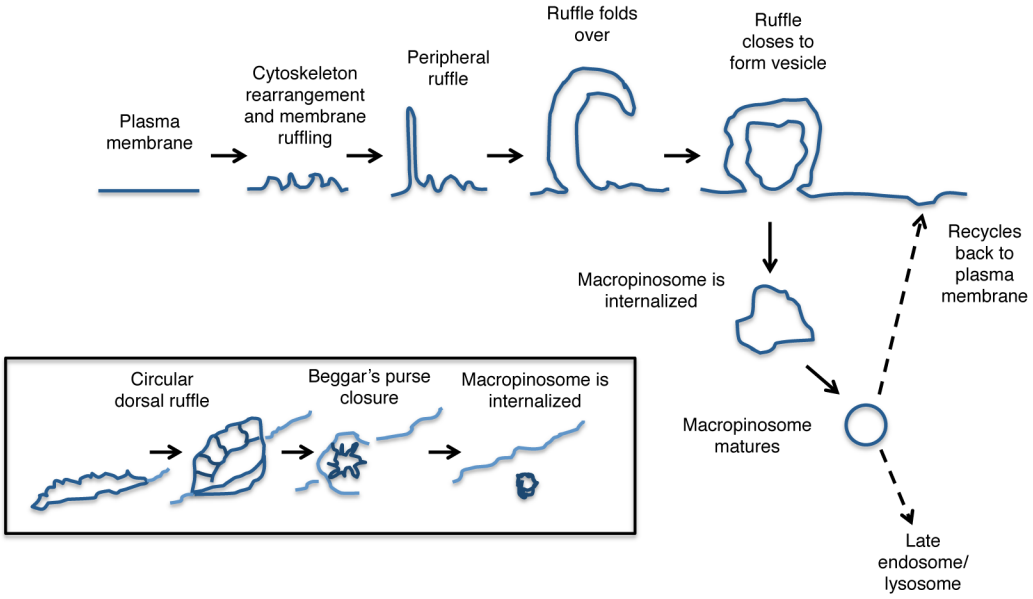

Adapted from Lim and Gleeson, *Immunology and Cell Biology*, 2011

Figure 7. Evolution of membrane ruffles into macropinosomes

During macropinocytosis, actin rearrangement at the plasma membrane creates membrane ruffles. These ruffles can be peripheral to the cell (main), or circular dorsal ruffles (inset). Peripheral ruffles often fold back onto themselves, trapping extracellular solutes and fluid, and fuse with the cell. They are internalized as macropinosomes and mature within the endocytic pathway. They can progress to the late endosome or lysosome, where their contents are degraded, or they can be recycled back to the plasma membrane surface. Circular dorsal ruffles close via a "Beggar's purse closure," named for its appearance, before being internalized.

Macropinocytosis

Macropinocytosis is a cellular process morphologically defined by membrane extensions of outwardly polymerizing actin, or membrane ruffles. The presence of outwardly polymerizing actin, in addition to the large and pleomorphic size of the internalized vesicles, distinguish macropinocytosis from other types of endocytosis, such as clathrin-mediated, caveolae -mediated, lipid raft-mediated, and from phagocytosis. Membrane ruffles often result in non-specific internalization of fluid cargo into large vesicles, or macropinosomes (Figure 7) (Hansen and Nichols, 2009; Kerr and Teasdale, 2009; Swanson and Watts, 1995). Macropinocytosis includes peripheral ruffles and lamellipodia at cell margins and circular dorsal ruffles on the dorsal cell membrane (Swanson, 2008). Macropinosomes rapidly traffic to the perinuclear region and acidify through the endocytic pathway as their fluid contents are absorbed into the cytosol (Swanson and Watts, 1995). Membrane ruffling is involved in cell migration, cell-cell interactions, environmental sampling, recycling of surface proteins and membranes, and delivery of bulk material to endosomes and lysosomes (Gu et al., 2011; Hewlett et al., 1994; Nobes and Marsh, 2000; Orth and McNiven, 2006). While all cells are capable of macropinocytosis, it most commonly occurs in immune cells and cells that form endothelial and epithelial barriers. Macropinocytosis can be induced by exogenous growth factors or oncogenes (Hewlett et al., 1994; Veithen et al., 1996), by activation of tyrosine kinase receptors, including EGFR, phosphitdyl serine receptor, or α_5 integrins, and involves many cellular factors including actin; Rho GTPases such as Cdc42 and Rac1 (Nobes and Hall, 1995); cellular kinases p21-activated kinase 1 (Pak1), phosphatidylinositol 3-kinase (PI3K), and protein kinase C (PKC) (Amyere et al., 2002);

and the Na^+/H^+ exchanger (Amyere et al., 2000; Araki et al., 1996; Dharmawardhane et al., 2000; Nobes and Marsh, 2000; Swanson and Watts, 1995; West et al., 2000) (Figure 8). Macropinocytosis can be inhibited chemically by blocking key pathway regulators, most specifically by blocking the Na^+/H^+ exchanger, which is inhibited by ethyl isopropyl amiloride (EIPA) (Figure 9). This specificity exists because the Na^+/H^+ exchanger is not known to be involved in other endocytic pathways or in phagocytosis (Koivusalo et al., 2010). Macropinocytosis pathway members can also be inhibited by using siRNAs or dominant negative constructs. Fluid phase uptake can be measured or visualized by dextran or nanoparticle uptake and by markers of acidification and lysosomal targeting.

In Chapter III, I report my results that define macropinocytosis during coronavirus infection and discuss why this process is important for viral replication. Macropinocytosis has been identified as an entry mechanism for several bacterial and viral pathogens including *Salmonella enteritica, Neiserria gonorrhea,* Rubella virus, Cocksackie B virus, Influenza, Ebola, Vaccinia, and HIV (Mercer and Helenius, 2009) (Figure 10). In each of these studies, membrane ruffling began with the addition of pathogen to cell culture and ceased after pathogen internalization. While subversion of the macropinocytosis pathway for pathogen entry is described, induction of constitutive macropinocytosis has been described only when induced by growth factors or oncogenes, or by dendritic cells surveying the environment (Mercer and Helenius, 2009). Our studies demonstrating constitutive macropinocytosis with MHV infection in cells that do not natively display macropinocytosis raise important questions about virus-host interactions responsible for macropinocytosis during infection, including whether the process is

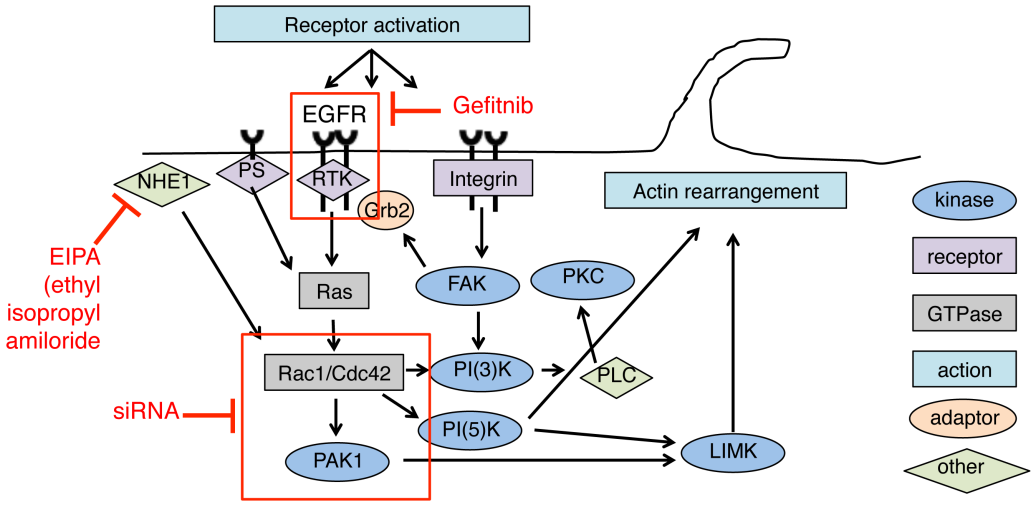

Adapted from: Mercer and Helenius, **Gulping rather than sipping: macropinocytosis as a way of virus entry,** Current Opinion in Microbiology Volume 15, Issue 4 2012 490 – 499, http://dx.doi.org/10.1016/j.mib.2012.05.016

Figure 8. Macropinocytosis activation pathway

Macropinocytosis can be induced by activation of tyrosine kinase receptors (RTK), phosphitdyl serine receptors (PS), or α_5 integrins, and involves many cellular factors including key kinases (blue ovals), GTPases (grey boxes), and adapter proteins (orange ovals). Macropinocytosis can be inhibited chemically by blocking the Na^+/H^+ exchanger (NHE1), which is inhibited by ethyl isopropyl amiloride (EIPA), by inhibitors of the receptor, including gefitinib inhibition of EGFR, and through siRNA knockdown of pathway members (red boxes). Grb2- Growth factor receptor-bound protein 2, Rac1- Ras-related C3 botulinum toxin substrate 1, Cdc42- Cell division control protein 42 homolog, FAK- Focal Adhesion Kinase, PI (3) K- Phosphatidylinositol 3-kinase, PI (5) K- phosphatidylinositol 5-kinase, PLC-phospholipase C, LIMK- LIM domain kinase

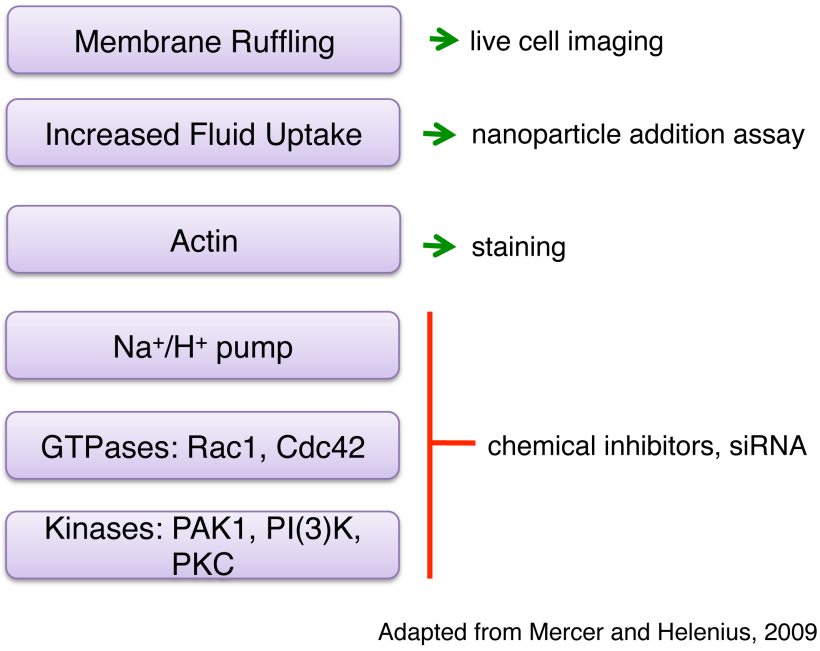

Figure 9. Testing for macropinocytosis

A rubric for testing for macropinocytosis, including confirmation of membrane ruffling, demonstration of bulk fluid uptake, and dependence on macropinocytosis pathway members, including actin, Na^+/H^+ pump, GTPases, including Rac1 and Cdc42, and kinases, including Pak1, PI(3)K, and PKC. In order to demonstrate the dependence on these pathway members, chemical inhibitors or siRNA can be used.

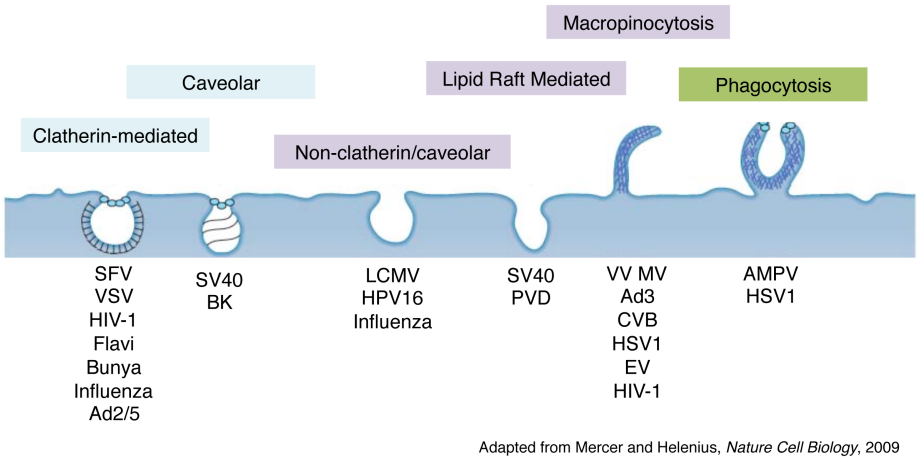

Figure 10. Viruses use endocytosis for entry

Endocytic mechanisms of eukaryotes are divided into two classes: pinocytosis for uptake of fluid and solutes, and phagocytosis (green box) for larger particles. Pinocytosis is further divided into those requiring dynamin for vesicle scission (light blue boxes), clathrin-mediated and caveolar, and those that do not, non-clathrin/caveolar, lipid raft mediated, and macropinocytosis. (purple boxes). Any of these pathways can be subverted for viral entry, and viruses may enter via more than one pathway. Viruses shown include: semliki forest virus (SFV); vesicular stomatis virus (VSV); human immunodeficiency virus 1(HIV-1); flaviviruses (Flavi); bunyaviruses (Bunya); influenzavirus (Influenza); adenovirus 2/5 (Ad2/5); simian virus 40 (SV40); BK virus (BK); human papilloma virus 16 (HPV16); lymphocytic choriomeningitis virus (LCMV); polyomavirus (PVD); vaccina virus mature virion (VV MV); adenovirus 3 (Ad3); coxsackievirus B (CVB); herpes simplex virus 1 (HSV1); echovirus 1(EV1) and mimivirus (AMPV). Blue circles-dynamin, dark blue lines-actin.

specifically induced and required by MHV for productive infection, and what viral and cellular pathways are involved in this process.

Summary

Coronaviruses are known to orchestrate the rearrangement of cellular membranes for replication through the formation of replication complexes. In contrast, prior to this work, little was known of coronavirus modifications of host cell plasma membranes. Live-cell imaging of cells infected with GFP-expressing MHV resulted in the observation that MHV infection is associated with profound rearrangements of the plasma membrane, including peripheral ruffles, circular dorsal ruffles, and the formation of long filopodia.

Chapter II describes the engineering, recovery and use of MHV reporter viruses. Chapter III describes studies demonstrating that MHV induced ruffling events are macropinocytosis, which is important for efficient viral replication, likely as a mechanism of cell-cell spread. Chapter IV extends studies to MERS-CoV, demonstrating the development of antibodies against MERS-CoV nonstructural proteins and visualization of replication complexes in infected cells. Chapter V includes methods used for the experiments in this dissertation and Chapter VI discusses important implications of this work and the new questions it raises for continued study and discovery. Research into virus-cell interactions has a history of resulting in profound insights into normal cell biology. Coronaviruses appear to be profligate in their exploitation and modification of host cell membrane biology, both on the interior and the exterior of the cell. This work sought to investigate pathways long ago discovered by coronaviruses.

Chapter II: CORONAVIRUS REPLICASE-REPORTER FUSIONS PROVIDE QUANTITATIVE ANALYSIS OF REPLICATION AND REPLICATION COMPLEX FORMATION

Introduction

At the beginning of this dissertation, replicase proteins nsps 3, 4 and 6 were predicted to be involved in membrane modifications (Angelini et al., 2013) leading to formation of double membrane vesicles (DMVs), which are essential for replication. Each MHV nsp studied has been shown to localize to virus-induced DMVs and other modified host membranes, collectively referred to as replication complexes (RCs) (Gosert et al., 2002). While much has been learned about virus-induced host cell modifications, little is known of the process of replication complex formation or changes over time. It is known that nucleocapsid is associated with sites of RNA synthesis, but also at sites of virus assembly in the ERGIC / Golgi distinct from sites of replication (Bost et al., 2001). The mechanisms by which RCs form, RNA synthesis occurs, and nucleocapsids transit to sites of virion assembly, however, remain unknown. Coauthors of this publication corresponding to this chapter, Rachel Graham and Xiaotao Lu, generated the viruses used in these studies, the initial growth characterization, and performed the immunoprecipitation studies. Rachel Graham also assisted with some of the immunofluorescence images. I performed the majority of the immunofluorescence studies, and all of the competition assays, live-cell imaging, and comparative luciferase and replication studies.

To date, studies of CoV replication complex formation and evolution have involved immunofluorescence imaging of fixed cells using antibodies against native proteins (Brockway et al., 2003; Brockway et al., 2004; Sims et al., 2000; Snijder et al., 2006). For assessment of kinetics of replication, fluorescent and luminescent reporters have been expressed with replicase proteins either from expression plasmids, with reporter proteins replacing replication non-essential accessory ORFS, or with replicase protein-reporter fusions expressed in place of accessory ORFS (Bosch et al., 2004; Das Sarma et al., 2002; de Haan et al., 2003; Fischer et al., 1998). Reporters also have been utilized within CoV replicon genomes (Hertzig et al., 2004). Studies with such constructs have provided insights into the function and interaction of replicase proteins and viral replication, as well as serving as reporters for studies of CoV inhibitors (Ge et al., 2007; Hertzig et al., 2004; Roberts et al., 2006; Zhao et al., 2013). While these strategies have been useful for reporting on overall virus replication, they were not designed to test the expression or localization of specific proteins, nor were they designed to report replicase gene expression. A successful replicase reporter virus has been constructed for equine arteritis virus, an arterivirus with a genome size less than half that of MHV, with the insertion of EGFP in between nsp1 and nsp2 (van den Born et al., 2007). The capacity of the CoV replicase gene to accept foreign genes, however, is not known, nor has foreign gene insertion within the replicase gene of any replicating CoV been tested without compensatory deletion of viral genetic material. In this chapter, I defined quantitative translation of the MHV replicase gene and formation of replication complexes by using the reporters green fluorescent protein (GFP) and Firefly Luciferase (FFL) as in-frame fusions with viral replicase proteins nsp2 and nsp3. Nsp2 is a 65-kDa protein that has

been shown to localize to CoV replication complexes, but is dispensable for virus replication in culture (Graham et al., 2005). Nsp3 is a 210-kDa protein that contains two essential proteases and other functional protein domains, and is required for both virus-induced membrane modifications and virus replication (Angelini et al., 2013). Reporter fusions with nsp2 and nsp3 can be stably cloned into the MHV genome, permit efficient virus replication, target replication complexes, and provide the earliest indicators of MHV replication and direct measurement of replication complex formation. The results also demonstrate the capacity of the MHV genome to tolerate genomic expansion and identify sites for possible virus mediated expression of foreign proteins within the replicase polyprotein.

Generation and recovery of MHV replicase reporter viruses

Since nsp2 is dispensable for replication (Graham et al., 2005), I first tested the tolerance for reporter expression in place of deleted nsp2. This approach also was used since engineered genome length would not exceed WT MHV. Constructs were engineered in which enhanced green fluorescent protein (EGFP) (0.71 kb/26.8 kDa) or firefly luciferase (FFL) (1.65 kb/ 60.7 kDa) (Figure 11) replaced the nsp2 coding sequence. All constructs were initially designed with PLP1 specific cleavage sites at N and C termini of the reporter, based on the hypothesis that processing of the reporter from nsp1 and nsp3 would be required for viability. Following electroporation of *in vitro*-transcribed genome RNA into BHK cells layered on permissive DBT cells, cytopathic effect (CPE) of syncytia was detected by 24 h post electroporation for both recombinant viruses. Media supernatants from electroporated cultures were used to infect fresh DBT cells and RNA

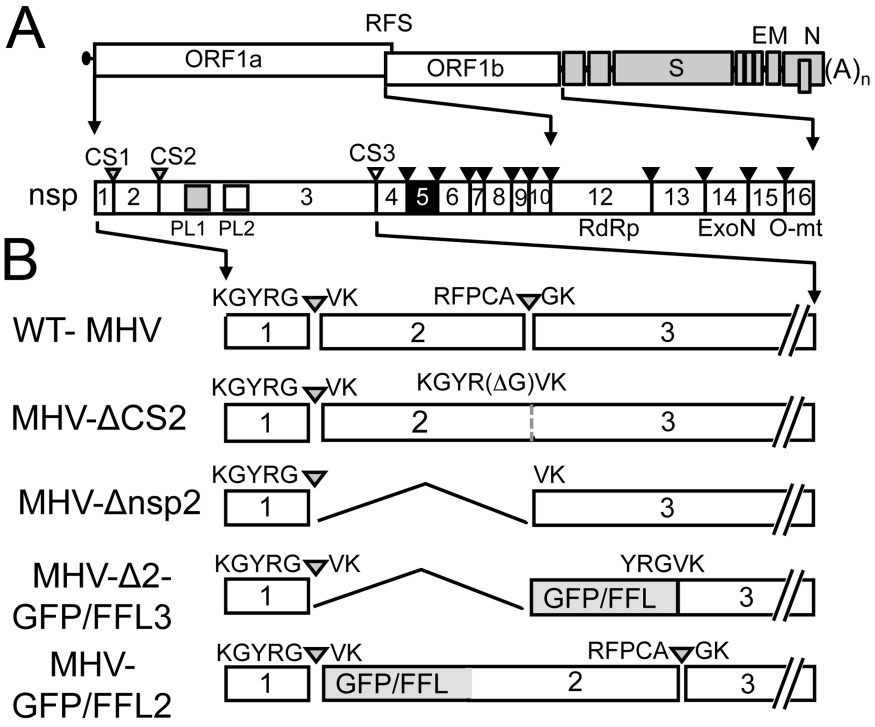

Figure 11. Generation and recovery of MHV replicase reporter viruses

A. Schematic of MHV genome organization with ORF1a and ORF1b connected by ribosomal frameshift (RFS), and downstream structural / accessory ORFS: S-spike, E-envelope, M-membrane, N-nucleocapsid. The ORF1ab polyprotein of MHV is shown, with nonstructural protein domains 1-16 (nsp). Papain-like proteinase domains PL1 and PL2 are indicated by grey and white boxes in nsp3. Nsp5 protease (3CLpro, Mpro) is indicated by the black box. Cleavages mediated by each domain are indicated by correspondingly colored arrowheads (CS1-cleavage site 1). Deletion is indicated by the Δ sign. **B.** Design of reporter fusion viruses. The top schematic shows WT-MHV-A59 nsp1-3, with cleavage site residues P5-P2' and cleavage sites marked by carets. The next schematics show previously described MHV-ΔCS2 (lacking P1-Gly at nsp2-3 cleavage site) and MHV-Δnsp2 with in frame deletion of nsp2 and functional engineered nsp1-nsp3 cleavage site. GFP and FFL reporter gene insertions are indicated in grey. All confirmed functional cleavages indicated by grey arrowheads. MHV-Δ2-GFP/FFL3: MHV with deletion of nsp2 and fusion of GFP or FFL to nsp3. MHV-GFP/FFL2: MHV with addition of GFP or FFL as fusion to nsp2.

was harvested and amplified by RT-PCR for sequencing of the entire genome. Viral genome sequencing demonstrated retention of reporter genes without additional mutations in the genome. Passage of the P0 virus in culture demonstrated stability of the inserted GFP and FFL sequences for more than 5 passages (data not shown). This confirmed the capacity of MHV to accept proteins of differing size and structure in place of deleted nsp2. These viruses will be referred to as MHV-Δ2-GFP3 and MHV-Δ2-FFL3. I next investigated the capacity of the MHV replicase to accept additional genetic material into its genome without deletion of viral sequence. GFP and FFL were engineered between nsp1 and nsp2 while retaining all viral proteins. Since I sought to test whether reporter fusions with nsp2 could be recovered, the cleavage site between nsp1 and the reporter was retained, but the cleavage site between the reporter and the nsp2 amino terminus was deleted (Figure 11B). Both recombinant viruses were recovered, sequence confirmed, and passaged for > 5 passages with retention of the introduced sequences (data not shown). These viruses will be referred to as MHV-GFP2 and MHV-FFL2.

Polyprotein expression and processing in MHV replicase reporter viruses

MHV-Δ2-GFP3 and MHV-Δ2-FFL3 mutant viruses were engineered with predicted functional cleavage sites at the nsp1 and nsp3 junctions. To define the processing of nsp1-reporter-nsp3 from the replicase polyprotein, DBT cells were infected with WT MHV, MHV-Δ2-GFP3, or MHV-Δ2-FFL3, radiolabeled, and proteins immunoprecipitated from lysates of infected cells with antibodies specific for nsps 1, 2, 3, and 8 (Figure 12A). Immunoprecipitation of lysates from WT MHV-infected cells

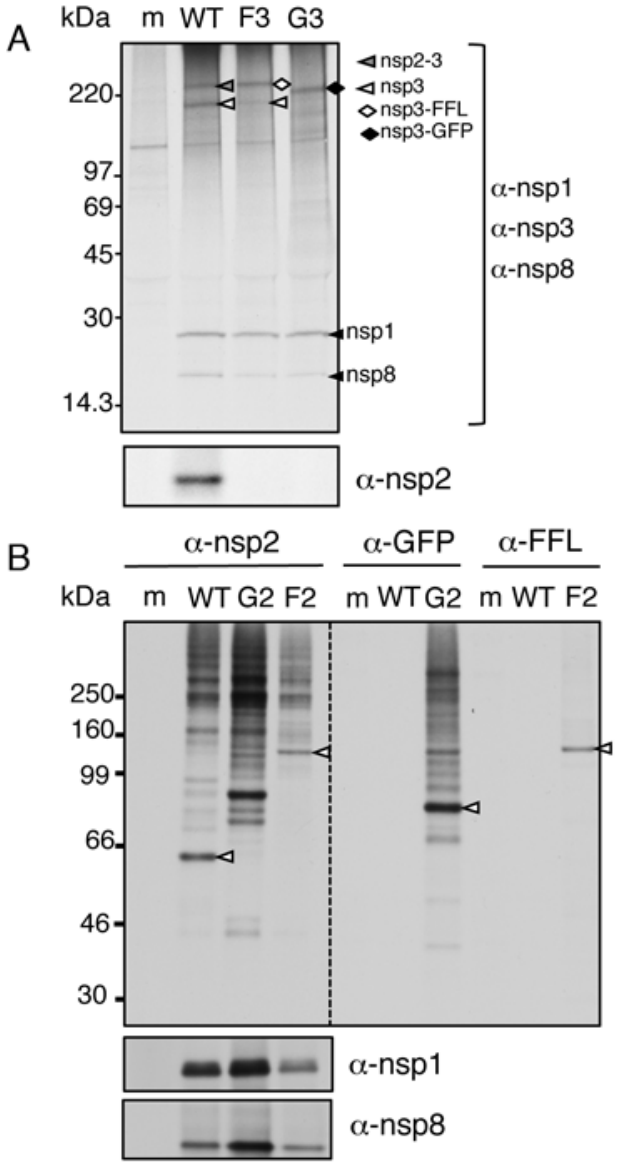

Figure 12. Polyprotein expression and processing in MHV replicase reporter viruses

A. DBT cells were infected with WT MHV, MHV-Δ2-GFP3 (G3), and MHV-Δ2-FFL3 (F3). Radiolabeled proteins were immunoprecipitated by combined antibodies for nsp1, nsp3 and nsp8, and detected by fluorography. The molecular weight marker is indicated on the left. nsp3, nsp2-3, FFL-nsp3, and GFP-nsp3 are indicated in panel. m=mock **B.** DBT cells were infected with WT MHV, MHV-GFP2 (G2), and MHV-FFL2 (F2) as indicated by top labels and radiolabeled proteins were harvested by immunopreciptation and detected by fluorography. Antibodies used are indicated to the right or above. The dashed line represents the same gel with different exposure times, overnight on the left, and one week on the right. The molecular weight marker is indicated on the left. nsp2, GFP-nsp2, and FFL-nsp2 are indicated by white arrowheads. m=mock

detected nsps 1, 2, 3, 2-3, and 8. Immunoprecipitation of proteins from cell lysates of MHV-Δ2-FFL3 and MHV-Δ2-GFP3 infected cells detected both nsp1 and nsp8, but not nsp2, as expected. This indicated that processing was occurring at the junction between nsp1 and FFL/GFP, and that expression and processing of downstream proteins from the replicase polyprotein was intact. Immunoprecipitation with α-nsp3 in WT infected cells detected the 210-kDa nsp3 as well as the known nsp2-nsp3 intermediate precursor (275 kDa). In contrast a 210-kDa-nsp3 protein was barely detectable following infection with MHV-Δ2-FFL3 and not detected from cells infected with MHV-Δ2-GFP3. Instead, α-nsp3 antibodies detected a protein of ~271 kDa in MHV-Δ2-FFL3 infected cells (the predicted mobility of nsp3 plus FFL) and ~237 kDa in MHV-Δ2-GFP3 infected cells (the predicted mobility of nsp3 plus GFP). These results indicate that reporter molecules are efficiently processed at the nsp1-reporter junctions, but minimally or not processed at the engineered cleavage sites between the reporter and nsp3. This suggested that while P1'-P5' residues are required for cleavage, the context of P5-P1 also is important. The result serendipitously demonstrated that viable recombinant MHV could be engineered with a reporter fusion with the 210-kDa nsp3 protein.

This outcome served as the rationale for design of the "second-generation" reporters, with a retained cleavage site between nsp1 and the reporter, and deletion of the cleavage site between the reporter and nsp2. For MHV-GFP2 and MHV-FFL2, immunoprecipitation of infected cell lysates with α-nsp1 and α-nsp8 detected the respective proteins. Antibodies against nsp2 detected the 65-kDa nsp2 in WT-infected lysates, but did not detect nsp2 in either reporter virus. Instead, α-nsp2

immunoprecipitated proteins of 92 kDa or 126 kDa, consistent with the predicted sizes of GFP-nsp2 and FFL-nsp2 fusion proteins, respectively (Figure 12B). To confirm this, lysates were immunoprecipitated with α-GFP and α-FFL antibodies. The α-FFL detected a protein of identical mobility from MHV-FFL2 infected cells as detected by α-nsp2. The α-GFP immunoprecipitation of MHV-GFP2 infected lysates detected a protein with mobility slightly differing from that of α-nsp2, but consistent with a fusion of nsp2-GFP. The reason for the difference in mobility is not clear, but suggests different migrating forms of nsp2-GFP with different available epitopes recognized by α-nsp2 and α-GFP. The complete lack of nsp2 and detection of new proteins consistent with nsp2-GFP and nsp2-FFL strongly supported the expression of stable fusion proteins that are not cleaved during infection. Overall, these results indicated that the recombinant viruses expressed the reporters as fusions with nsp3 or with nsp2.

Replication of MHV-Δ2-GFP3, MHV-Δ2-FFL3, MHV-GFP2, and MHV-FFL2

Previous work in our lab has shown that MHV-Δnsp2 replicates with similar kinetics to WT-MHV, but with a lower peak titer (Graham et al., 2005), while MHV mutants engineered to abolish cleavage site 2 between nsp2-nsp3 (MHV-ΔCS2) demonstrate a prolonged eclipse phase but ultimately achieve WT-like peak titer (Graham and Denison, 2006). Finally, loss of cleavage between nsp1 and nsp2 has been demonstrated to result in decreased viral yield but WT-like timing of exponential replication (Gadlage and Denison, 2010). To test the effect of reporter fusions with nsp2 or nsp3, murine DBT cells were infected with MHV-Δ2-GFP3, MHV-Δ2-FFL3, MHV-GFP2, or MHV-FFL2 viruses in direct comparison with WT-MHV, MHV-Δnsp2, and MHV-ΔCS2, with

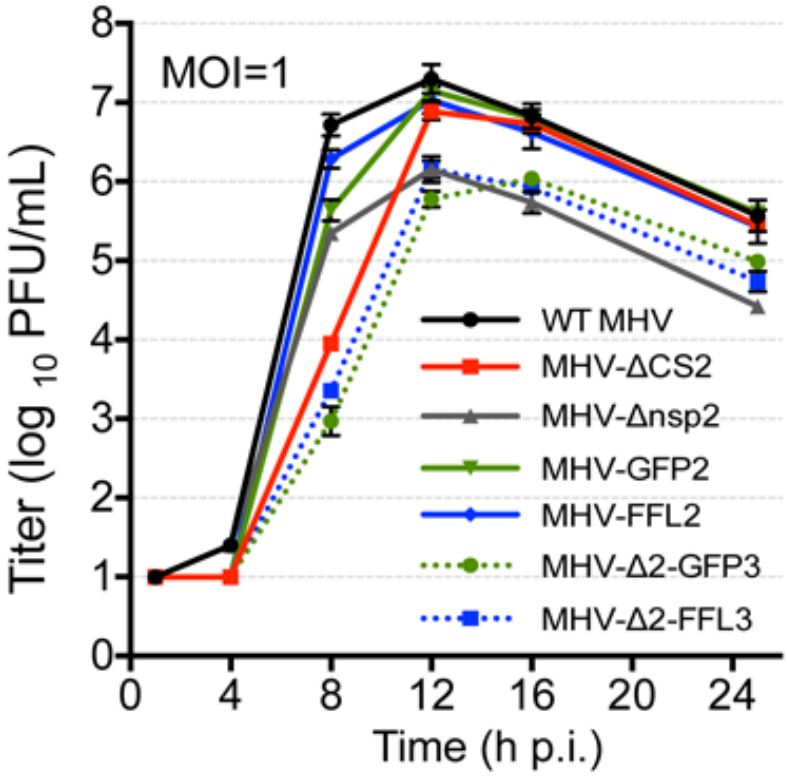

Figure 13. Replication of MHV reporter fusion viruses

DBT cells were infected with recombinant WT MHV, MHV-Δnsp2, MHV-ΔCS2, MHV-Δ2-GFP3, MHV-Δ2-FFL3, MHV-GFP2, and MHV-FFL2 at an MOI of 1 PFU/cell. Supernatant was sampled at indicated times p.i., and titer determined by plaque assay. Titer reported is the mean of three replicates, +/- SD.

measurement of supernatant virus titer by plaque assay at multiple time points post infection (Figure 13). MHV-Δnsp2 replicated with 1-$\log_{10}$ impairment in viral titer but normal timing of exponential replication. MHV-ΔCS2 (nsp2-3 fusion) also replicated as previously reported, with delayed exponential replication but WT-like virus yield. MHV-Δ2-GFP3 and MHV-Δ2-FFL3 replication resulted in a cumulative phenotype: A 4h delay in exponential replication similar to MHV-ΔCS2, and decreased viral yield similar to MHV-Δnsp2. In contrast, both MHV-GFP2 and MHV-FFL2 demonstrated replication in culture with exponential replication and viral yield similar to WT-MHV. This suggests that the replication phenotypes of MHV-Δ2-GFP3 and MHV-Δ2-FFL3 result from deletion of nsp2 and fusion of nsp2 with nsp3, not the insertion of foreign genes themselves. These results support previous studies from my lab proposing that cleavage at the nsp3 N-terminus is required for efficient onset of exponential replication (Graham and Denison, 2006). Similarly, the WT-like replication of MHV-GFP2 and MHV-FFL2 further shows that it is cleavage at the C-terminus of nsp1 that is required for WT-like yield. Finally, the results demonstrate that expansion of the replicase gene and polyprotein can still allow for WT-like replication.

Subcellular localization of nsp2 and nsp3 fusion reporters

Next, the expression and localization of nsp2 and nsp3 reporter fusions in virus-infected cells were tested. DBT cells on glass coverslips were infected with reporter-expressing MHV at an MOI of 1 PFU/cell, fixed at 10 h p.i, stained for replicase proteins, and examined by confocal microscopy (Figure 14). DBT cells infected with WT MHV and stained with antibodies for nsp2, nsp3, nsp8, or membrane protein (M) demonstrated the

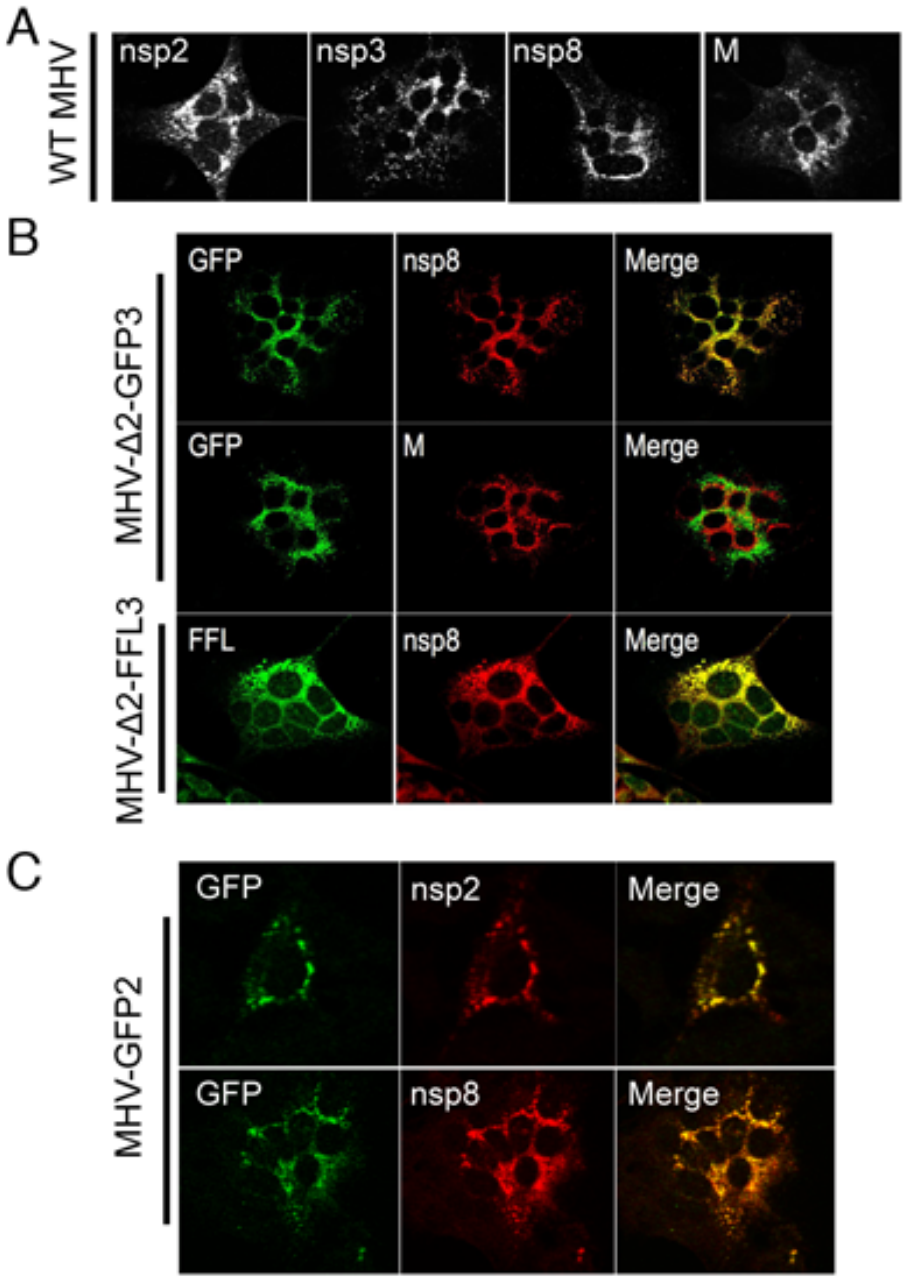

Figure 14. MHV nsp2 and nsp3 fusion reporters localize to replication complexes

DBT cells were infected with WT MHV **(A)**, MHV-Δ2-GFP3, MHV-Δ2-FFL3 **(B)**, or MHV-GFP2 **(C).** At 10 h p.i. cells were fixed, stained with antibodies as indicated (α-FFL, α-nsp2, α-nsp3, α-nsp8, α-M) and imaged by confocal microscopy. GFP was detected by native fluorescence. M – membrane protein.

established punctate cytoplasmic pattern of localization (Figure 14A). Cells infected with MHV-Δ2-GFP3 or MHV-Δ2-FFL3 also exhibited punctate, perinuclear cytoplasmic localization of reporter molecules by native fluorescence (GFP) or by IF with a-FFL. GFP and FFL both colocalized with nsp8 (Figure 14B), a replicase protein known to localize to replication complexes, but were distinct from M, which localizes to sites of viral assembly in the ERGIC / Golgi (GFP, Figure 14A, FFL, data not shown). The punctate nature of reporter localization suggests a mechanism for specific targeting to replication complexes. In addition, these results demonstrate that GFP fluorescence is intact when the reporter is fused to the N-terminus of nsp3. DBT cells infected with MHV-GFP2 (Figure 14C) also exhibited punctate, perinuclear cytoplasmic localization, and colocalized with nsp2 and nsp8, again demonstrating specific targeting to replication complexes and indicating that native fluorescence is intact in the nsp2-reporter fusion protein.

Competitive fitness of WT MHV vs. MHV-GFP2

Since MHV-FFL2 and MHV-GFP2 demonstrated WT-like kinetics during replication in culture, I investigated whether there was a fitness cost associated with introduction of a foreign protein in the replicase polyprotein. Cells were infected with WT MHV or MHV-GFP2 alone, or at WT MHV: MHV-GFP2 ratios of 1:1, 1:10, or 10:1 at a combined MOI of 0.1 PFU/cell, followed by 10 passages of supernatant onto fresh flasks of DBTs. GFP expression was compared with expression of replicase protein nsp8 to determine the relative competitiveness of the MHV-GFP2 virus. DBT cells seeded on glass coverslips were infected with P1, P3, and P10 passages of each combination of viruses for 8 hours. Following immunostaining for nsp8, coverslips were imaged and scored for nsp8

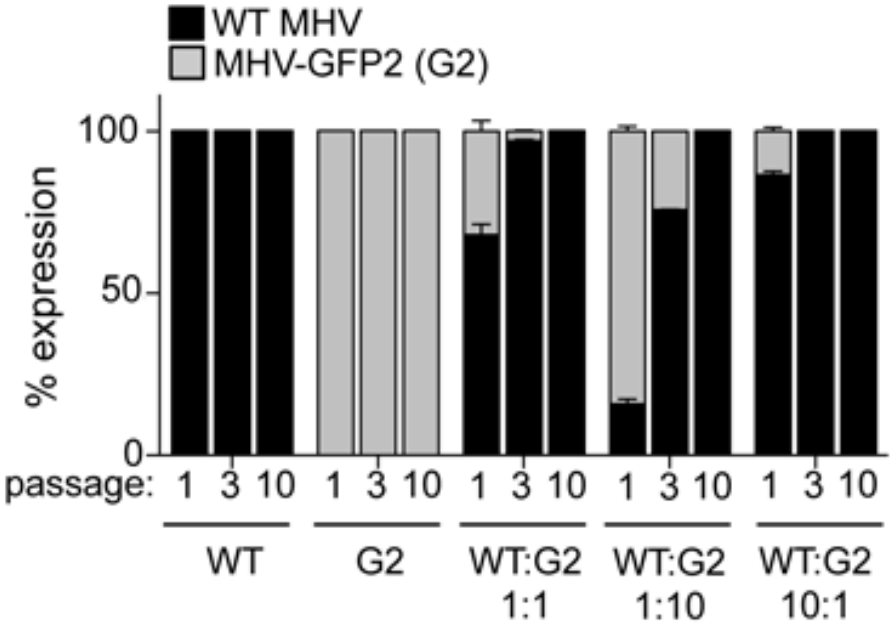

Figure 15. Competitive fitness of WT-MHV and MHV-GFP2

DBT cells were infected with WT MHV or MHV-GFP2 alone or at 1:1, 1:10, or 10:1 ratios of WT-MHV:MHV-GFP2. DBT cells on glass coverslips were infected at an MOI of 1 PFU/cell with P1, P3, and P10 passages of each combination. At 8 h p.i., cells were fixed and imaged for nsp8 (red) and GFP (green). Cells containing green (MHV-GFP2) or red (WT MHV or MHV-GFP2) replication complexes were scored. Thirty images from two independent experiments were photographed and scored for cells infected only with WT MHV or only with MHV-GFP2, while for the WT:G2 1:1, 1:10, and 10:1 samples, 50 images from two independent experiments were scored.

(indirect immunofluorescence-red) and GFP (native green fluorescence). At all passages, WT MHV-infected cells exhibited only nsp8 (red) signal, while MHV-GFP2-infected cells demonstrated colocalized nsp8 (red) and native GFP in all cells (Figure 15). In competition experiments, at P1 MHV-GFP2 infected cells were detected, but not at levels equivalent to the input ratios. By P3 to P10, even when a 10-fold advantage was given to MHV-GFP2, the recombinant virus could not compete with WT. Thus, while GFP as a fusion with nsp2 had no effect on replication as measured by plaque assay, the insertion of the gene was associated with a fitness cost compared to WT virus.

GFP-nsp2 allows quantitation of replication complex formation in live cells

I tested whether reporter-nsp fusions could be used to track the quantity and movement of these proteins within a single infected cell over time. DBT cells cultured in glass-bottomed dishes were infected with MHV-GFP2 and at 5 h p.i., were imaged in a 37°C live imaging chamber incubator on a wide-field fluorescence microscope. Images were collected in the differential interference contrast (DIC) and green filter sets every thirty seconds for 2.5 hours from the same field (Figure 16). Every tenth image was analyzed for corrected total cell fluorescence (CTCF) by selecting the cell as the region of interest (ROI) and correcting for the background within each individual image (Burgess et al., 2010). Green fluorescence is evident from the first frame and the CTCF nearly triples in value throughout infection until it peaks at 6.75 h p.i. At the conclusion of imaging at 7.5 h p.i., CTCF has decreased by 30% from the peak value. Throughout the collection of images, green fluorescence is localized perinuclearly, with both increasing numbers and intensity of GFP foci from 5 to 7.5 h p.i. The increase in fluorescence intensity during infection indicates that more copies of GFP-nsp2 are being produced and accumulating,

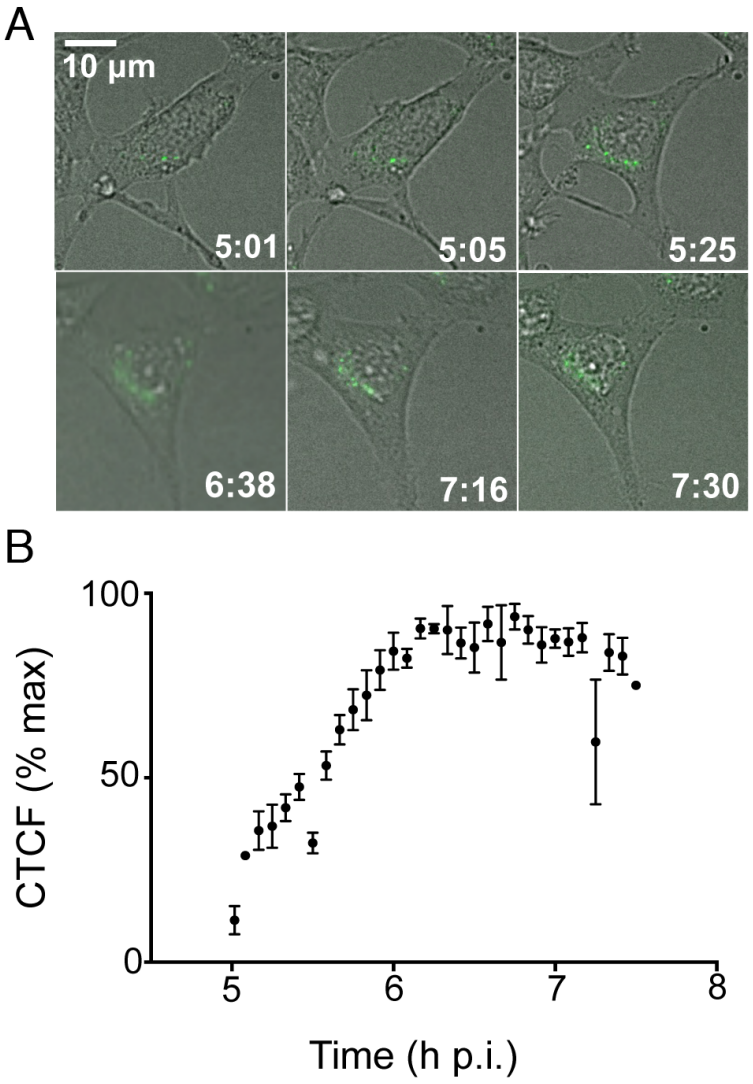

Figure 16. MHV-GFP2 quantitation of replication complex formation in live cells

A. DBT cells on glass bottom culture dishes were infected with MHV-GFP2 at an MOI of 1 PFU/cell. At 5 h p.i., dishes were transferred to the 37°C chamber incubator, with imaging of DIC and GFP every 30 seconds for 2.5h. Individual frames were used to generate this panel. The video sequence corresponding to this figure can be seen as Fig. S1. **B.** Corrected total cell fluorescence (CTCF) was measured for the cell utilizing ImageJ. CTCF was calculated for every ten frames and plotted over time. Data shown is calculated from three independent infected cells.

as each copy of nsp2 is fused only to one fluorescent molecule, in contrast to indirect fluorescence where multiple fluorescent molecules have the capacity to bind to one viral protein. These results indicate that MHV-GFP2 and MHV-Δ2-GFP3 reporter viruses can be used to directly measure the progression of RC formation in real time in single infected cells, as well as tracking the localization and movement of nsp2 and nsp3 over time.

FFL-nsp2 is a highly sensitive quantitative measure of genome translation

Translation of input genome RNA is the first step in virus replication, and ORF1a–encoding nsp2 and nsp3 domains, is translated 100% of the time. I hypothesized that this would allow translation of luciferase to provide an earlier marker of viral replication. I inquired whether FFL expression as fusions with nsp2 or nsp3 could quantitatively measure replication, and if so, whether it was as sensitive as virus titer. DBT cells were infected with MHV-FFL2 or MHV-Δ2-FFL3 viruses at an MOI of 1 PFU/cell, supernatants collected for plaque assays, and cells harvested for luciferase assays at multiple times post infection (Figure 17). MHV-FFL2 and MHV-Δ2-FFL3 both replicated as expected with MHV-Δ2-FFL3 demonstrating delayed exponential replication and decrease in virus yield compared with MHV-FFL2. Luciferase activity (yield in relative light units – RLU) for MHV-FFL2 showed signal >3 log10 higher than the corresponding titer for the at 4 h p.i., while increasing in signal over time. At 8 h p.i., measurements of luciferase activity and titer were very similar. MHV-Δ2-FFL3-infected cells also demonstrated a >3 log10 increase in FFL signal compared to viral titer at 4 h p.i., but this increased signal was retained until 16 h p.i. Most importantly, for both

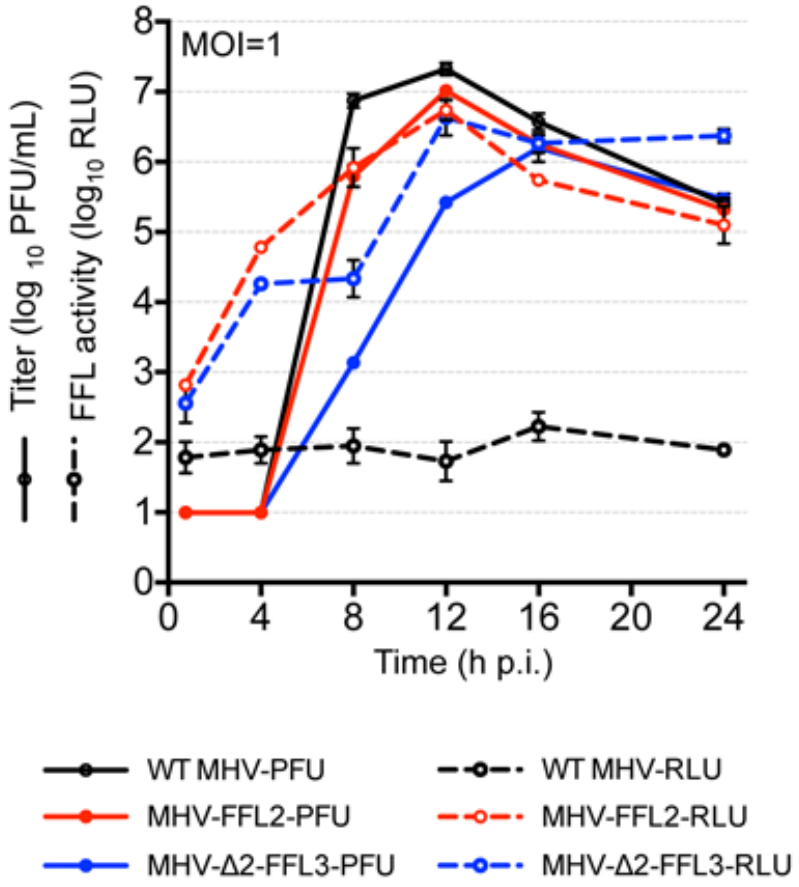

Figure 17. MHV-FFL2 and MHV-Δ-FFL3 are quantitative measures of replication

DBT cells were infected with MHV-Δ2-FFL3 or MHV-FFL2 at an MOI of 1 PFU/cell in replicate wells. At indicated times h p.i., supernatant was collected for measurement of virus titer by plaque assay and cells harvested for measurement of FFL activity. Titer (PFU/solid) and luminescence (RLU/dotted) are plotted. Data is represented as the mean +/- SD of three replicates.

viruses, FFL activity was detected earlier and 100 fold greater than virus titer during eclipse phase. The amplification trend for MHV-FFL2 luminescence mirrors replication, as does the trend for MHV-Δ2-FFL3, suggesting that this assay can serve as a robust early surrogate for viral replication. Further, the results demonstrate that replicase gene translation is occurring continuously and genome used as a translational template is being amplified, even in virus with delayed exponential increase in virus titer. These results establish that expression of the FFL reporter from the MHV replicase serves as a sensitive, quantitative marker of replicase polyprotein translation and as a discriminating indicator of viral replication. They also suggest that it may be possible to uncouple measurement of genome translation and genome replication from measurement of infectious virus, and might act as a much earlier biological marker for studies of virus inhibition or studies or constitutive or conditional mutations.

Discussion

In this chapter, I demonstrated that the CoV genome is capable of tolerating large substitutions or additions of foreign genetic material within the replicase protein as in-frame protein domains. Further, I showed that fusion of reporters to replicase proteins is tolerated in efficiently replicating virus, allowing quantitative assessment of multiple stages in the virus life cycle. Specifically, the studies show that measurement of viral replication by using FFL can be a highly sensitive, early and powerful surrogate for genome replication and that GFP fusions with nsp2 and nsp3 can allow for quantitative assessment of replication complex formation and evolution during the course of infection.

Finally, the results show that insertion of very different proteins are tolerated at each of these locations.

Most studies of CoV replication using addition of reporters have involved substitution of accessory ORFs. These have been used as general indicators of overall viral replication, mostly for testing inhibitors or attenuation of replication (Curtis et al., 2002; de Haan et al., 2003; Fischer et al., 1998; Ge et al., 2007; Hertzig et al., 2004; Kilianski et al., 2013; Pfefferle et al., 2011; Roberts et al., 2006; Zhao et al., 2013). However, these strategies are limited as direct indicators of genome replication since they require subgenomic mRNA transcription for expression of the engineered reporters or are not contained within infectious virus. While reporters expressed from downstream ORFs are valuable as indicators of overall viral replication, they cannot distinguish genome replication from subgenomic mRNA transcription. Reporters also have been employed for analysis of coronavirus host interactions and cell biology. Specifically, expression of nsp2-reporter or nsp4-reporter fusions as substitutions of MHV ORF4 or HE have been described and used to define localization and movement of nsps (Gadlage et al., 2008; Hagemeijer et al., 2011; Hagemeijer et al., 2010). While informative, these studies are limited in their interpretation by nsp expression from non-native locations in the genome. Previous work in the Denison lab has shown that alternative expression of nsp2 can be detrimental to replication, even when expressed as a duplication with native nsp2 (Gadlage et al., 2008). These results suggest that the context of nsp2 location in the polyprotein is important for its interaction with adjacent replicase proteins. Although nsp2 is dispensable for

replication (Graham et al., 2005), altering expression by deletion or cleavage site alteration impacts replication and fitness.

The observation that GFP or FFL fusions with nsp2 had no detectable effect on the MHV replication cycle in culture was surprising and suggests significant flexibility in this region of the polyprotein for additional genetic information. A recent study of the evolution of the genomes of nidoviruses from the small arteriviruses (~15 kb) to the largest coronaviruses (up to 32 kb) proposed that proto-CoVs emerged due to incorporation of a cassette of proteins including the proofreading exonuclease in nsp14, which allowed more stability of larger genomes (Lauber et al., 2013). It also was proposed that increased genetic robustness to mutations also was required for genome expansion and increased complexity. This study supports that argument, with incorporation of FFL expanding the MHV genome by ~5.3%. The virus can be recovered at P0 and P1 with high titer stocks for use *in vitro* and *in vivo* and the FFL coding sequence is maintained for at least 5 passages. However, introduction of GFP as an nsp2 fusion results in a fitness cost during direct competition with MHV. It will be interesting to see if this fitness cost is similar for FFL or other foreign genes. It will also be of interest to see whether foreign genes are retained over long passage in absence of competition, or if the subtle fitness cost results in selection against the foreign sequences in the long term.

The implications of stable replicase nsp-reporter fusions are significant for several reasons. It has not previously been possible to directly quantitate translation of the CoV

replicase/ transcriptase polyproteins in infected cells. CoV ORF1a expresses ~495 kDa polyprotein (pp1a). Translation of ORF1b, which encodes critical replication enzymes including nsp12-RdRp and nsp14-ExoN, requires a ribosomal frameshift between nsp10 and nsp12. *In vitro* studies have suggested frameshift efficiencies ranging from 10-40% (Somogyi et al., 1993). Dual luciferase systems have been used to examine structures and sequences in this region, however this has never been tested utilizing infectious virus (Plant et al., 2005; Plant et al., 2013). Expression of different quantitative reporters from ORF 1a and ORF1b could allow direct testing of timing and stoichiometry of replicase polyprotein translation. Our lab has recently recovered recombinant viruses expressing GFP as a fusion with nsp14 (unpublished results), providing encouraging evidence that ORF1b reporter expression is possible. The early exponential signal from FFL-nsp2 is consistent with rapid amplification of genome RNA prior to virus assembly and release, and thus may be an early and sensitive reporter for studies of inhibitors of virus replication. Similarly, it has not previously been possible to track the expression and localization of replicase proteins from their native locations in the genome. Native expression of fluorescent reporters fused to replicase proteins creates the opportunity to track replication complex formation in real time in a single cell, without potential artifacts due to cellular fixation for immunofluorescence or due to altered expression from subgenomic mRNAs or exogenous plasmids. These results suggest that it may be possible to engineer reporter-fusions with multiple replicase proteins for testing and visualization of protein-protein and protein-membrane interactions in live cells.

Chapter III: CORONAVIRUSES INDUCE CONTINUOUS, ENTRY-INDEPENDENT MACROPINOCYTOSIS

Introduction

At the beginning of this dissertation, coronaviruses were known to initiate extreme rearrangements of host cell membranes to promote replication. These membrane structures on the interior of the cell include double membrane vesicles and convoluted membranes (Perlman and Netland, 2009). Modified membranes are thought to concentrate critical viral replication materials and to provide protection from host immune surveillance (Knoops et al., 2008). While several viral proteins, specifically nsps 3, 4, and 6, are thought to orchestrate this process in addition to other cellular proteins and pathways, including small GTPases and autophagy components (Prentice et al., 2004; Verheije et al., 2008), little is known about virus-host interactions required for cellular membrane reorganization. In addition to these internal membrane organizations, coronaviruses modify the plasma membrane during several stages of their life cycle, including entry via direct membrane fusion at the plasma membrane or endocytosis and non-lytic exocytosis. For several CoVs, including murine hepatitis virus (MHV) and SARS-CoV, cell surface expression of proteolytically mature spike protein mediates interactions with receptors on adjacent cells, resulting in cell fusion and syncytia formation. Expression of spike alone may be sufficient for formation of syncytia (Belouzard et al., 2009; Bertram et al., 2011). Syncytia formation is a well-described cytopathic effect for many viruses in cell culture or in animal model systems, and has been suggested to increase viral cell-cell spread (Yamada et al., 2009). However, for

coronaviruses, syncytia formation has not been tested for a role in replication or cell spread.

A live-cell imaging experiment at the beginning of this dissertation project revealed an intriguing and somewhat unexpected phenotype. Late during infection with MHV, the plasma membrane underwent extreme morphologic changes with the extension of filopodia, peripheral ruffles, circular dorsal ruffles, and the internalization of large and pleomorphic vesicles that collected toward the nuclei of the cell. Plasma membrane ruffling has been previously described to be a defining characteristic of macropinocytosis. The initial live-cell imaging studies were performed by Mark Denison and repeated many times by Chris Peek and me. I also had some assistance with the BSL3 work to complete the experimental portion of the SARS-CoV studies by Michelle Becker and Clint Smith, though all of the data was analyzed by me. Chris Peek assisted with the development of the nanoparticle uptake assay and methods for image analysis. I generated all other experimental data.

In this chapter, I demonstrate that, in addition to internal membrane rearrangements, CoVs also induce plasma membrane changes consistent with macropinocytosis. Macropinocytosis is a type of endocytosis, morphologically defined by the presence of membranous extensions of outwardly polymerizing actin, termed membrane ruffles. Membrane ruffles non-specifically surround and internalize fluid cargo into large vesicles, or macropinosomes (Hansen and Nichols, 2009; Kerr and Teasdale, 2009; Swanson and Watts, 1995). Membrane ruffling is involved in cell migration, cell-cell

interactions, environmental sampling, recycling of surface proteins and membranes, and delivery of bulk material to endosomes and lysosomes (Gu et al., 2011; Hewlett et al., 1994; Nobes and Marsh, 2000; Orth and McNiven, 2006). While all cells are proposed to be capable of macropinocytosis, it is generally associated with immune cells that monitor the environment for pathogens, as well as for apoptotic body clearance (Henson et al., 2001). Macropinocytosis is usually transient, but is constitutive in cells transformed by the SRC oncogene (Amyere et al., 2002). Macropinocytosis may be initiated by activation of the epidermal growth factor receptor (EGFR) and involves signaling though GTPases and kinases including Rac1, Cdc42, and Pak1. Further, macropinocytosis requires sodium hydrogen exchangers (NHE) and thus is specifically inhibited by 5-(N-Ethyl-N-isopropyl)-amiloride (EIPA) (Mercer and Helenius, 2009, 2012). Macropinocytosis has been identified as an entry mechanism for several pathogens including *Salmonella enteritica*, *Neiserria gonorrhea*, cocksackie B virus, influenza virus, Ebola virus, vaccinia virus, Nipah virus, and HIV (Mercer and Helenius, 2009; Pernet et al., 2009). In each of these studies, membrane ruffling or blebbing is induced by addition of the pathogen to cell culture, and membrane modifications cease after pathogen internalization. To date, no role for macropinocytosis other than entry has been described as a host-pathogen interaction of viruses or bacteria.

In this study, I show that cells infected with CoVs MHV or SARS-CoV induce macropinocytosis with well-defined characteristics: membrane ruffling and extensive filopodia formation, large vesicle internalization, increased bulk fluid uptake, actin polymerization, dependence on signaling through Cdc42, Rac1, and Pak1, and sensitivity

to EIPA. MHV-induced macropinocytosis is continuous once initiated ≥ 4 hours post infection, significantly after viral entry is completed. Replicating virus is required for induction of macropinocytosis, and inhibition of macropinocytosis impairs viral titer and cell-cell fusion. MHV-induced macropinocytosis requires fusogenic spike glycoprotein, and is dependent on EGFR activation. The results support a role for CoV-induced macropinocytosis in cell fusion and virus cell-cell spread, representing novel exploitation of macropinocytosis machinery for virus use.

Infection with MHV or SARS-CoV induces continuous membrane ruffling

During live-cell imaging of murine hepatitis virus (MHV)-infected cells, we observed that MHV-infected cells displayed plasma membrane ruffling and extensive filopodia. We therefore examined the etiology and role of plasma membrane ruffling during CoV infection. Murine delayed brain tumor (DBT) astrocytoma cells were infected with MHV strain A59 (MHV-A59) expressing GFP as a fusion with the replicase protein nsp3 (Freeman et al., 2014) and cells were imaged continuously from 4 to 12 hours post infection (h p.i.), until the monolayer was entirely involved in syncytia or was lost (Figure 18A and Figure 19). Cell infection was confirmed both by the presence of GFP-nsp3 at replication complexes, and by syncytia formation, a characteristic cytopathic effect of MHV infection. Membrane ruffling on multiple edges of the cell was noted to begin after 5 h p.i., similar to the time of appearance of GFP-nsp3 fusion proteins at replication complexes and was continuous throughout infection. The plasma membrane changes were extensive, and included lamellipodia, filopodia, peripheral dorsal ruffles, and circular dorsal ruffles (Figure 18A, Figure 19). The membrane ruffling associated

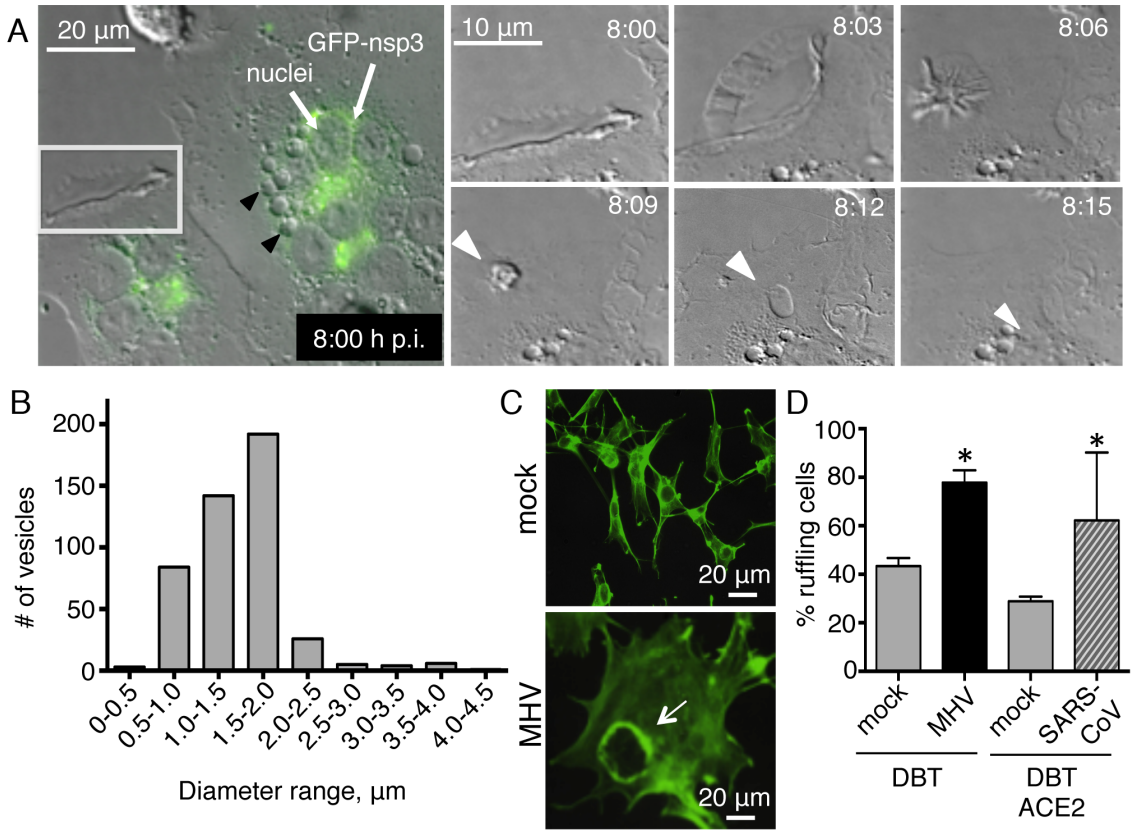

Figure 18. Infection with MHV or SARS-CoV induces membrane ruffling and vesicle internalization

A) DBT cells were infected with MHV-Δ2-GFP3, at an MOI of 1 PFU/cell and imaged from 4-12 h p.i. Small panels to the right correspond to the white box and are enlarged to show detail. Green fluorescence indicates nsp3. Black arrowheads denote vesicles. White arrowheads follow the evolution of a vesicle over time. **B)** Vesicle diameter was measured from 5 movies of infected cells, MOI=1 PFU/cell, n=386 vesicles. **C-D)** DBT cells were infected with MHV-A59 at an MOI of 1 PFU/cell for 8 h. DBT-hACE2 cells were infected with SARS-CoV at an MOI of 0.1 PFU/cell for 24 h. Cells were fixed with 10% formalin and stained for F-actin (green). Arrow denotes ruffle (**C**). Every third infected (or mock) cell was imaged and scored for ruffling by 3 blinded reviewers. Data is represented as averages +/- SEM of two replicates in duplicate. Significance was assessed using one-way ANOVA with Dunnett's post-hoc test. n≥30 fields per replicate. *$p<0.05$.

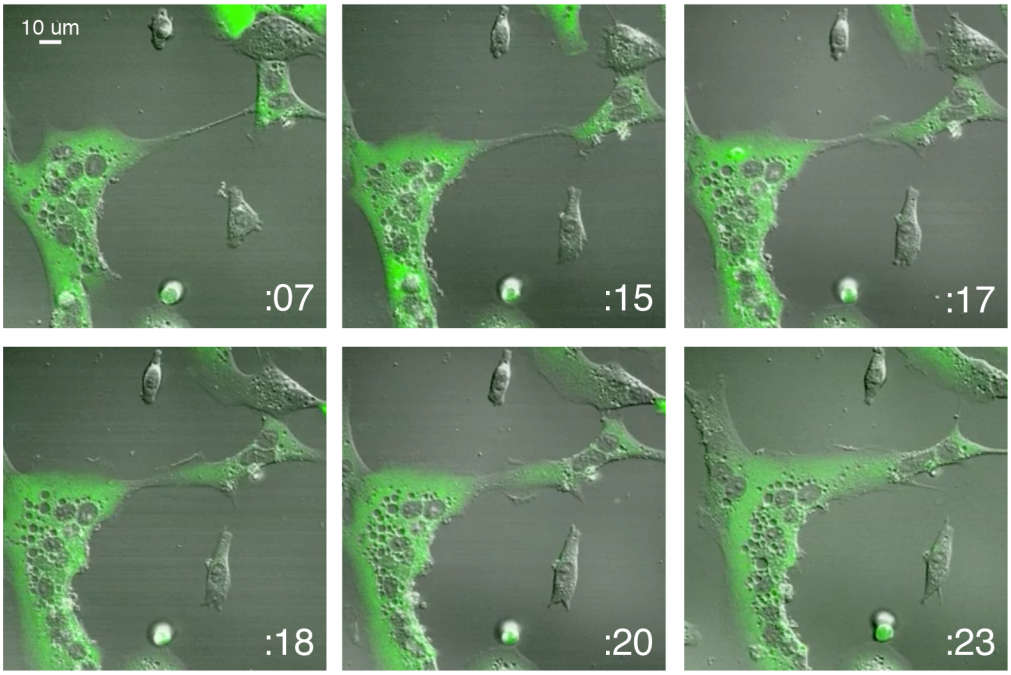

Figure 19. MHV-infected cells form long filopodia

DBT cells transfected with a GFP-expressing plasmid were infected with MHV-A59 at an MOI of 1 PFU/cell for 6 h and visualized using live cell imaging for several hours. This image is a series of stills from a video demonstrating that infected cells form long filopodia that create contacts with neighboring cells, leading to their fusion with the original infected cell. Time stamps are in minutes.

with infection frequently resulted in the internalization of large vesicles. We measured the diameters of 386 vesicles from five live imaging movies of MHV-infected cell monolayers. Vesicle diameters ranged from 0.49 μm to 4.14 μm with a mean diameter of 1.45 μm (Figure 18B). This large vesicle diameter was similar to that reported for macropinosomes in multiple systems, and much larger and more variable in size than that of endosomes generated by other forms of endocytosis (Swanson, 2008). In addition to ruffling and vesicle formation, MHV-infected cells reproducibly manifested long filopodia that extended from infected cells and contacted distant cells resulting in fusion at the point of contact and subsequent recruitment of cells into syncytia (Figure 19).

To determine the composition of these membrane ruffles, we tested for the presence of actin by staining MHV-infected, fixed cells with fluorescent phalloidin (Figure 18C-D). Because macropinocytosis has not previously been reported in CoV-infected cells, we tested whether it occurred during infection with other CoVs, specifically SARS-CoV. To control for variations in cell type, DBT cells expressing the human ACE2 receptor for SARS-CoV (DBT-hACE2) (Sheahan et al., 2008) were infected with SARS-CoV for 24 h and compared with mock-infected DBT-hACE2 cells, mock-infected DBT cells, and MHV-infected DBT cells. Cells were fixed, stained with fluorescent phalloidin, imaged, and the cells were scored for ruffling (Figure 18C). Both MHV-and SARS-CoV-infected cells demonstrated a significantly increased number of cells exhibiting membrane ruffles compared to mock-infected cells (Figure 18D). Cellular ruffling was also confirmed in MHV-infected HeLa-R and BHK-R (each expressing CEACAM1, the MHV receptor), and 17Cl1 cells (data not shown).

Infection with MHV or SARS-CoV induces bulk fluid uptake consistent with macropinocytosis

A hallmark of macropinocytosis is bulk fluid uptake from the surrounding environment. To test whether CoV-infected cells were inducing bulk fluid uptake, we used Nile Red neutral polystyrene nanoparticles with a diameter of 800 nm as markers, since their size is excluded from all endocytic pathways except macropinocytosis. MHV-infected DBT cells (Figure 20A-B) and SARS-CoV-infected DBT-hACE2 cells (Figure 20B) were incubated with nanoparticles for the last 3 h of infection. Cell monolayers infected with either MHV or SARS-CoV demonstrated a significantly higher percentage of cells with internalized nanoparticles than mock-infected cells (Figure 20B). Macropinocytosis has been described as a means of pathogen entry in several different systems. However, since our data suggested MHV-induced ruffling was occurring much later during infection, we next determined the timing of bulk fluid uptake during MHV infection. Cells were mock-infected or infected with MHV, then incubated with nanoparticles for two-hour intervals beginning at infection, and fixed immediately afterwards (Figure 20C). Significantly increased nanoparticle uptake was first detected between 4-6 h p.i. and was also prominent at 6-8 h p.i., indicating that increased fluid phase uptake initiates at 4 h or later post-entry and continues through the remainder of infection. This result was consistent with our visual and quantitative measurement of ruffling and vesicle formation. Because nanoparticle uptake occurred late during infection, we next tested whether replicating MHV was required to induce bulk fluid uptake. Cells were mock-infected, infected with MHV, or incubated with an equal concentration of UV-inactivated or heat-inactivated MHV and incubated with nanoparticles for two-hour intervals, beginning at infection

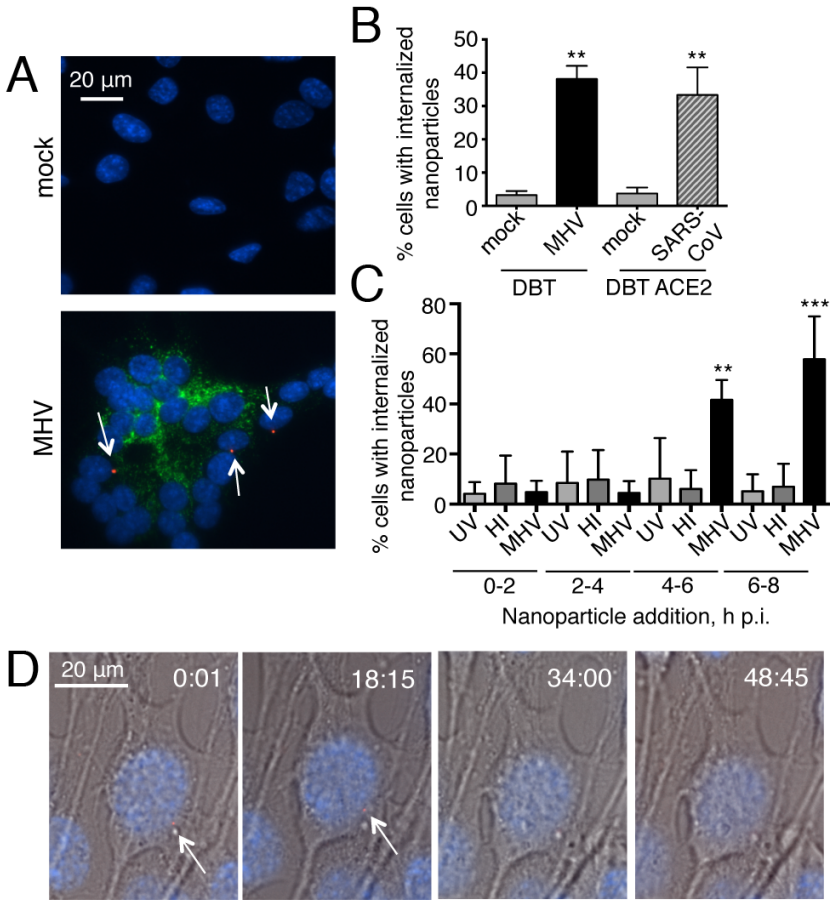

Figure 20. Infection with MHV or with SARS-CoV induces nanoparticle internalization that requires replicating virus

A-B) DBT cells were infected with MHV-A59 at an MOI of 1 PFU per cell for 8 h. DBT-hACE2 cells were infected with SARS-CoV at an MOI of 0.1 PFU/cell for 24 h. Nanoparticles were added 3 h prior to fixation, and cells washed, fixed, stained, and imaged. Arrows denote nanoparticles (red). DAPI (blue), nsp8 (green). **B)** Data is represented as the mean +/- SEM of two replicates in duplicate. n≥30 fields per replicate. **C)** Cells were mock-infected or infected with MHV, UV-inactivated MHV (UV), or heat-inactivated MHV (HI) at an MOI=1 PFU/cell (or equivalent volume for noninfectious virus) for 8 h. Nanoparticles were added in 2h increments, as designated, and cells were washed, fixed, stained and imaged. Data is represented as the mean +/- SEM of two replicates in duplicate. **D)** DBT cells on a glass- bottom dish were infected with DiI labeled MHV (white arrows) at an MOI of 25 PFU/cell, incubated at 4°C for 30 m, and imaged in the 37°C chamber incubator for 1 h. Time is in minutes:seconds. Virus fusion with the cell was observed, but membrane ruffling was absent. A representative image is shown of triplicate experiments. Significance was assessed using one-way ANOVA with Dunnett's post-hoc test. **p<0.005, ***p<0.0001.

(Figure 20C). UV-inactivated MHV did not result in increased nanoparticle uptake, suggesting that surface receptor interactions were insufficient to induce macropinocytosis. Heat-inactivated MHV also did not cause nanoparticle internalization, suggesting that the membrane ruffling phenotype observed was not a cellular response to foreign particles. In addition, in order to confirm that macropinocytosis is not utilized for entry of coronaviruses, we labeled virions with DiI and added them to DBT cells grown on a glass-bottom dish at a high MOI of 25 PFU/cell (Figure 20D). Virions were adsorbed for 30 minutes at 4°C to synchronize the infection before transferring them to the 37°C chamber incubator surrounding the microscope. Cells were then live-imaged for 1 hour. While we did visualize viruses entering cells at the plasma membrane, we did not observe any evidence of cellular membrane ruffling at the site of entry or elsewhere on the cell. Thus, virus infection is required for induction of bulk fluid uptake, and MHV-induced macropinocytosis is not associated with virus entry.

MHV-induced macropinocytosis is dependent on the classical macropinocytosis pathway

We next determined whether MHV-induced macropinocytosis required known mediators of cellular macropinocytosis. We selected Rac1, Cdc42, and Pak1 from the classical macropinocytosis pathway for siRNA inhibition. Inhibition of RhoA was chosen as a negative control, since it is not associated with macropinocytosis. For each siRNA molecule, target knockdown ≥80% was confirmed by immunoblot (Figure 21A, B). Transfection efficiency was tested with siRNA-AllSTARS-GFP and found to be >96% (data not shown). Inhibition of Pak1, Cdc42, and Rac1 resulted in significantly decreased

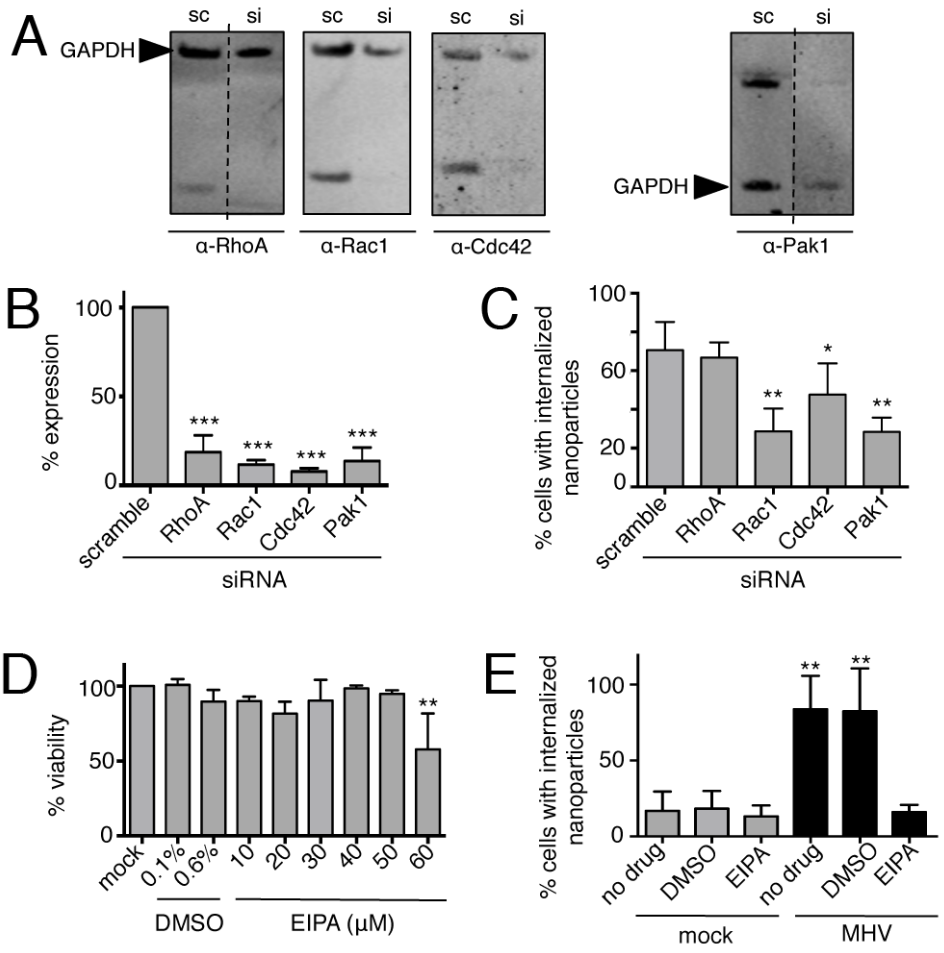

Figure 21. Nanoparticle uptake during MHV infection is dependent on classical macropinocytosis pathway members

A-B) Cells were reverse transfected with siRNA for 72 h and protein knockdown was confirmed by immunoblot (**A**) and standardized to GAPDH (**B**). Scramble (sc) and siRNA (si)-treated samples are from the same gel for each protein. RhoA and Pak1 are from discontinuous lanes denoted by dashed lines. Data are represented as the means +/- SEM in triplicate. **C)** Cells were reverse transfected for 68 h and infected with MHV for 8 h. Nanoparticles were added during the final 3 h, cells were washed, fixed, stained, and imaged. Data are represented by averages +/- SEM of two replicates in duplicate, n≥30 fields per replicate. **D)** 12 h toxicity was assessed for EIPA with CellTiter Glo. **E)** Cells were mock-infected or infected with MHV at an MOI of 1 PFU/cell for 8 h with no drug, DMSO, or 40 μM EIPA. Nanoparticles were added during the final 3 h of infection. Cells were washed, fixed, stained, and imaged, and the percentage of cells with internalized nanoparticles was calculated. Data are represented as averages +/- SEM of two replicates in duplicate. Significance was assessed using one-way ANOVA with Dunnett's post-hoc test. *p<0.05, **p<0.01, ***p<0.0001.

nanoparticle internalization following MHV infection, while nanoparticle uptake was unchanged in cells transfected with a scrambled siRNA or with siRNA targeting RhoA (Figure 21C). These results demonstrate that MHV-induced macropinocytosis signals through a known cellular macropinocytosis pathway.

EIPA is an inhibitor of sodium-hydrogen exchangers (NHE) and is the most specific known chemical inhibitor of macropinocytosis. Other endocytic pathways do not use NHE and are not impacted by treatment (West et al., 1989). We compared nanoparticle internalization in MHV-infected and uninfected cells treated with nontoxic doses of EIPA (Figure 21D) or with DMSO, the vehicle control. EIPA-treated, infected cells internalized significantly fewer nanoparticles than DMSO-treated, infected cells (Figure 21E). Thus, all data collected to this point are consistent with the hypothesis that MHV is inducing macropinocytosis during infection: membrane ruffling, bulk fluid uptake, dependence on classical pathway members, and sensitivity to EIPA.

Inhibition of macropinocytosis impairs MHV replication

We next tested the requirement for macropinocytosis during MHV replication (Figure 22). We utilized siRNA knockdown of Pak1, treatment with *C. difficile* toxin A (CdtA), or treatment with EIPA and determined the effect on viral replication. CdtA decreases ADP-ribosylation of Rho family proteins, including Rac1, RhoA, and Cdc42, and thus we used this as an independent mechanism to confirm the relationship between macropinocytosis and viral replication (Just et al., 1995). Inhibition of Pak1 with siRNA

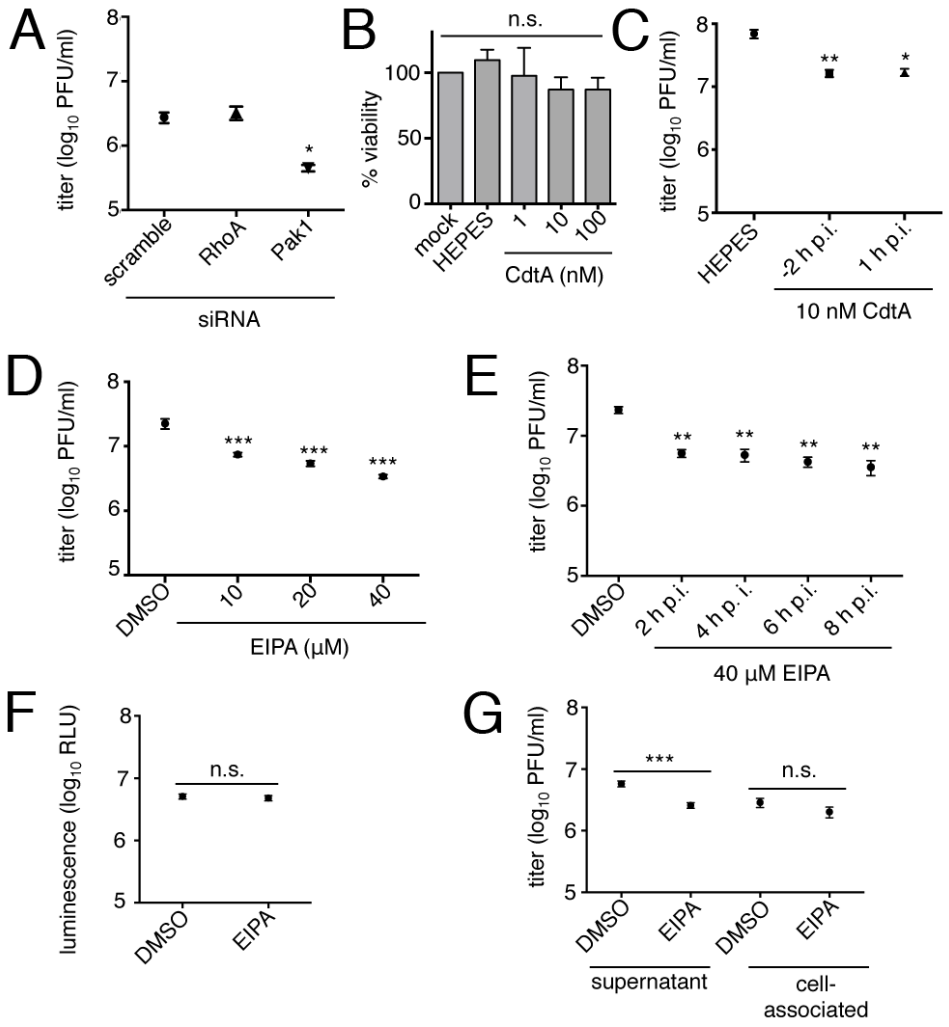

Figure 22. Inhibition of macropinocytosis impairs MHV replication

A) Cells were reverse transfected for 68 h and infected with MHV for 12 h. Supernatant samples were titered via plaque assay. Data are represented by averages +/- SEM of two replicates in duplicate. **B)** 12 h toxicity was assessed for *C. difficile* toxin A (TcdA) with CellTiter Glo. **C)** Cells were treated with HEPES buffer, or 10 nM TcdA for 2 hours prior to infection with MHV-A59 at an MOI of 1 PFU/cell. Viral titer was measured at 10 h p.i. Data are represented by averages +/- SEM of an experiment in triplicate. **D-E)** Cells were infected with an MOI of 1 PFU/cell with MHV. 0.4% DMSO, or 10, 20, or 40 μM EIPA were added times indicated post infection. Viral titer was measured at 12 h p.i. EIPA was added at 6 h p.i. **(D)** or at a concentration of 40 μM EIPA **(E)**. Data are represented as mean +/- SEM of two replicates in duplicate. **F-G)** Cells were infected with MHV-FFL2 at an MOI of 1 PFU/cell. 0.4% DMSO or 40 μM EIPA was added at 8 h p.i. Supernatant was collected at 10 h p.i. and titered. Cells were collected in luciferase lysis buffer and assessed for luminescence **(F)**, or in DMEM and subject to three rounds of freeze-thaw before being titered **(G).** Data are represented as averages +/- SEM of two replicates in duplicate. Significance was assessed using one-way ANOVA with Dunnett's post-hoc test. *$p<0.05$, **$p<0.005$, ***$p<0.0005$.

prior to infection caused a ≥ 80% decrease in MHV titer at 12 h p.i., while use of scramble siRNA or an siRNA against RhoA did not have a significant effect on titer (Figure 22A). Treatment with CdtA also caused a significant decrease in MHV titer at 10 h p.i. (Figure 22B-C). EIPA was added to MHV-infected cell monolayers at different concentrations and times post-infection (Figure 22D-E). EIPA treatment resulted in a ≥ 75% decrease in virus titer when added anytime after 2 h p.i. To test the effect of EIPA on different stages in the virus life cycle, we infected cells with MHV expressing firefly luciferase as a fusion with the replicase protein nsp2 (Freeman et al., 2014) and measured FFL activity in the presence or absence of EIPA added at 8 h p.i. (Figure 22F). In replicate experiments, supernatant was collected at 10 h p.i. and cell-associated virus was collected by freezing and thawing infected cells three times. Titer was assessed in each sample by plaque assay (Figure 22G). Intracellular FFL-nsp2 expression from the viral genome was not altered by EIPA treatment. In addition, viral titer was significantly decreased in the supernatant of cells treated with EIPA, while intracellular virus titer was not affected by addition of EIPA. Together, these results indicate that EIPA does not effect intracellular virus replication, assembly, or maturation, but alters the overall peak of infectious virus in the supernatant, consistent with an effect on late stages of virus release or cell-cell spread.

The presence of fusogenic spike protein at the plasma membrane is required to induce macropinocytosis

Having determined that MHV-induced macropinocytosis requires active virus replication and occurs at a late stage in the virus life cycle, we investigated the role of the spike

protein in CoV-induced macropinocytosis, using MHV-A59 and recombinant MHV-2S. In MHV-A59, spike is cleaved by furin in the trans-Golgi network during virion maturation (de Haan et al., 2004), resulting in fusogenic spike on nascent virions and on the plasma membrane of infected cells. Interaction of the MHV-A59 spike with cellular receptor results in either virus-cell fusion and cell entry or cell-cell fusion and syncytia formation (de Haan et al., 2004). In contrast, the spike protein of another strain, MHV-2, is not cleaved by furin during exit of nascent virions, but rather is cleaved by cathepsins following endocytosis during entry (Qiu et al., 2006). Thus, released infectious MHV-2 does not have fusogenic spike, and cells infected with MHV-2 do not express fusogenic spike on the cell surface or generate syncytia in culture.

To test for the role of spike and spike fusogenic activity in MHV-induced macropinocytosis, we mock-infected or infected cells with MHV-A59 or with recombinant MHV-A59 encoding MHV-2 spike (MHV-2S) (Navas et al., 2001) and tested nanoparticle internalization (Figure 23). MHV-2S-infected cells internalized significantly fewer nanoparticles than MHV-A59-infected cells (Figure 24A). To test the specific requirement for spike cleavage, we infected cells with an MHV-A59 mutant C12 (MHV-C12) containing an amino acid mutation (H716D) that abolishes the furin cleavage site (Hingley et al., 1994). During infection with MHV-C12 there was no significant difference in nanoparticle internalization compared to mock-infected cells (Figure 24A). We next used a furin inhibitor, peptidyl chloromethylketone (dec-RVKR-cmk) (de Haan et al., 2004) to block furin cleavage of the MHV-A59 spike (Figure 24B). Treatment with dec-RVKR-cmk decreased both nanoparticle uptake and syncytia

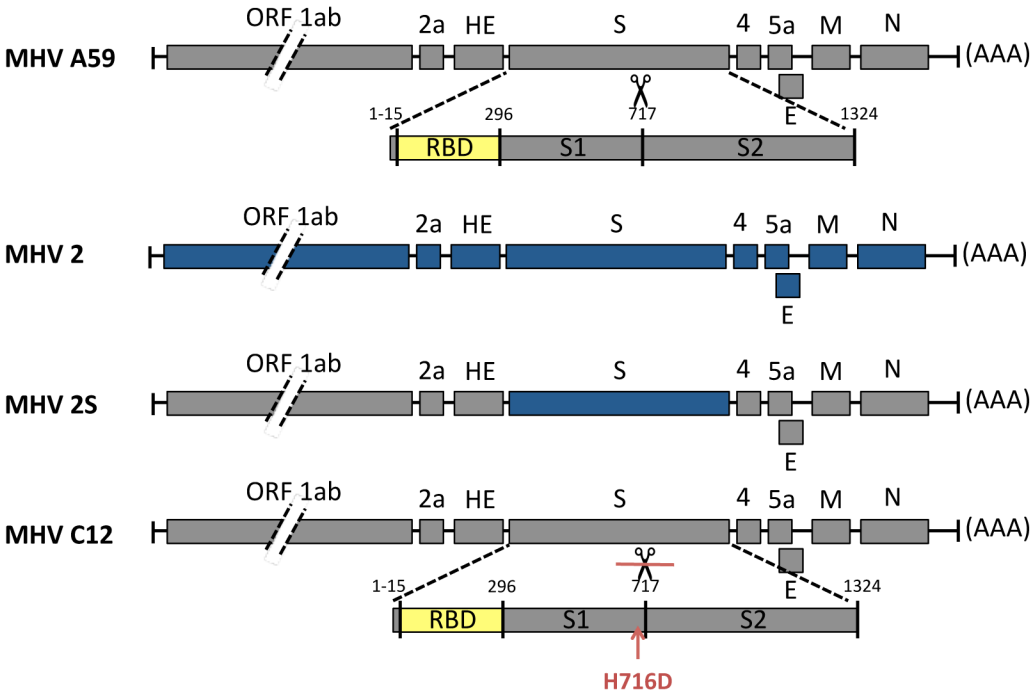

Figure 23. Panel of spike viruses

A schematic representation of the viruses used in this work with changes in the spike protein. MHV-A59 is considered "WT" in this work. MHV-2 is a different strain of MHV. MHV-2S contains only the spike protein of MHV-2 in an isogenic MHV-A59 background. MHV-C12 contains a one amino acid mutation in the furin cleavage sequence of MHV-A59, H716D.

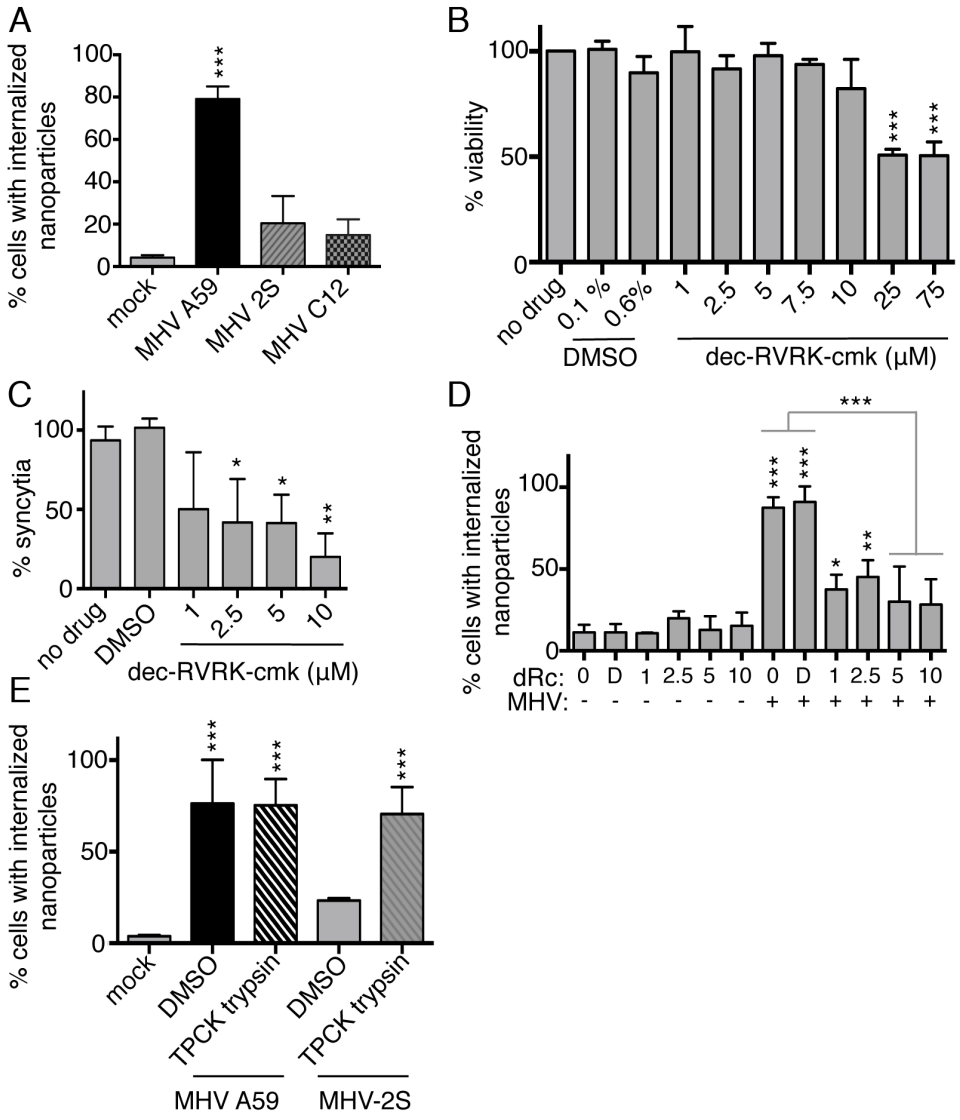

Figure 24. Fusogenically active spike protein is required to induce macropinocytosis

A) Cells were mock-infected or infected with MHV-A59, MHV-2S, or MHV-C12 at an MOI of 1 PFU/cell. Nanoparticles were added at 5 h p.i. for 3 h and cells were washed, fixed, stained, and imaged. **B-D)** DBT cells were mock-infected or infected with MHV-A59 at an MOI of 1 PFU/cell in DMEM or DMEM with DMSO or dec-RVKR-cmk (dRc) at infection for 8 h. dec-RVKR-cmk was added to cells for 12 h and toxicity assessed with CellTiter Glo **(B)**. Nanoparticles were added 3 h prior to fixation, cells washed, fixed, stained, and imaged. % syncytial cells **(C)** and % cells with internalized nanoparticles **(D)** were measured. **E)** Cells were mock-infected or infected with MHV-A59, MHV-2S at an MOI of 1 PFU/cell. At 5 h p.i., cells were treated with TPCK trypsin for 5 m, washed, then nanoparticles were added for 3 h. Cells were washed, fixed, stained, and imaged. Data are represented as mean +/- SEM from two replicates in duplicate. n≥30 cells per replicate. Significance was assessed using one-way ANOVA with Dunnett's post-hoc test, ***$p<0.0001$, **$p<0.01$, *$p<0.05$.

formation in a concentration-dependent manner (Figure 24C-D). To test whether spike cleavage alone was sufficient to induce macropinocytosis, we treated cells infected with MHV-2S with TPCK-trypsin in order to generate fusogenic spike protein on the cell surface, and assessed nanoparticle uptake. Cells infected with MHV-2S and treated with trypsin recovered the capacity for nanoparticle internalization (Figure 24E). Together, these results demonstrate that expression of fusion-competent spike protein at the plasma membrane is necessary for MHV macropinocytosis induction.

MHV-induced macropinocytosis is associated with, but independent from, syncytia formation

The necessity for cleaved spike in macropinocytosis induction could be explained by either a requirement for spike mediated cell-cell fusion, or by a direct role for spike in macropinocytosis induction. To distinguish between these possibilities, we used two approaches: induction of syncytia by different methods and blockade of syncytia formation with anti-receptor antibodies. To test the cell-fusion hypothesis, cells were chemically treated with PEG-1500 or transfected with the G protein of Vesicular Stomatitis Virus (VSV) (Figure 25A) to induce cell-cell fusion, then incubated with nanoparticles. While MHV induces syncytia of ≥ 30 nuclei, both PEG-1500 treatment and VSV-G expression resulted in small syncytia with fewer than 10 nuclei. Nanoparticle uptake was compared between syncytia with 10 nuclei or less from MHV-infected cells, PEG-1500 treated cells and VSV-G transfected cells. PEG-1500 treatment resulted in nanoparticle uptake greater than mock-infected cells but significantly less than during

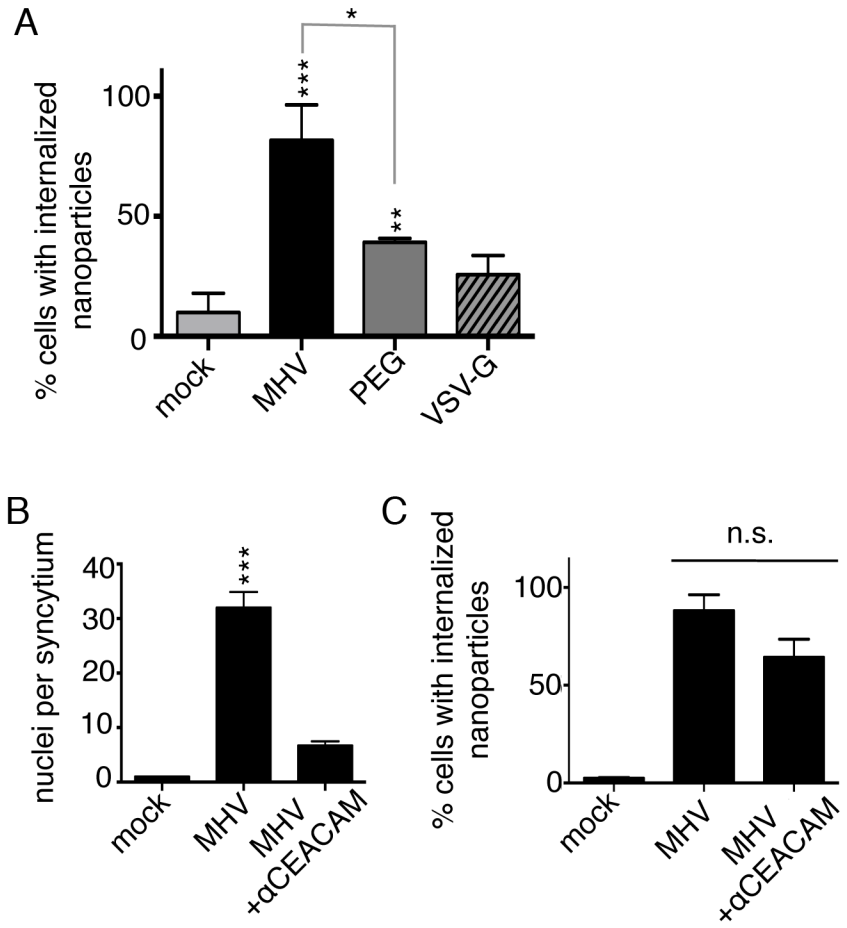

Figure 25. MHV-induced macropinocytosis is associated with, but independent from, syncytia formation

A) DBT cells were mock-infected or infected with MHV-A59 at an MOI of 1 PFU/cell for 8 h, treated with PEG for 1 m, washed and incubated for 3 h, or transfected with VSV-G for 24 h. Nanoparticles were added 3 h prior to fixation, cells washed, fixed, stained, and imaged. Syncytia with ≤10 nuclei were analyzed. Data are represented as mean +/- SEM from two replicates, each in duplicate, n≥30 cells per replicate. **B-C)** Cells were mock-infected or infected with MHV at an MOI of 1 PFU/cell. α-CEACAM blocking antibodies were added at 2 h p.i., nanoparticles were added at 5 h p.i., and at 8 h p.i., cells were washed, fixed, stained and imaged. Nuclei per syncytium **(B)** and % cells with internalized nanoparticles **(C)** were measured. Significance was assessed using one-way ANOVA with Dunnett's post-hoc test. ***$p<0.0001$, **$p<0.01$, *$p<0.05$.

MHV infection. Expression of VSV-G did not result in increased nanoparticle uptake compared mock-infected cells. We next blocked the interactions of MHV-A59 spike with its cellular receptor, carcinoembryonic antigen (CEACAM), by adding α-CEACAM blocking antibodies at 2 h p.i., and measured the effect on syncytia size and nanoparticle uptake (Figure 25B). The α-CEACAM antibodies resulted in a significant reduction in syncytia cell number and size, but did not significantly decrease nanoparticle uptake by infected cells (Figure 25C). Together these results demonstrate that cleaved spike protein at the cell surface, and not cell fusion alone, is required to initiate and to sustain macropinocytosis.

Coronavirus-induced macropinocytosis is dependent on activation of epidermal growth factor receptor (EGFR)

Signaling through EGFR is essential for induction of macropinocytosis in several systems (Haigler et al., 1979; Mercer et al., 2010; Sanchez et al., 2012). To test whether EGFR activation is required for CoV-induced macropinocytosis, we utilized gefitinib, which specifically inhibits EGFR autophosphorylation and prevents EGFR activation (Moasser et al., 2001). DBT cells were mock-infected or infected with MHV-A59, gefitinib was added after viral entry at 1.5 h p.i., and cells were analyzed for nanoparticle uptake and syncytia size (Figure 26A-C). Addition of gefitinib to MHV-infected cells significantly decreased the percentage of syncytia with internalized nanoparticles (Figure 26B). We also observed that gefitinib significantly decreased the number of nuclei in a syncytium, with only half as many nuclei as in a DMSO-treated syncytium (Figure 26C). We then

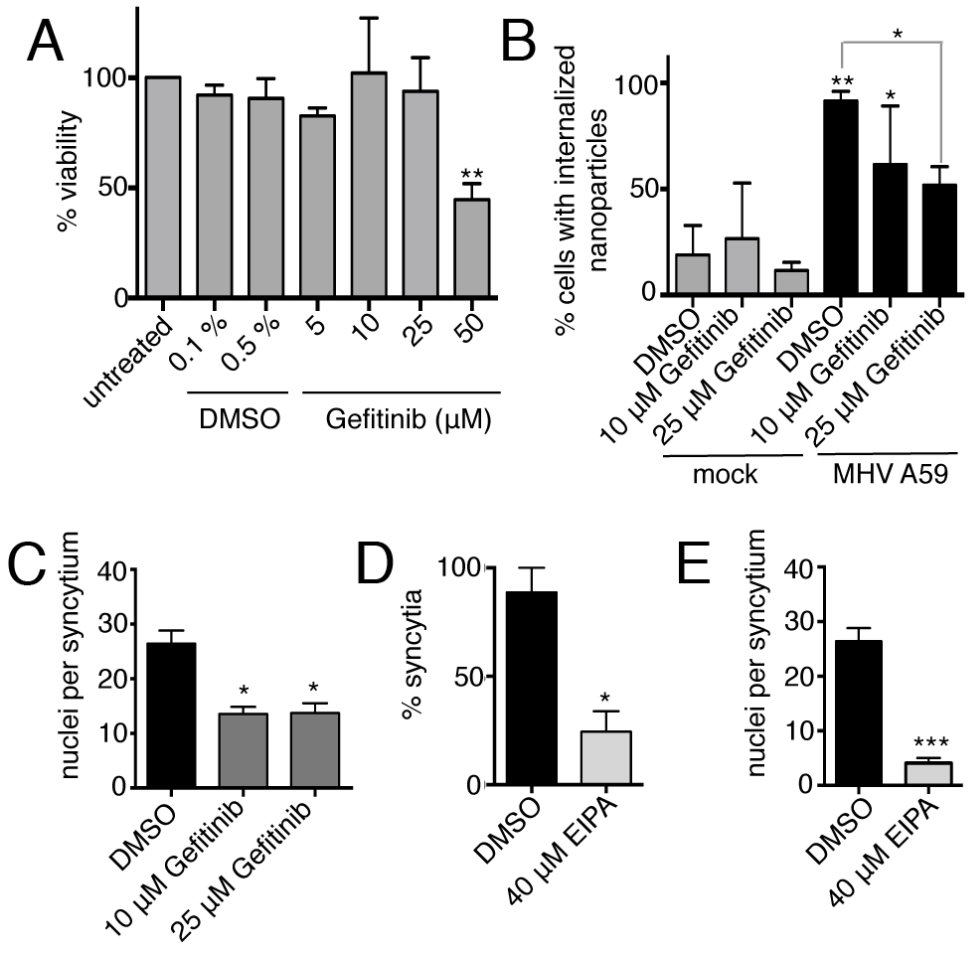

Figure 26. CoVs induce macropinocytosis via EGFR

A) Gefitinib was added to cells for 12 h and toxicity assessed with CellTiter Glo. **B-C)** DBT cells were mock-infected or infected with MHV-A59 at an MOI of 1 PFU/cell in DMEM or DMEM supplemented with DMSO or gefitinib at 1.5 h p.i. Cells were fixed at 8 h p.i. Nanoparticles were added 3 h prior to fixation, cells washed, fixed, stained, and imaged. % cells with internalized nanoparticles **(B)** and # nuclei per syncytium **(C)** were measured. **D-E)** DBT cells were mock-infected or infected with MHV-A59 at an MOI of 1 PFU/cell in DMEM or DMEM supplemented with DMSO or EIPA at 1.5 h p.i. Cells were fixed at 8 h p.i., stained, and imaged. % infected cells involved in syncytia **D)** and # nuclei per syncytium **(E)** were measured. Data are means +/- SD in triplicate, n≥30 fields per replicate. Statistical significance was assessed using one-way ANOVA with Dunnett's post-hoc test. ***$p<0.0001$, **$p<0.01$, *$p<0.05$.

evaluated the effect of EIPA on syncytia size, and discovered that treatment with EIPA decreased both the percentage of infected cells involved in syncytia (Figure 26D) and the size of the syncytia (Figure 26E). These data suggest that CoVs are utilizing EGFR activation to induce macropinocytosis and to initiate cell-cell spread.

Discussion

In this study, we demonstrate that MHV infection induces macropinocytosis, as defined by characteristic membrane ruffling, internalization of large pleomorphic vesicles, increased fluid phase uptake, dependence on Rac1, Cdc42, and Pak1, and sensitivity to EIPA. MHV-induced macropinocytosis requires cell-surface expression of cleaved, fusogenic spike and spike-mediated induction of macropinocytosis is dependent on direct or indirect interactions of spike with EGFR. We have summarized these data in the model shown in Figure 27.

CoVs have been shown previously to modify cytoplasmic membranes to form viral replication complexes (Angelini et al., 2013). Here, we report that CoVs also have the capacity to modify the plasma membrane through the activation of the macropinocytosis pathway. Prior to this study the only role demonstrated for virus-induced macropinocytosis has been in virus entry. MHV-associated macropinocytosis, in contrast, is initiated relatively late during infection and is continuous once activated. MHV-2S does not stimulate cell-cell fusion or macropinocytosis in infected cells, but still causes disease *in vivo*, suggesting that macropinocytosis may not be required for fitness or pathogenesis of all strains of MHV or for all coronaviruses. The disease phenotypes for

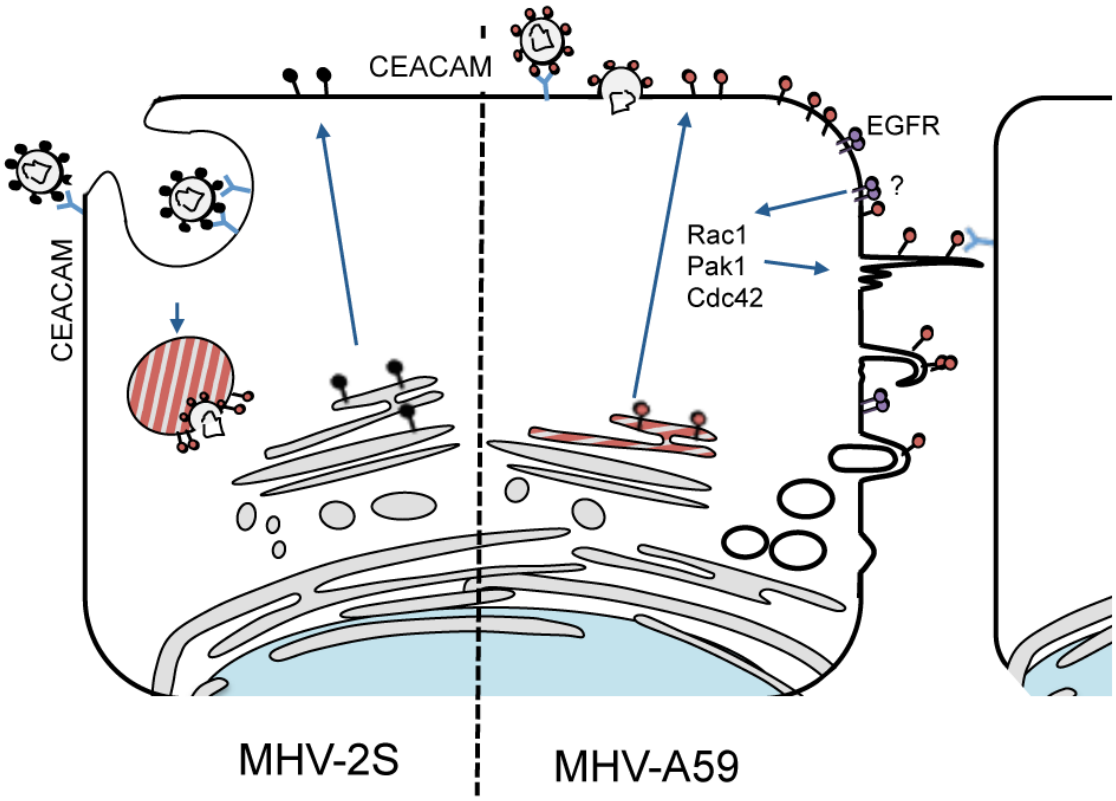

Figure 27. Model of macropinocytosis during CoV infection

MHV-2S enters the cell via endocytosis after the spike protein interacts with the CEACAM receptor. Spike is cleaved to its fusogenic form by cathepsins after entry via endocytosis and the virus fuses with the endosomal membrane to release the genome to the cytoplasm. Replication occurs and virions are assembled in the ERGIC, then packaged and released via exocytosis. Spike protein that reaches the surface of the cell is uncleaved (black ball and stick) and cannot mediate syncytia formation with neighboring cells. MHV-A59 enters the cell via fusion at the cell membrane after spike interacts with the CEACAM receptor. The genome immediately enters the cytoplasm and replication occurs. Packaging of nascent virions occurs in the ERGIC, and free spike proteins and spike incorporated into virions is cleaved by furin in the trans Golgi. Virions are packaged and released via exocytosis. Spike protein that reaches the cell surface is cleaved and fusogenically active (red ball and stick), and can mediate fusion events with neighboring cells. This cleaved, activated spike protein can also mediate interactions, potentially through EGFR (purple ball and stick), that induce the macropinocytosis pathway within the cell, which relies on Rac1, Cdc42, and Pak1. Actin modifications at the cell surface then cause membrane ruffling and macropinosome internalization, in addition to filopodia that can facilitate spike-receptor interactions with neighboring cells. The location of spike cleavage is denoted by the red-striped regions.

MHV-A59 and MHV-2S differ, as infection with MHV-A59, but not MHV-2S, causes spinal cord demyelination (Das Sarma et al., 2000), suggesting that macropinocytosis driven cell-cell spread could be a tissue-specific strategy. The conservation of macropinocytosis during MHV and SARS-CoV infection, however, suggests that macropinocytosis induction could be an important determinant of pathogenesis for viruses capable of maintaining cleaved spike protein on the surface of infected cells.

Our results demonstrate two consistent and dramatic phenotypes associated with MHV-induced macropinocytosis: ruffling with vesicle internalization, and filopodia associated with cell fusion and recruitment into syncytia. The fact that inhibition of MHV-induced macropinocytosis impairs overall virus titer while not affecting entry or intracellular infectious virus, suggests the possibility of multiple functions that favor overall virus fitness: specifically recruitment of membranes and nutrients into infected cells and syncytia, enhancement of virus release, or virus cell-cell spread. MHV-A59 acquires its viral envelope by budding through the ERGIC, and is released from the cell without lysis via the exocytic pathway. No previous role for a traditionally endocytic pathway such as macropinocytosis has been reported to be used during viral release (Tooze et al., 1984; Tooze et al., 1987). The observed increase in formation of long filopodia from infected cells that contact and recruit uninfected cells into syncytia suggests a role for macropinocytosis as a mechanism by which CoVs potentiate cell communication over significant distances. Filopodia could act as mediators of CoV cell-cell fusion by concentrating spike protein and virus at the filopodia tip. Actin modifications have been previously implicated in cell-cell spread for other viruses. Vaccinia virus utilizes actin

tails to infect distant cells at a rate faster than infecting adjacent cells (Cudmore et al., 1995; Doceul et al., 2010). HIV and HTLV use filopodia to create virological synapses to transfer infectious material from one cell to another (Igakura et al., 2003; McDonald et al., 2003). Macropinocytosis can occur in polarized cells (Mettlen et al., 2006), and could represent a novel mechanism of virus cell-cell spread over tight junctions within airway epithelium. Viral spread in this manner has several advantages over viral spread via exocytosis, specifically immune evasion, concentration of reagents, speed, and the capacity to circumvent physical barriers. Increasing the extent and duration of plasma membrane extensions could increase opportunities for interactions with adjacent or distant cells.

Our results also show that expression of cleaved, fusogenic spike on the cell surface is necessary to induce macropinocytosis, whether by furin-mediated cleavage in the cell or by exogenous cleavage by trypsin on the cell surface. Induction of macropinocytosis also requires EGFR activation and signaling through the known macropinocytosis cellular pathway. Based on our results, we propose a model in which fusogenic spike protein on the plasma membrane results in EGFR activation, leading to a signaling cascade that manifests as increased membrane ruffling and filopodia formation to facilitate cell-cell fusion and virus spread. Spike-EGFR interactions could occur at several cellular locations and be either direct or indirect. Spike protein localized at the plasma membrane could directly interact with neighboring EGFR. EGFR is also a highly trafficked receptor, which translocates to the mitochondria after activation (Demory et al., 2009), then promptly back to the plasma membrane, providing opportunities for interactions between

spike and EGFR within the cell. Proteins from other viruses have been previously shown to activate tyrosine kinase receptors in a ligand-independent fashion through transmembrane domain interactions, such as E5 of bovine papillomaviruses (DiMaio and Petti, 2013), or through the production of a cellular ligand, as in human papillomavirus 16 (DiMaio and Petti, 2013).

Our results raise many important questions for future studies. What is the relationship of GTPase and EGFR activation to specific stages in the viral life cycle? Does the virus receptor play a role in facilitating activation of EGFR and induction of macropinocytosis? How does the capacity to induce macropinocytosis favor fitness of MHV-A59? The results of our studies define novel roles for coronavirus spike protein and for macropinocytosis during coronavirus infection and raise the possibility that other RNA viruses may usurp macropinocytosis machinery for purposes other than virus entry.

Chapter IV: MERS-CoV ANTIBODIES

Introduction

In June 2012, MERS-CoV was isolated from a man with acute pneumonia and renal failure in Saudi Arabia (Zaki et al., 2012). The number of cases has increased to 827 with 287 deaths by July 2014, with a majority of the case burden in the Arabian Peninsula. Evidence of MERS-CoV has been detected in Nycteris, Pipistrellus, and Taphozous bats (Annan et al., 2013) (Memish et al., 2013) as well as in dromedary camels. Person-person transmission has also been confirmed, though at this time it is less communicable than SARS-CoV (Reusken et al., 2013) (Meyer et al., 2014). Serological evidence suggests that MERS-CoV has been circulating in camels since at least 1992 (Alagaili et al., 2014). Presently, vaccines and specific antiviral pharmaceuticals are unavailable, so understanding the molecular mechanisms is incredibly important.

All positive sense RNA viruses replicate on modified host cytoplasmic membranes. All Beta-CoVs investigated form two types of ER membrane modifications: double membrane vesicles and convoluted membranes (Knoops et al., 2008). Replication complexes are formed on these membranous structures. Coronaviruses contain large RNA genomes that range form 26-32kb and two-thirds of the genome encodes the replicase gene (Orf1a/b), which is translated into a large polyprotein that is cleaved into up to 16 nonstructural proteins (nsps 1-16) that are associated with viral replication (Perlman and Netland, 2009). The remainder of the genome encodes the structural proteins, spike, membrane, nucleocapsid, and envelope, as well as accessory proteins. All

replicase proteins investigated colocalize at the replication complexes, which are associated with the membrane modifications (Bost et al., 2000; Brockway et al., 2003; Gosert et al., 2002; Knoops et al., 2008; Snijder et al., 2006; van der Meer et al., 1999). Replication complexes appear to exclude most cellular marker but partially colocalize with ER proteins, PDI and sec61α (Knoops et al., 2010). The structural proteins localize to the ER-Golgi intermediate complex (ERGIC), which is the site of viral assembly (Sims et al., 2000).

A great deal of progress has been made while studying this new pathogen since its emergence, but its intracellular replication strategies have not been investigated. It is unknown if nsps accumulate to form replication complexes, as in other coronaviruses, or if these complexes are morphologically and temporally similar to other coronaviruses. This chapter describes a collaborative study by our lab contributing to new knowledge of the newly emergent pathogen, MERS-CoV. Our lab has developed antibodies that specifically recognize MERS-CoV replication proteins. Clint Smith and Xiaotao Lu were responsible for protein design, purification, and initial testing of epitope recognition via dot blot, and I describe these portions of the project only briefly. I was responsible for clearing the antibodies on cells and initial testing of their function for immunofluorescence studies, including specificity testing, time course evaluation, and colocalization with other viral antibodies. Also included is some work done in collaboration with Barney Graham's lab at the NIH testing antibodies directed against the MERS-CoV spike protein. Dia Beachboard completed the studies describing localization

of MERS-CoV antibodies with cellular markers. Clint Smith and Michelle Becker completed BSL3 work.

This work demonstrates that these antibodies are specific and robust. It also shows that viral proteins are expressed long before cellular cytopathic effects are present. Viral proteins partially colocalize with PDI, the ER marker and colocalize with other replicase proteins. Spike protein colocalized with actin and WGA, a marker of the Golgi complex and did not colocalize with the replicase proteins. Because this pathogen is newly emerging, has many unknowns, and is very deadly, it is important to better understand its replication strategies such that they might be effectively targeted for therapeutic intervention.

Purified antibodies specifically recognize MERS-infected cells

Regions of MERS-CoV corresponding to replicase proteins nsp1, nsp8, nsp9, and nsp10 were cloned into a SUMO expression vector, expressed in *E. coli* and purified (Figure 28). Nsp5 protein was a gift from Andrew Messecar's lab at Purdue University. Each purified protein was sent to Cocalico Inc., injected into rabbits or guinea pigs, and several bleeds were collected and tested for protein recognition via dot blot (data not shown). Antibodies were then cleared on DBT cells to eliminate non-specific binding.

To test whether purified antibodies specifically recognized epitopes in MERS-CoV-infected cells via immunofluorescence assays, WHO-Vero cells on glass coverslips were infected with MERS-CoV at an MOI of 1 PFU/cell for 24 hours, fixed in MeOH,

immunostained utilizing the new MERS-CoV antibodies, and examined by wide field microscopy (Figure 29). To control for specific expression, the preimmune serum of each

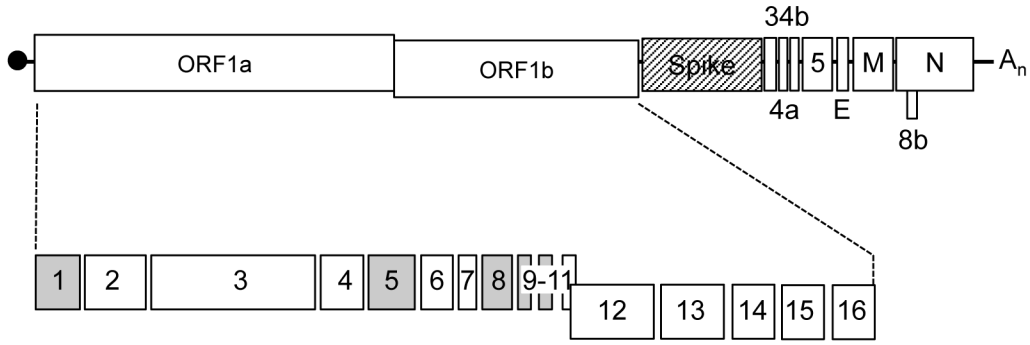

Figure 28. Design of antibodies specific for MERS-CoV nsps

Schematic of MERS-CoV genome is shown. The first 2/3 of the genome encodes the replicase gene that is translated to a polyprotein that is cleaved into 16 nsps (nsp 1-16). The last 1/3 encodes structural and accessory proteins. Full-length proteins were cloned into pSUMO vectors for protein expression of nsp1, 8, 9, and 10 (grey boxes). MERS-CoV nsp5 was a gift from Andrew Messecar's lab (Purdue University). Antibodies against the spike protein (striped box) were a gift from Barney Graham's lab (NIH).

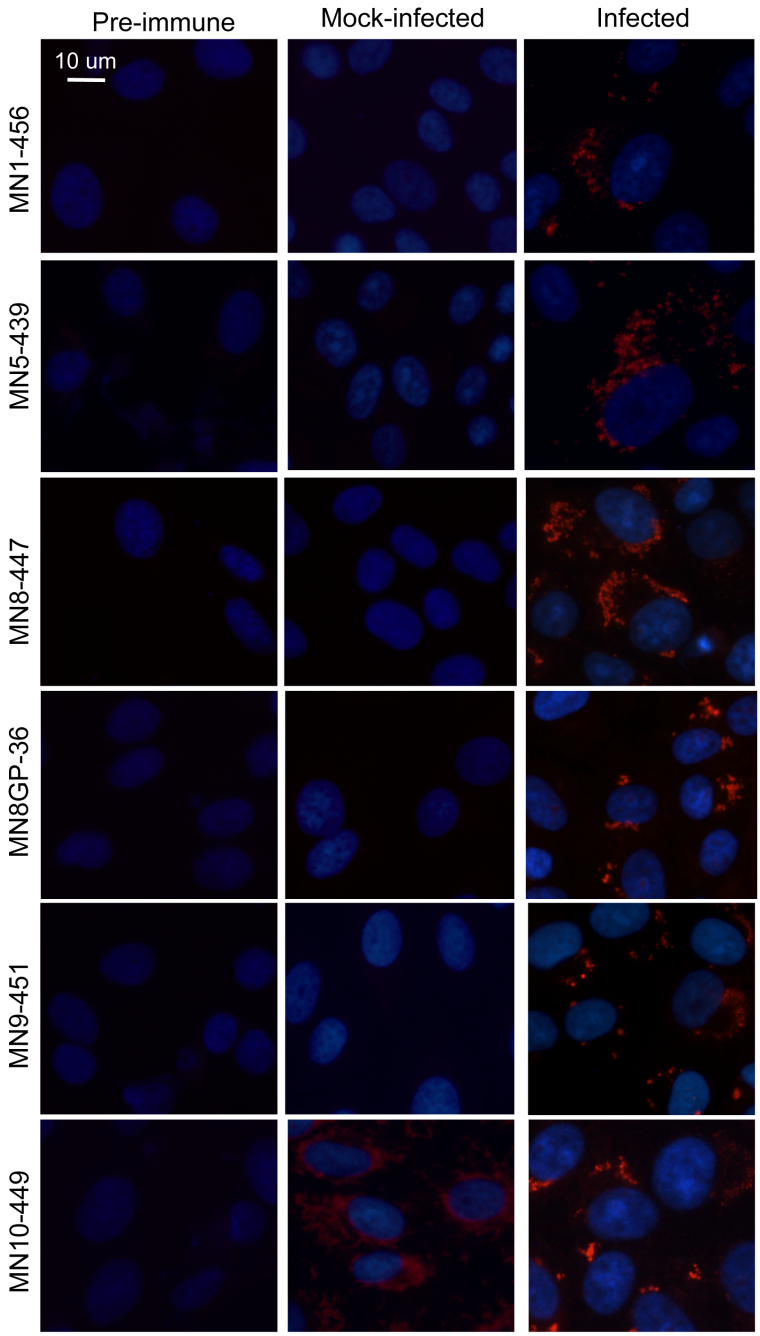

Figure 29. Antibodies directed against MERS-CoV nsps are specific for MERS-CoV infected cells

WHO-Vero cells were mock-infected or infected with MERS-CoV at an MOI of 1 PFU/cell. At 24 h p.i., cells were fixed in MeOH, stained with antibodies or pre-immune serum as indicated (α-nsp1, α-nsp5, α-nsp8, α-nsp9, α-nsp10) and secondary antibodies labeled with Alexa 546 and imaged by wide field microscopy. Nuclei are stained by DAPI. All images are at the same magnification.

antibody was also applied to infected cells, and the antibodies were tested against mock-infected WHO-Veros. We also confirmed specific expression by testing our primary antibodies alone and our secondary antibodies alone (data not shown), and as expected, no fluorescence was detected.

WHO-Vero cells infected with MERS-CoV and stained with antibodies directed toward nsp1, nsp5, nsp8, nsp9, and nsp10 demonstrated a punctate cytoplasmic pattern of localization that often formed a semicircular ring near the nucleus (Figure 29). Each of the antibodies, except for the antibody directed to nsp10, demonstrated very low background signal in contrast to the bright signal visualized in infected cells. None of the antibodies had signal present in the preimmune serum-stained samples. I used wide field microscopy for these experiments such that the background in the entire field could be discerned, instead of only the background within a z-slice. I used confocal imaging for all other images in this chapter. Because of the high background of the nsp 10 antibody, I did not evaluate it in additional studies.

MERS-CoV replication proteins are evident as early as 6 hours post infection

To test how early MERS-CoV replicase proteins could be recognized and visualized in infected cells, samples were prepared as before, but fixed at 6, 12, and 24 hours post infection (Figure 30). Specific signal was not expected at earlier times post infection, as MERS-CoV creates a very subtle CPE in our hands 1-2 days post infection. Surprisingly, robust signal for each antibody tested was visualized as early as 6 h p.i., although there

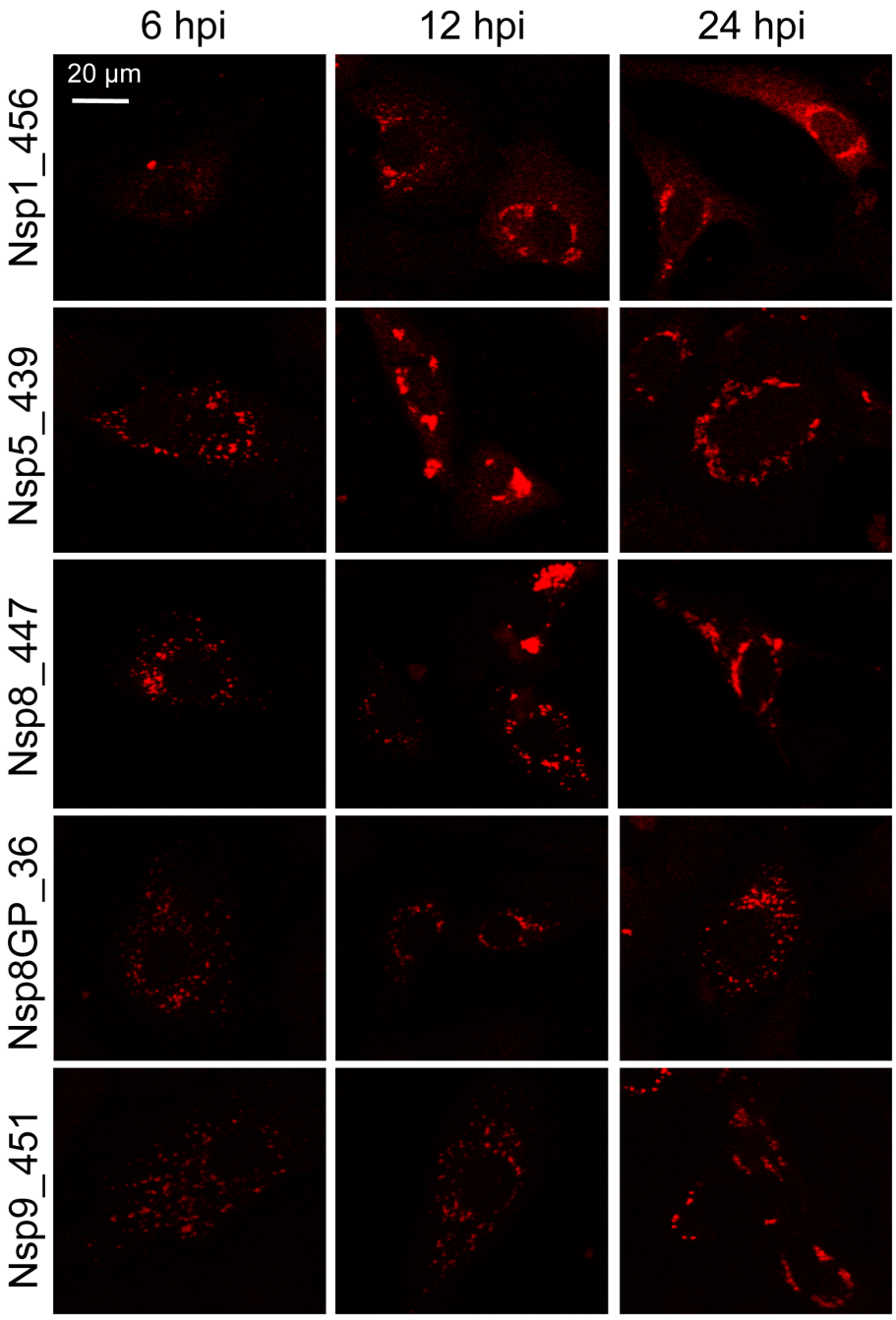

Figure 30. MERS-CoV proteins can be visualized as early as 6 h p.i.

WHO-Vero cells were infected with MERS-CoV at an MOI of 1 PFU/cell. At 6, 12, or 24 h p.i., cells were fixed in MeOH, stained with antibodies as indicated (α-nsp1, α-nsp5, α-nsp8, α-nsp9) and secondary antibodies labeled with Alexa 546. Cells were imaged by confocal microscopy. All images are at the same magnification.

were fewer cells with fluorescent signal in these samples than there were in the 12 h or 24 h samples.

MERS-CoV replication proteins colocalize with Golgi and ER markers

In order to determine whether MERS-CoV replicase proteins colocalize with ER, Golgi, mitochondria or actin, co-immunostaining was performed (Figure 31). First, in order to determine whether MERS-CoV replicase proteins colocalize with ER markers, MERS-CoV infected cells on glass coverslips were co-stained for each nsp and PDI. Both nsp8 and nsp9 demonstrated partial colocalization with PDI, similar to previous studies with SARS-CoV nsp3 (Knoops et al., 2010). Other studies have demonstrated that some nsps relocalize to the site of viral assembly, the ERGIC, at late times post-infection (Bost et al., 2001). In order to test whether MERS-CoV nsps localize to the Golgi at 24 h p.i., we tested co-localization of each nsp with WGA (WGA N-acetyl-D-glucosamine and sialic acid residues). Foci from all nsps tested were distinct from the Golgi, suggesting that, at least at this time post-infection, replicase proteins do not relocalize to the Golgi, which may be important for future studies of viral assembly.

Next, in order to determine whether other organelle markers were excluded from replication complexes, we analyzed colocalization of the nsps with mitochondria using the mitochondrial protein pyruvate dehydrogenase (PDH). Nsp1, nsp5, and nsp9 do not colocalize with PDH. There was partial colocalization of nsp8 and PDH, but it was only at the periphery of distinct foci, suggesting that the two compartments may be in close proximity. Current electron microscopy studies in our lab have demonstrated that

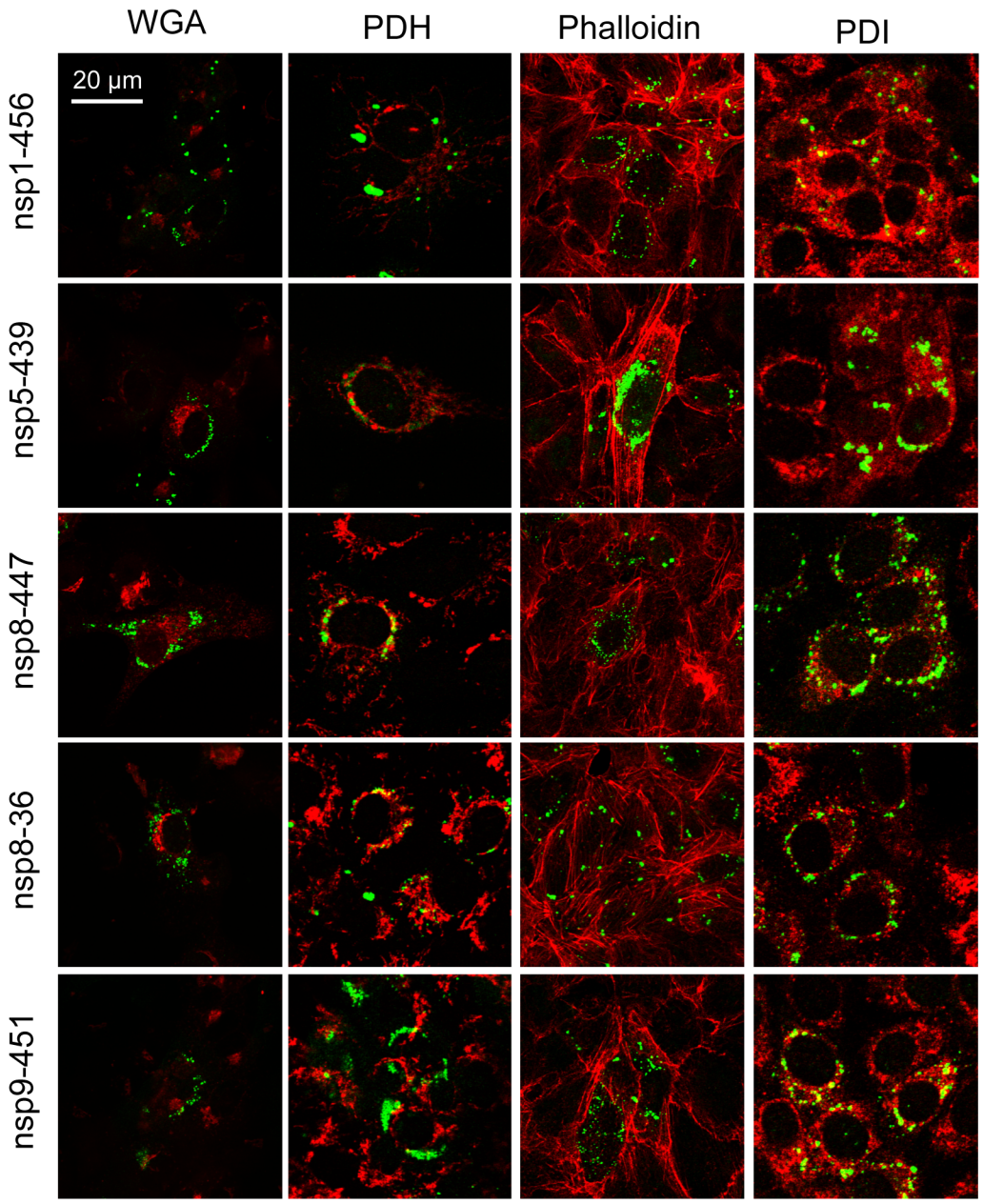

Figure 31. MERS-CoV replicase proteins and cellular markers

WHO-Vero cells were infected with MERS-CoV at an MOI of 1 PFU/cell. At 24 h p.i., cells were fixed in MeOH, stained with antibodies as indicated. MERS-CoV replicase proteins are labeled with green and cellular markers are labeled in red. Confocal images. WGA-Golgi, PDH-mitochondria, Phalloidin-F-actin, PDI-ER. Yellow pixels correspond to colocalization of green and red. All images are at the same magnification.

mitochondria are often incredibly near, but distinct from double membrane vesicles (data not shown). Additionally, we tested colocalization with the actin cytoskeleton. For this, we labeled F-actin with phalloidin. As expected, none of the nsps evaluated colocalized with the actin cytoskeleton. Collectively, these data suggest that MERS-CoV forms replication complexes that are similar to other beta-CoVs, both in punctate expression in the perinuclear region of the cell and in patterns of localization with cellular markers.

MERS-CoV antibodies directed against the spike protein are specific and robust

In addition to the antibodies directed against the replicase proteins, I also have been working in collaboration with Barney Graham's lab at the NIH to evaluate antibodies directed against the MERS-CoV spike protein. To test whether these antibodies specifically recognized epitopes in MERS-CoV-infected cells during immunofluorescence assays, WHO-Vero cells on glass coverslips were infected with MERS-CoV at an MOI of 1 PFU/cell for 24 hours, fixed in MeOH, immunostained utilizing the MERS-CoV antibodies directed against spike protein, and examined by wide field microscopy (Figure 32). Each of the Spike antibodies, D12, F11, G2, and G4, demonstrated specificity for MERS-CoV infected cells.

MERS-CoV antibodies directed against the spike protein coloclalize with actin and Golgi markers.

To investigate the cellular localization of the spike protein, WHO-Vero cells on glass coverslips were infected with MERS-CoV at an MOI of 1 PFU/cell for 24 hours, fixed in 10% formalin, permeabilized with 1% Triton X-100, co-immunostained utilizing the

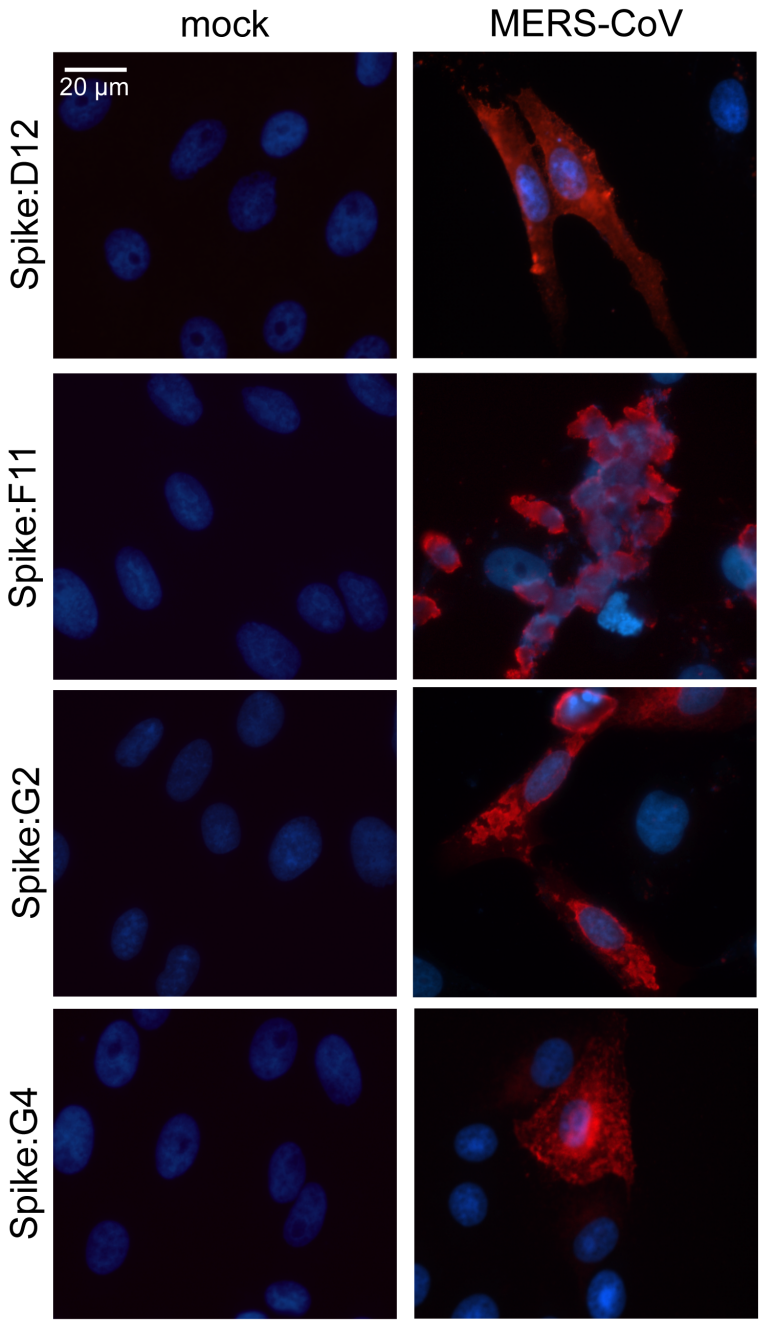

Figure 32. Different antibodies designed against MERS-CoV Spike protein specifically recognize infected cells

WHO-Vero cells were infected with MERS-CoV at an MOI of 1 PFU/cell. At 24 h p.i. cells were fixed in MeOH, stained with antibodies as indicated and secondary antibodies labeled with Alexa 546. Cells were imaged by wide field microscopy. Nuclei are stained with DAPI. All images are at the same magnification.

MERS-CoV antibodies directed against spike protein (G2) and antibodies directed either against the WGA, to represent the Golgi, or with phalloidin toxin, to stain the actin cytoskeleton (Figure 33). Coverslips were examined by confocal microscopy. Spike staining of infected cells was discovered to coloclalize both with actin at the cell surface and with WGA, the Golgi marker. This staining pattern is consistent with the spike protein of other coronaviruses, and corresponds to mature spike in the Golgi trafficking out to the cell surface.

Replicase proteins localize to replication complexes, while spike protein exists in the Golgi and at the surface of the cell

In order to evaluate colocalization of MERS-CoV nsps and spike, WHO-Vero cells on glass coverslips were infected with MERS-CoV at an MOI of 1 PFU/cell for 24 hours, fixed in MeOH, and co-stained with each of our nsp antibodies raised in rabbits with the nsp8 antibody raised in guinea pigs and the spike antibodies raised in mice (Figure 34). During co-staining experiments, the all nsps colocalize with nsp8 at perinuclear foci, and spike has a distinct pattern of localization separate from the nsps. Visually, there appeared to be differences in the number of foci or intensity of some proteins. When testing nsp5 and nsp8, all of nsp8 colocalizes with nsp5 but there are some nsp5 foci that do not colocalize with nsp8. This suggests that, while all of the nsps tested localize to sites of viral replication, nsps may be present at the replication complexes in different quantities or arrive there with temporal differences.

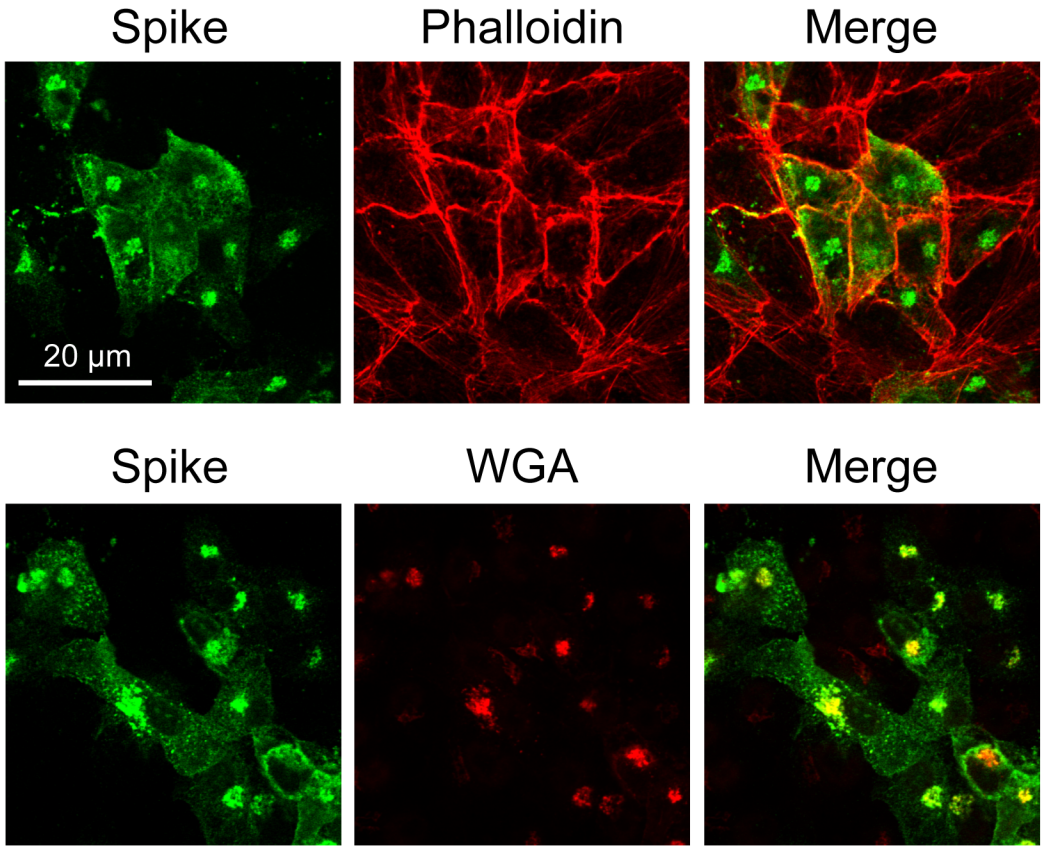

Figure 33. MERS-CoV spike protein localizes to the interior and exterior of the cell

WHO-Vero cells were infected with MERS-CoV at an MOI of 1 PFU/cell. At 24 h p.i., cells were fixed with 10% formalin, permeabilized where indicated, and stained with antibodies (α-spike G2) and secondary antibodies labeled with Alexa 488. Cells were costained with WGA directly conjugated to Alexa 555 or phalloidin conjugated to Alexa 546. Cells were imaged by confocal microscopy. All images are at the same magnification.

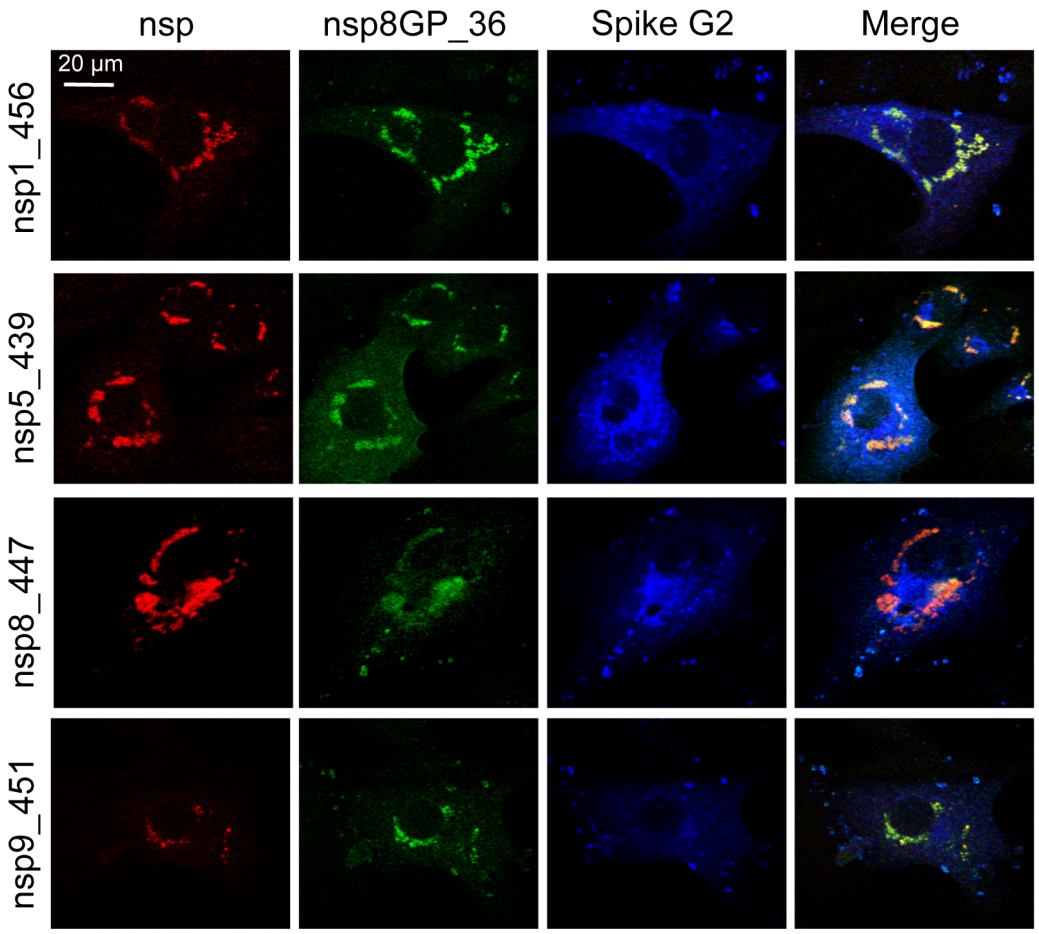

Figure 34. MERS-CoV nsps colocalize to replication complexes, while spike localizes to the interior and exterior of the cell

WHO-Vero cells were infected with MERS-CoV at an MOI of 1 PFU/cell. At 24 h p.i., cells were fixed in MeOH, stained with antibodies as indicated and secondary antibodies labeled with Alexa 546 (rabbit nsps), 488 (guinea pig nsp8), or 633 (mouse spike). Cells were imaged by confocal microscopy. Yellow pixels correspond to colocalization of green and red. All images are at the same magnification.

Discussion

MERS-CoV is an important infectious agent with severe consequences for human health. In this work, we have developed antibodies specific for several MERS-CoV nonstructural proteins. We have tested these proteins to determine that they are highly specific and robust for use in immunofluorescence studies. We have determined that MERS-CoV nsps localize to punctate perinuclear foci, as is seen for other coronaviruses. Specific signal is visualized for each antibody as early as 6 h p.i. Each nsp tested colocalizes with nsp8, another of the replicase proteins. Antibodies directed against the nonstructural proteins do not coloclalize with markers against actin, the Golgi network, or mitochondria, but do partially coloclalize with ER markers. Antibodies directed against the spike protein coloclalize with actin and with the Golgi, but not with replicase proteins.

Interestingly, the patterns of localization seen in immunostaining for MERS-CoV nonstructural proteins has similarities and differences from other previously studied coronaviruses. While each nsp demonstrated a pattern of punctate, perinuclear localization, much like other CoVs studied, the signal for MERS-CoV seemed to often form a distinct semi-circular ring around the nucleus with less thickness than seen in the other CoVs. The foci also seemed to be fewer in number than in other viruses studied, although each was very bright in its intensity. This could suggest that there is a tight special regulation associated with this virus. Patterns of colocalization between nsps were as expected, as were patterns of colocalization between evaluated nsps and cellular markers, with nsps demonstrating some degree of colocalization with ER markers, but not with any of the other cellular markers tested. Antibodies against the spike protein

demonstrated expected colocalization as well, with overlap in signal with both actin and markers for the Golgi. The timing of protein expression in MERS-CoV-infected cells was also surprising. In our hands, MERS-CoV does not have a robust expression of CPE, and even when it is visualized, it is multiple days post-infection. Protein production was visualized as early as 6 h p.i., which is an indicator that cells are actively infected at this point.

Interestingly, while we had great success with the strategy of utilizing the entire nsp as an antigen for most of the nonstructural proteins tested, this was less effective for nsp10. This brings to light a potential immunogenicity difference between different proteins or regions of the genome. Other strategies, such as truncations of the protein or peptide antigens, may be employed with greater success for nsp10.

Antibodies generated against MERS-CoV nonstructural proteins are specific and robust. They will be a valuable resource for future studies of MERS-CoV replication. These reagents and additional nsp-specific antibodies being developed in the laboratory will be critical in future studies of protein processing, nonstructural protein interactions, and protein localization.

Chapter V: MATERIALS AND METHODS

Viruses, cells, plasmids, and antibodies

Recombinant murine hepatitis virus strain A59 (WT), GenBank sequence AY910861 (Denison et al., 2004; Sperry et al., 2005), was used as WT for MHV experiments. Work with SARS-CoV was completed using the reverse genetics infectious clone based on the Urbani strain (Yount et al., 2003). Work with MERS-CoV was completed with the recombinant clone (Scobey et al., 2013). Viral studies with SARS-CoV and MERS-CoV were preformed in a Select Agent certified BSL-3 laboratory using protocols reviewed and approved by the Institutional Biosafety Committee of Vanderbilt University and the Centers for Disease Control for the safe study and maintenance of SARS-CoV. MHV-Δnsp2 virus with in-frame deletion of nsp2, and MHV-ΔCS2 with deletion of the nsp2-3 cleavage site P1 Glu, were previously described (Graham et al., 2005). MHV-2S and MHV-C12 were kind gifts from Susan Weiss (U Penn) and have been previously described (Gombold et al., 1993; Navas et al., 2001). Delayed brain tumor (DBT) cells (Hirano et al., 1976), WHO Vero cells (Scobey et al., 2013) and baby hamster kidney cells expressing the MHV receptor (BHK-MHVR) (Chen et al., 1997; Lin et al., 1996) were grown in Dulbecco's Modified Eagle Medium (DMEM) with 10% fetal bovine serum (FBS), 1% 1M HEPES, 100 units/ml of penicillin, 100 μg/ml streptomycin, and 0.23 μl/mL amphotericin B. Medium for BHK-MHVR cells was supplemented with G418 (0.8 mg/ml) for selection of cells expressing the receptor. DBT cells expressing the SARS-CoV receptor (DBT-hACE2) (Sheahan et al., 2008) were cultured as previously described. VSV-G plasmid was a kind gift from Michael Whitt (UTHSC) (Robison and

Whitt, 2000). The polyclonal antibodies used in biochemical and imaging experiments have been previously described. All polyclonal antibodies were raised in rabbits unless indicated. For MHV, these include antibodies specific for nsp1 (VU221) (Brockway et al., 2004), nsp2 (VU154) (Sims et al., 2000), nsp3 (VU164) (Graham et al., 2005), and nsp8 (VU123) (Bostwick et al., 2000). Mouse monoclonal α-firefly luciferase (FFL), clone LUC-1, was purchased from Sigma-Aldrich. Mouse monoclonal antibody specific for full-length GFP was purchased from SantaCruz Biotechnology. Mouse monoclonal antibody against the viral Membrane protein (M) was generously provided by J. Fleming (University of Wisconsin, Madison). Alexa Fluor 488 phalloidin (Molecular Probes) was used to stain for F-actin. Rabbit polyclonal α-CDC42-c terminal ab155940, rabbit polyclonal α-RhoA ab86297, mouse monoclonal α-GAPDH [6C5] ab8245, mouse monoclonal α-Rac1 [0.T.127] ab33186, and rabbit monoclonal α-Pak1 (phosopho S144) [EP656Y] ab40795 were purchased from abcam. Rabbit polyclonal antiserum specific for CEACAM was a kind gift from Tom Gallagher (Loyola University Chicago) (Thorp and Gallagher, 2004). Mouse monoclonal antibodies against protein disulfide isomerase (PDI; BD Transduction Laboratories) and pyruvate dehydrogenase (PDH, Invitrogen) were used. WGA directly conjugated to Alexa 555 (Invitrogen) was used to stain the Golgi complex and phalloidin directly conjugated to Alexa 546 (Invitrogen) was used as a probe for F-actin. *C. difficile* toxin A was a kind gift from Borden Lacy (Vanderbilt University) (Chumbler et al., 2012). The spike antibodies were a gift from Barney Graham (NIH).

Generation of antibodies directed against MERS-CoV replicase proteins

For generation of antibodies directed against the MERS-CoV replicase proteins, the MERS-CoV genome was used as a template for reverse-transcription-PCR amplification of full-length proteins, cloned into pSUMO protein expression vectors, and purified. Protein generated for antibody production were the following: nsp1, nsp 8, nsp9 and nsp10. Additionally, nsp5 protein was received from Andrew Mesecar. New Zealand White rabbits were immunized with the purified proteins for antibody production (Cocalico, Inc.). After initial inoculation, rabbits were boosted at day 14 and day 21, and test bleeds were performed. Rabbits were boosted again at day 49, and sera from production bleeds on day 56 were used in the experiments in this report. For all studies, preimmune sera from the same rabbits were matched with immune sera.

Construction of mutant MHV cDNA plasmids

Insertions of reporter genes in place of the nsp2 coding sequences of MHV were engineered using PCR with primers as shown in Table 1. For ABCDEF primer sets, primers A and B generated an A/B PCR product, primers C and D generated a C/D PCR product, and primers E and F generated an E/F PCR product. AB, CD, and EF PCR amplicons were ligated into an ABCDEF product using the class IIs restriction enzyme method, and ligation products were cloned into the appropriate fragment A vector using unique sites: 5'-Sac II and 3'-Nde I. Successful insertions of reporter gene sequences were confirmed by restriction digestion and sequencing. The infectious cDNA fragment A construct (pCR-XL-Topo-A), which consists of genome nts 1 to 4882, was used as

template DNA (Yount et al., 2002). Reporter genes were cloned from pEGFP-C1 (GFP, Clontech) and pGEM-Luc (firefly luciferase, Promega).

Generation of MHV reporter viruses

Viruses containing PCR-generated insertions within the viral coding sequence were produced using the infectious cDNA assembly strategies for MHV as previously described, with modifications (Denison et al., 2004; Sperry et al., 2005; Yount et al., 2003; Yount et al., 2002). Plasmids containing the seven cDNA cassettes of the MHV genome were digested using Mlu I, BsmB I, and Sfi I for fragment A, Bgl I and BsmB I for fragments B and C, BsmB I and Nci I for fragments D and E, BsmB I for fragment F, and BsmB I and Sfi I for fragment G. Digested, gel-purified fragments were ligated together in a total reaction volume of ~100 µl overnight at 16^{o}C. Following chloroform extraction and isopropanol precipitation of ligated DNA, capped, polyadenylated full-length RNA transcripts of MHV infectious cDNA were generated in vitro using the mMessage mMachine T7 Transcription Kit (Ambion) following the manufacturer's protocol with modifications. Twenty-microliter reactions were supplemented with 3 µL of 30 mM GTP, and transcription was performed at 40.5^{o}C for 25 minutes, 37.5^{o}C for 50 minutes, and 40.5^{o}C for 25 minutes. In parallel, capped, polyadenylated RNA transcripts encoding the corresponding nucleocapsid proteins (N) were generated in vitro using N cDNA generated from PCR (Yount et al., 2003; Yount et al., 2002). N transcripts and mutant viral transcripts were then mixed and electroporated into BHK-MHVR cells. Cells were grown to sub-confluence, trypsinized, then washed twice with PBS and resuspended in PBS at a concentration of 10^7 cells/ml. Six hundred µl of cells were then added to

RNA transcripts in a 4-mm gap electroporation cuvette (BTX), and three electrical pulses of 850 V at 25 μF were delivered with a Bio-Rad Gene Pulser Xcell electroporator. Transfected cells were then seeded onto a layer of 10^6 uninfected DBT cells in a 75-cm^2 flask and incubated at 37^{o}C for 30-90 h. Virus viability was determined by syncytia formation. T25s of cells were infected with supernatant, then the RNA was harvested using TRIzol (Invitrogen) according to the manufacturer's instructions, and retention of reporters was verified by RT-PCR and sequencing.

Microscopy

DBT cells grown to 60% confluency on 12-mm glass coverslips were infected with designated viruses. At 10 h p.i., medium was aspirated from cells, and cells were fixed and permeabilized in methanol at -20^{o}C overnight. WHO-Vero cells grown to 60% confluency on 12-mm glass coverslips were infected with MERS-CoV at an MOI of 1 PFU/cell for the time designated. Vero cells grown to 60% confluency on 12-mm glass coverslips were infected with SARS-CoV at an MOI of 1 PFU/cell for the time designated. Viral studies with MERS-CoV or SARS-CoV were preformed in a BSL-3 laboratory using protocols reviewed and approved by the Institutional Biosafety Committee of Vanderbilt University and the Centers for Disease Control for the safe study and maintenance of MERS-CoV and SARS-CoV. Cells were rehydrated in PBS for 20 min and blocked in PBS containing 5% bovine serum albumin (BSA). Blocking solution was aspirated, and cells were washed with immunofluorescence (IF) assay wash solution (PBS containing 1% BSA and 0.05% Nonidet P-40) at room temperature. Cells were incubated in primary antibodies where indicated, 1:1000; or α-FFL (Sigma-

Aldrich), 1:1000 for 45 m. Cells were washed in IF wash solution 3 times for 5 min per wash. Cells were incubated in secondary antibodies (Goat α-rabbit-AlexaFluors 488 (1:1000) or 546 (1:1500), Invitrogen Molecular Probes) for 30 min. Cells were washed 3 times for 5 min per wash, followed by a final wash in PBS, and then rinsed in distilled water. Coverslips were mounted with Aquapolymount (Polysciences) and visualized by confocal immunofluorescence microscopy on a Zeiss LSM 510 laser scanning confocal microscope at 488 and 543 nm with a 40X oil immersion lens. Images were processed and assembled using Nikon Elements, ImageJ, and Adobe Photoshop CS5 (12.0x64). All images were processed side-by-side with mock images.

Protein immunoprecipitations

For protein labeling and immunoprecipitation experiments, cells were infected with MHV and incubated at 37^{o}C. At 2.5 h p.i., medium was aspirated and replaced with medium lacking methionine and cysteine and supplemented with actinomycin D (Sigma) at a final concentration of 20 μg/ml. At 3.5 h p.i., cells were labeled with [35S]-Methionine/Cysteine ([35S]-Met/Cys) at a concentration of 0.08 mCi/ml. Radiolabeled cells were lysed in 1 ml no-SDS lysis buffer (1% NP-40, 0.5% sodium deoxycholate (DOC), 150 mM sodium chloride (NaCl), and 50 mM Tris pH 8.0) at 10-14 h p.i. Cellular debris and nuclei were pelleted by centrifugation at 14,000 × g for 3 min at RT, and the supernatant was transferred to a fresh tube. Fifty microliters of cell lysate was subsequently used per 400 μl of immunoprecipitation reaction buffer. Lysate was combined with protein A-sepharose beads and a 1:200 dilution of antibody in no SDS lysis buffer supplemented with 1% SDS. After incubation at 4°C for 18 h, beads were

pelleted and washed with low-salt lysis buffer (no-SDS lysis buffer with 150 mM NaCl) followed by high-salt lysis buffer (no-SDS lysis buffer with 1 M NaCl) and a final low-salt wash. After rinsing, proteins were eluted by the addition of 2X LDS (lithium dodecyl sulfate) + 1X DDT buffer (NuPage, Invitrogen) to the pelleted beads, which were heated at 70^{o}C for 10 minutes prior to electrophoresis of the supernatant on 4-12% Bis-Tris or 3-8% Tris-Acetate gels (NuPage, Invitrogen). Gels were imaged by autoradiography.

Viral replication assays

For viral replication analysis, DBT cells were infected in triplicate with WT MHV or mutant viruses at the MOI indicated for each experiment. Following a 30-minute adsorption with rocking at RT, media was aspirated, and cells were washed 3 times with PBS and then incubated with pre-warmed media at 37^{o}C. Aliquots of media were collected from 1 to 24 h p.i., and virus titers were determined by plaque assay on DBT cells in duplicate as described previously (Lavi et al., 1984). EIPA (Sigma) was applied during infection as indicated.

Competition assay

Confluent monolayers of DBT cells in T25 flasks were infected with WT MHV or MHV-GFP2 alone or at a 1:1, 1:10, or 10:1 ratio of WT MHV to MHV-GFP2 at a total MOI of 0.1 PFU/cell. Each flask was passaged 10 times as described for serial virus passage and 1 mL supernatant was collected and stored at −80°C. DBT cells were seeded on glass coverslips and infected at an MOI of 1 PFU/cell with P1, P3, and P10 of each combination of viruses. At 8 h p.i., slides were fixed with cold MeOH. Coverslips were

immunostained with primary antibodies specific for nsp8 and secondary antibodies, goat α-rabbit AlexaFluor 546, as described above. Coverslips were mounted with Aquapolymount (Polysciences) and visualized by immunofluorescence microscopy on a Nikon Eclipse TE-2000S wide field fluorescent microscope. Cells were imaged using a 40X oil-immersion lens through DIC, FITC, Cy3, and DAPI filters. Resulting images were merged and assembled using Nikon Elements, ImageJ, and Adobe Photoshop CS2. Infected and mock-infected cells were processed in parallel. Competition was assessed by counting the number of cells expressing GFP-nsp2 costained for nsp8 with Alexa 546 versus the number of cells stained for nsp8 with Alexa 546 alone.

Luciferase activity versus viral replication assay

DBT cells in 6-well plates were infected with MHV-Δ2-FFL3 or MHV-FFL2 at an MOI of 1 PFU/cell and incubated at 37^{o}C for 30 min. At 0.5 h p.i., media was aspirated to remove inoculum, cells were washed three times with PBS, and supplemented with pre-warmed media. At time points through 24 h p.i., supernatant was harvested, or cells were lysed in Reporter Lysis Buffer (Promega) and subjected to one freeze-thaw cycle. Following freeze-thaw, lysates were vortexed and centrifuged briefly at top speed, and supernatants transferred to new tubes. To measure luciferase activity, 20 μL of lysate was added to each well of an opaque 96-well plate. Plates were loaded onto a Veritas luminometer and the automatic injector was used to add 100 μl of reconstituted Luciferase Assay Reagent (Promega) to each well as the samples were being read, 5 s per well, 0 s delay. Viral replication was determined from harvested supernatants by plaque assay as above.

Live-cell imaging of MHV infected cells

DBT cells were seeded onto 35mm MatTek glass bottom culture dishes for 48 hours. Cells were then infected with MHV-Δ2-GFP3 at an MOI of 1 PFU/cell. In a separate experiment, cells were transfected with a GFP-expressing plasmid before being infected with MHV-A59 at an MOI of 1 PFU/cell. Plates were transferred to a live-cell incubator surrounding the objective stage of a Nikon Eclipse TE-2000S widefield fluorescent microscope. In the viral entry experiment, cells were infected with DiI labeled MHV-A59 at an MOI of 25 PFU/cell and the infection was synchronized at 4° C for 30 minutes before imaging. Cells were imaged using a 40X oil-immersion lens through DIC and FITC short pass filters, with images captured at 30-second intervals. Resulting images were assembled into movies using Nikon Elements, ImageJ, Adobe Photoshop CS5 and Quicktime Pro.

Determination of bulk fluid uptake and fixed ruffling

DBT cells grown to 80% confluency on 12-mm glass coverslips were infected with MHV-A59 at an MOI of 1 PFU/cell. At designated times p.i., 100μg/ml 800nm fluorescent polystyrene nanoparticles (Corpuscular Inc.) were added to cells and incubated for 3 h at 37ºC. DBT-hACE2 cells were infected with SARS-CoV for 24 h at an MOI of 0.1 PFU/cell and 100μg/ml nanoparticles were added during the final 3 h prior to fixation. Cells were washed with media 3 times for 5 minutes. Drugs were added where indicated. Cells were fixed in 100% methanol or 10% formalin, then put at -20°C or 4°C, respectively, overnight. Cells were rehydrated in PBS for 10 min and blocked in PBS containing 5% bovine serum albumin (BSA). The coverslips were immunostained and imaged as described above in “Microscopy”. Scores for ruffling events were

calculated by encrypting the images and allowing three independent blinded reviewers to evaluate if a cell was positive or negative for ruffling, utilizing fixed criteria and a binary system. Cells were determined to have internalized nanoparticles based on a binary scoring system. Number of cells analyzed per sample as indicated.

Fluorescent labeling of virions

Viral stocks of MHV-A59 were grown on DBT cells and purified using a sucrose cushion with 5.5mL of 20% sucrose (20% sucrose, 0.1 M MgSO4, 50 mM HEPES, 150mM NaCl, pH 7.4, 0.2μM filtered) layered over 1.5 mL of 60% sucrose (20% sucrose, 0.1 M MgSO4, 50 mM HEPES, 150mM NaCl, pH 7.4, 0.2μM filtered) and spun at 27,000 RPM at 4° C for 90 min. Virions were then incubated with 5 uM 1,1'-Dioctadecyl-3,3,3',3'-Tetramethylindocarbocyanine Perchlorate (DiI) (Life Technologies) for 1 h at room temperature and purified using a sucrose cushion with 1.5 mL 20% sucrose layered over 1 mL 60% sucrose and spun at 28,000 RPM at 4° C for 90 min to remove free dye.

Toxicity assays

Cellular toxicity for EIPA (Sigma), C. difficile toxin A (CdtA) (Lacy lab, Vanderbilt), peptidyl chloromethylketone (dec-RVKR-cmk) (Calbiochem), and Gefitinib (Selleck Chemicals) were tested at 12 h post treatment with DBT cells using Cell Titer Glo (Promega) protocol at following manufacturer's instructions.

siRNA assays

siRNA SMARTpools for murine Cdc42, Rac1, Pak1, RhoA, and scramble were obtained from ThermoScientific. DBT cells were reverse transfected per the protocol for Lipofectamine RNAiMAX (Life technologies). For siRNA and infection, cells were reverse transfected for 68 h, infected with MHV at an MOI of 1 for 8 h, and nanoparticle and fixation protocols were completed as described above. To test protein knockdown, cells were reverse transfected, incubated for 72 h, harvested with non-SDS lysis buffer, subjected to immunoblot analysis, and imaged with the Odyssey Imaging System (Licor). Band intensity was quantified and normalized to GAPDH using ImageJ. siRNA transfection efficiency was tested with transfection of AllStars Negative siRNA AlexaFluor 488 (Qiagen).

UV-inactivation and heat-inactivation assays

MHV was UV-inactivated by placing 1 mL of stock in an open 30 mm dish in a UV cross-linker for 45 minutes. MHV was heat-inactivated by placing 1 mL of stock at 70°C for 45 minutes. Inactivated virus was titered by plaque assay and determined to be inactivated when plaque formation was absent. DBT cells were mock-infected or infected with MHV-A59, UV-inactivated virus, or heat inactivated virus at an MOI of 1 or an equivalent volume of non-infectious virus for 8 h.

Cell-associated assay

DBT cells were infected with MHV-FFL2 at an MOI of 1 PFU per cell. At 8 h p.i., cells were washed 2x with PBS, then DMSO or EIPA was added. At 10 h p.i., supernatant was

collected and cell monolayers were harvested in DMEM and subject to 3 rounds of freeze-thaw. Each fraction was titered by plaque assay as previously described. Cells from a parallel experiment were collected in Luciferase Assay Buffer (Promega) and assessed for luminescence via the manufacturer's protocol.

Furin inhibition assay

DBT cells grown to 80% confluency on 12-mm glass coverslips were mock-infected or infected with MHV-A59 at an MOI of 1 PFU per cell. Cells were untreated, treated with 0.25% DMSO, or treated with increasing concentrations of peptidyl chloromethylketone (dec-RVKR-cmk) (Sigma) at the time of infection. Nanoparticle assays were completed, cells fixed and stained as described above, then imaged, and assessed for nanoparticle uptake and syncytia formation.

Fusion assays

DBT cells grown to 80% confluency on 12-mm glass coverslips were treated for 1 min with PEG-1500 (Sigma) and rinsed 3x with PBS before incubation with nanoparticles for 3 h. Nanoparticle assays were completed, cells fixed and stained, imaged, and assessed for nanoparticle uptake and syncytia formation. Alternatively, cells were grown to ~60% confluency and transfected with VSV-G per the protocol for Lipofectamine 2000 (Life Technologies) for 24 h before nanoparticle incubation for 3 h. DBT cells grown to ~80% confluency on 12-mm glass coverslips were infected with MHV-A59 or MHV-2S at an MOI of 1 PFU per cell. At 5 h p.i., cells were treated with 2.5 μg/ml TPCK trypsin (Sigma) for 5 m, washed 1x with PBS, nanoparticles were added and incubated for 3 h,

washed, fixed, stained, and imaged. DBT cells grown to 80% confluency on glass coverslips were mock-infected or infected with MHV at an MOI of 1 PFU per cell. α-CEACAM blocking antibodies were added at 2 h p.i., nanoparticles were added at 5 h p.i. for 3 h and cells were washed, fixed, stained and imaged. DAPI was used to stain nuclei. Number of nuclei per syncytium were measured, and the number of fields counted are as indicated.

Antibody clearance

WHO Vero cells were grown to 80% confluency in 6-well plates. Cells were rinsed of DMEM and 500 μL of antibody was applied to a well of cells and incubated with rocking at room temperature for 1 hour. Antibody was collected and centrifuged to remove cellular debris.

Statistical analysis

Statistical tests were applied as noted within the figure legends and were determined using GraphPad Prism (La Jolla, CA) software. Statistical significance is denoted as stated in the legends and was determined using a one-way analysis of variance (ANOVA) with Dunnett's multiple-comparison test compared to uninfected or vehicle-treated samples. *P* values of <0.05 were considered to be statistically significant.

Table 1. Primers used for generation of reporter insertions

Primer Name	Sequence[a]	Used to amplify	Sense	Comments
MHV A	5'-AACGGCACTTCCTGCGTGTCCATG	MHV nsp1	+	Common MHV left nsp1 primer
MHV B	5'-CGTCTCCCTTAACACCGCGATAGCCCTTAAGAAGAG	MHV nsp1	-	Common MHV right nsp1 primer
MHV-GFP C	5'-CGTCTCCTAAGATGGTGAGCAAGGGCGAGGAGCTGT	GFP	+	
MHV-GFP D	5'-CGTCTCGTGCCCTTGTACAGCTCGTCCATGCCGAGAGT	GFP	-	MHV-Δ2-GFP3
MHV-GFP D	5'-CGTCTCGTAACCTTGTACAGCTCGTCCATGCCGAGAGT	GFP	-	MHV-GFP2
MHV-FFL C	5'-CGTCTCCTAAGATGGAAGACGCCAAAAACATAAAGAAAG	FFL[b]	+	
MHV-FFL D	5'-CGTCTCGTGCCCAATTTGGACTTTCCGCCCTTCTT	FFL	-	MHV-Δ2-FFL3
MHV-FFL D	5'-CGTCTCGTAACCAATTTGGACTTTCCGCCCTTCTT	FFL	-	MHV-FFL2
MHV E	5'-CGTCTCGTATCGCGGTGTTAAGAAAGTCGAGTTTAAC	MHV nsp3	+	Common MHV left nsp3 primer
MHV F	5'-ACTTGCACATATGAGACACAACGTCCCCA	MHV nsp3	-	Common MHV right nsp3 primer

[a]Underlining indicates residues added for cloning or mutagenesis purposes

[b]Firefly luciferase

Chapter VI: SUMMARY AND FUTURE DIRECTIONS

It is estimated that coronaviruses have been human pathogens for at least 500-800 years (Graham et al., 2013), though it wasn't until the 1960s that the first human coronaviruses, HCoV-229E and -OC43, were described as agents of the common cold. Coronaviruses became increasingly publicized with the outbreaks of SARS-CoV in 2002-2003 and MERS-CoV ten years later in 2012. Both the continued circulation of a SARS-CoV-like bat CoV capable of utilizing the SARS-CoV receptor ACE2 (Ge et al., 2013) and the emergence of MERS-CoV suggests that emergence of CoVs causing severe and lethal human disease might be more common than realized. Thus, understanding viral and host factors essential for efficient replication will enable us to prevent and treat infections, as well as control potential future pandemics.

The work in this dissertation specifically focuses on the unique capacity of coronaviruses, much like other positive-sense RNA viruses, to modify host cellular membranes during various stages of the viral lifecycle. This chapter will summarize the main findings of this dissertation in three parts: 1) the use of novel reporter viruses to visualize CoV replication in real-time, 2) the discovery that macropinocytosis occurs constitutively post-entry during CoV infection and is likely important for viral spread, and 3) the use of newly developed antibodies that provide the first images of MERS-CoV replication complexes. Finally, this chapter will highlight interesting new questions and future directions generated as a result of these studies.

Visualizing CoV replication in real-time using novel reporter viruses

Reporter protein sequences have been introduced into genomes of multiple coronaviruses to allow identification of infected cells or as surrogates for virus replication. However, these approaches have used either replicons or expression of reporter molecules in place of "accessory" proteins from 3' open reading frames. Reporters expressed from 3' ORFS are diffuse in the cytoplasm, thus limiting the usefulness of these viruses to detection of infected cells. By contrast, the reporters described in this dissertation are the first to express GFP or FFL from within the replicase gene. This design of recombinant reporter viruses resulted in expression of GFP as a fusion with nsps 2 or 3, and specific targeting of the GFP-nsps. This enabled the viruses to be used to study viral replication, replication complex formation, and ORF1a protein expression kinetics in live-infected cells. Although we had previously demonstrated that nsp2 could be deleted from the replicase polyprotein (Graham et al., 2005), viruses lacking nsp2 showed up to 90% decrease in peak replication. By contrast, recombinant viruses with reporters fused to nsp2 replicate with WT-like kinetics. The function of nsp2 is not known, and complementation by expression from other locations in the genome does not complement its deletion from its native encoded location (Gadlage et al., 2008). In addition, the reporter-nsp2 fusion viruses were unable to compete with WT virus. Thus, nsp2 appears to serve some role during infection that is not essential for replication but is important for overall virus fitness. The reporter-nsp2 viruses will allow direct testing of the expression, localization and functions of nsp2. As an example, the FFL-nsp2 virus allows direct measurement of translation of the replicase polyprotein 1a. I propose that multiple reporters might be

tolerated within one virus, as we have also successfully introduced GFP as a fusion with nsp14 in ORF1b (Eckerle, unpublished). Multiple reporters within one virus would be particularly useful to compare translation of ORF1a and ORF1b, to visualize protein interactions during replication complex formation, and to evaluate how viral proteins move from replication complexes to sites of assembly.

Recently, I have tested a panel of MHV and SARS-CoV recombinant viruses expressing fluorescent and luminescent reporters (Table 2) including fluorophores such as EGFP and mRFP. We have also generated fusion protein viruses with fluorescent proteins for use in super-resolution fluorescence microscopy and correlative EM/fluorescence. Specifically, we have introduced photoactivatable proteins including mEOS and PA-GFP. We have demonstrated the ability to use either STORM (stochastic optical reconstruction microscopy) or PALM (photoactivatable light microscopy) to achieve up to 10-fold increase in resolution of complexes containing localized proteins (Figure 35). To date, little is known of the timing and mechanisms of membrane modification, replication complex formation, stasis or movement of nsps between replication complexes, or movement of newly synthesized viral RNA and nucleocapsids. Our ability to perform super-resolution microscopy of individual and multiple replicase proteins will allow us to answer these questions. Each of these viruses could be imaged during the course of infection and fluorescence could help us to map the paths of the proteins in a single cell during the entire course of infection without having to choose a specific time to fix cells.

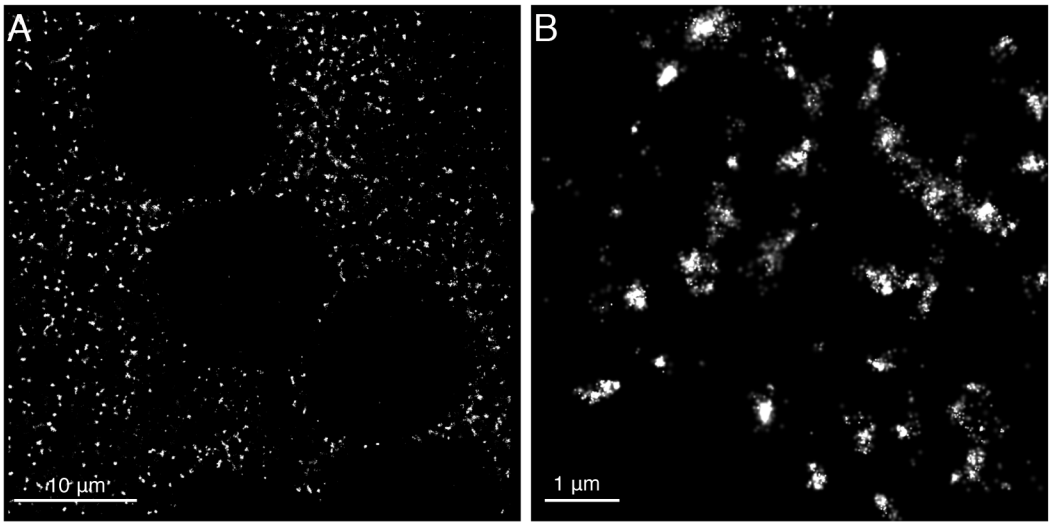

Figure 35. STORM imaging of DBT cells infected with MHV-mEos-nsp2

A) STORM image of a large area of an infected DBT cell. The fluorescence is directly from the mEos protein in the virus. Activated with low-level, continuous 405 nm laser, and collected images with the 546 nm laser. **B)** higher magnification of the same image.

While the reporter viruses generated in my study were stable for use up to five passages, with increased passage the reporter molecule was either inactivated or deleted. Specifically, with increased passage of MHV-Δ2-GFP3, the GFP sequence became unrecognizable and finally was completely excised by passage 20. Each incremental deletion of the reporter corresponded to a decreased eclipse phase in the replication curve, until upon complete removal of the GFP, the passage 20 version of MHV-Δ2-GFP3 replicated with kinetics of the parent MHV-Δ2 virus. With increasing passage of MHV-Δ2-FFL3, a mutation inactivated FFL substrate binding, while leaving the rest of the sequence intact. Viruses with the reporter-nsp2 fusions have not been tested for reporter inactivation or deletion. This data raises the possibility of evaluating different locations within the genome for increased stability, or for using the selective loss of reporter function to investigate questions of viral fidelity, with and without a mutation in the proofreading exonuclease. Codon optimization could be employed to investigate if an optimal reporter molecule could be designed for a specific viral genome. A series of reporter viruses could be used to measure recombination during viral infection.

Viruses containing reporters fused to nsp3 without a compensatory deletion of nsp2 have not been attempted, which would answer the question of if the replication defect was due to nsp2 loss alone or if it was more specifically related to the loss of a free nsp3 N terminus. The replication defect could be related to protease processing interference, difficulties in protein folding, or the interruption of localization signals. It could also be related to the size or shape of specific tags. This data raises the question of whether some

locations in the genome are better than others at creating either viable virus, or viable virus without replication defects.

Entry-independent, constitutive macropinocytosis during CoV replication

The capacity of CoVs to modify interior membranes during replication complex formation is well known. In contrast, prior to my studies little was known of coronavirus interactions with or modifications to the plasma membrane, apart from functions in virus entry and egress. This dissertation describes plasma membrane ruffling induced by both MHV and SARS-CoV infection that exhibit features of macropinocytosis. Prior to my work, macropinocytosis or a "macropinocytosis-like process" had been reported as an entry strategy utilized by 21 different viral pathogens since the first report in 2001 (Marechal et al., 2001) (Table 3). Interestingly, viruses that use macropinocytosis have surprisingly little in common. Genomes represented include both positive and negative sense single stranded RNA, double stranded RNA, and segmented RNA and DNA. Viral particles range in size from 20 nm for porcine parvovirus to 500 μm for the filamentous form of influenza. While macropinocytosis has previously been described to be an important means of cellular entry for many viruses and bacteria, the present work describes the first known viral induction of macropinocytosis not associated with virus entry. Coronavirus induction of macropinocytosis is significant, since it represents a novel exploitation of macropinocytosis by a virus, likely for cell-cell movement. It also describes a previously unknown function for the spike protein and suggests that the spike protein interacts with or indirectly activates epidermal growth factor receptor, to initiate subsequent signaling events and actin modification resulting in macropinocytosis.

Overall, my work raises many additional questions and important future directions that can be explored: What is the role of macropinocytosis during CoV infection? Does fusogenic spike interact with EGFR to activate macropinocytosis? Does macropinocytosis enhance cell-to-cell spread during infection?

What is the role of macropinocytosis during CoV infection?

Interestingly, MHV-A59 and MHV-2 spike proteins exhibit different capacities for macropinocytotic induction. These two viral strains differ in their entry mechanism, capacity for syncytia formation, and tropism, all of which are functions related to spike protein (Das Sarma et al., 2000; Navas et al., 2001). MHV-A59 is neurovirulent in mice, causing acute encephalitis and chronic demyelination, while MHV-2 has low neurovirulence, causing meningitis (Das Sarma et al., 2000). Spike is therefore an important mediator of tropism and pathogenesis, although it is not the sole regulatory factor of these parameters. Based on the results reported here, we conclude that MHV-2 is unable to induce macropinocytosis, but this does not seem to have negative consequences on viral replication for this virus. In contrast, blocking macropinocytosis in MHV A59 infection does result in a drop in viral titer. Macropinocytosis and syncytia formation with MHV-2 can be restored with exogenous trypsin cleavage of spike protein on the cell surface. Macropinocytosis may have evolved during MHV infection as a tissue-specific advantage, or as a means to a competitive edge over non-macropinocytotic variants. It is important to understand whether or not the capacity to induce macropinocytosis confers increased fitness *in vivo.* Additionally, there are other strains of MHV that have more specific hepatic tropism, such as JHM, which could assist in

answering this question by utilizing the JHM spike protein in an isogenic MHV A59 background.

SARS-CoV spike has complicated and incompletely characterized mechanisms of entry and spike cleavage. While it has been suggested that SARS-CoV is endocytosed and spike is subject to cleavage by cathepsins in the endosome, like MHV-2, other proteases have been demonstrated to cleave SARS-CoV spike at the cell surface, including trypsin, TMPRSS, HAT, and others (Bosch et al., 2008; Du et al., 2007; Kam et al., 2009). This leads me to hypothesize that any spike protein that traffics to the surface of the cell can then be cleaved by these proteases in order to induce macropinocytosis. Additional studies are necessary to elucidate this mechanism.

Does fusogenic spike interact with EGFR to activate macropinocytosis?

Epidermal growth factor receptor (EGFR) is a member of the ErbB family of tyrosine kinases that includes HER2, HER3, and HER4 (Earp et al., 2003). Dysregulation of these family members can lead to cancer. The clinical importance of this cellular receptor has led to the development of several inhibitors, including gefitinib (Iressa), which was used during this dissertation project to inhibit EGFR and study the effect on macropinocytosis in CoV-infected cells. In addition to EGFR, the phosphatidyl serine receptor (PSR) and α_v integrin are surface receptors that initiate macropinocytosis. Evaluating these additional pathways would determine if CoVs utilize multiple activating pathways for macropinocytosis. Additional data detailing when EGFR activation occurs during infection and the duration of activation would help to elucidate this novel viral-cell

interaction. Gefitinib has been shown to have some amount of cross reactivity, not with other family members, but with some other cellular targets, none of which are known activators of macropinocytosis (Brehmer et al., 2005). Use of some of the newer EGFR inhibitors may have less cross reactivity, and similar results with these alternative inhibitors would strengthen the conclusions already made.

Elucidating the nature of the spike-EGFR interaction is also important. Do they directly interact or is there an intermediate step such as an adaptor protein or ligand that is necessary for activation? Another question to be addressed is whether spike and EGFR interact at the surface or in the interior of the cell. Because EGFR is recycled, it would be possible for EGFR and spike to be exocytosed in the same vesicle. Viruses, particularly papillomaviruses, have been shown to interact with receptor tyrosine kinases in a variety of ways, including through a transmembrane domain surface interaction, the production of a ligand that then exogenously activates the receptor, and other viruses through direct binding to the receptor (DiMaio and Petti, 2013). Which phosphorylation site leads to its activation? Is spike acting as a cross-linker to create a permanent EGFR dimer, or is it causing the phosphorylation of an EGFR monomer that leads to the activation of the macropinocytosis pathway?

Does macropinocytosis enhance cell-to-cell spread during infection?

While my work has identified that macropinocytosis is a putative mechanism for creating virological synapses necessary for cell to cell spread through the formation of large membrane ruffles and also filopodia, more experiments are necessary to discover if cell-

cell spread is occurring in addition to syncytia formation. The length and frequency of filopodia should be measured during infection, as well as the change over time. Measurements of the interactions between filopodia and other cells should be noted, as well as the results of those interactions. More visual information about the relationship of budding virions or available surface spike protein and their relative position to filopodia forming would also be helpful in determining these relationships. An assay to measure cell-cell spread could also be a beneficial tool to evaluate changes in rate of formation or of plaque size. Polarized respiratory epithelial cells should be evaluated for their capacity for macropinocytosis after infection with coronaviruses. This system would help evaluate the hypothesis that CoVs are utilizing macropinocytosis to reach over tight junctions to infect neighboring cells. Other viruses have been shown to use cytoskeletal elements to form the virological synapse between cells; however, macropinocytosis has never been shown to be used for this purpose. In addition to the long extensions of actin, are the internalized vesicles also important for viral replication or are they simply a byproduct of the necessity for membranous extensions? What is in the vesicles, where do they deliver their cargo, and can they be halted independently of the membrane ruffles?

Visualizing MERS-CoV replication using newly developed antibodies

Chapter IV described the development of a panel of antibodies that recognized nonstructural proteins from the newly emergent pathogen, MERS-CoV. These antibodies were tested for specificity and used to investigate the spatial and temporal formation of replication complexes and their relationship to cellular markers. This work represents the first to visualize the formation of these complexes in this virus and also reports several

foundational, valuable, tested reagents that will be critical for future studies of these proteins for an important, newly emerged pathogen.

Significance and applications of research

CoVs will continue to pose a threat to human health, ranging from inconvenient common colds to life-threatening acute respiratory distress syndrome requiring significant medical intervention and supportive care. Even during the years spent working on this dissertation project, I have watched with fascination and awe the outbreak of a newly emergent coronavirus. It has provided an incredible exercise in epidemiology, frustration with the lack of information available, including the often inaccurate or inconsistent mortality and case counts, and curiosity about how the new virus works. It has been amazing to see how the scientific community reacted to a new virus. Papers emerged describing differences between this virus and SARS-CoV, serologic studies encompassing a wide variety of animals in the geographical area, the identification of the viral receptor, details about how best to screen and isolate new cases, and hypotheses about spread, emergence, and cross-species transmission. This outbreak has also presented learning opportunities about information sharing in the face of an emerging infection, regarding viral sequence information, samples, and reagents, what happens to the scientific enterprise if one group claims that an emerging virus is their intellectual property, and the importance of accurate case reporting from a region of the world with whom we do not always have cordial relations.

Historically, vaccination development has been a challenge for coronaviruses. Particularly, several vaccine strategies have been attempted for SARS-CoV including inactivating whole virus, spike (S) protein preparations, virus-like particles (VLPs), plasmid DNA and several vectors containing genes for SARS-CoV proteins (Tseng et al., 2012). None of these vaccines are presently licensed for use, as most strategies had problems during animal testing, some causing strong immunogenic reactions upon post-vaccination challenge with SARS-CoV. A strategy to attenuate viral fidelity showed promise during initial animal testing for safety and efficacy, and as proofreading activity is unique to coronaviruses, may represent a viable vaccination strategy for future emerging coronaviruses as well (Graham et al., 2012). Finding a strategy that could be applicable to future emerging coronaviruses is very appealing, as it would hasten our ability to control infections earlier in the initial period of emergence and uncertainty. Perhaps more important than the development of a vaccine, given these challenges, is the development of potent and effective anti-viral drugs that target coronaviruses. Through my work with macropinocytosis, in the understanding of a basic science mechanism, I utilized two inhibitors of this process that are used in clinical settings or are derivatives of approved drugs. Gefitinib, an EGFR inhibitor, is often used in cancer chemotherapy. Ethyl isopropyl amiloride is a derivative of amiloride, a blood pressure medication. Dosage information for halting macropinocytosis in humans is currently unknown, and the safety of blocking macropinocytosis in humans is also yet to be determined, as it is a process used by healthy cells, but because so many viruses without other shared characteristics utilize macropinocytosis, blocking it seems an interesting an uninvestigated strategy for a pan-viral inhibitor.

From a more basic-science perspective, my work also identified a new function for macropinocytosis in the life cycle of a virus, one unrelated to entry. It would be interesting to investigate other viruses that use macropinocytosis for entry for their capacity to use macropinocytosis at other points during the life cycle.

In conclusion, all scientific research serves to understand one tiny piece of the world in order to see how the pieces fit together to benefit society. The work described in this thesis represents years of my learning and development as a scientist and also my current contribution to furthering human understanding of host-pathogen interactions. It is my hope that the results of these studies will act as building blocks for many studies to follow exploring how viruses are able to exploit cellular processes for their own purposes. And in this way, one block at a time, we will be able to predict viral emergence, understand the intricacies of viral replication, and generate cures to alleviate human suffering.

Table 2. Generated reporter viruses

nsp1-repoter-nsp2 Virus	**P1 Titer**
mCherry	1.3x10^8
mEos2	3.3x10^8
EGFP	1.0x10^8
mRFP	7.0x10^7
FFL	6.8x10^7
nsp1-reporter-nsp3 Virus	
mCherry	1.0x10^7
mEos2	3.7x10^7
EGFP	7.0x10^7
mRFP	1.5x10^6
FFL	4.2x10^7

Table 3. Viruses that utilize macropinocytosis (MPC) for entry

Virus	Genome	Size	When	Main or Alternative ?	MPC	MPC-like	Reference
adenovirus 2	dsDNA	90-100 nm	egress from endosome	clathrin for entry	x		(Meier et al., 2002)
adenovirus 3	dsDNA	90-100 nm	entry	main	x		(Amstutz et al., 2008)
adenovirus 35	dsDNA	90-100 nm	entry	main	x		(Kalin et al., 2010)
African Swine Fever	dsDNA	200 nm	entry	main	x		(Sanchez et al., 2012)
bluetounge virus 1	dsRNA	86 nm	entry	main		x	(Gold et al., 2010)
Dengue virus	ssRNA +	50 nm	entry	clathrin main, MPC alternative	x		(Suksanpaisan et al., 2009)
ebola	ssRNA -	920 nm long, 80 nm diameter	entry	main	x		(Saeed et al., 2010)
				main	x		(Nanbo et al., 2010)
				main, clathrin as minor	x		(Aleksandrowicz et al., 2011)
				main, though atypical	x		(Mulherkar et al., 2011)
				main	x		(Wen et al., 2013)
Epstein Barr Virus	DNA	120-180 nm	apical to basolateral transcytosis	main	x		(Tugizov et al., 2013)
echovirus 1	ssRNA +	24-30 nm	entry	main	x		(Krieger et al., 2013)
HCMV	DNA	100-150 nm	entry	dendritic cells		x	(Haspot et al., 2012)
HIV-1	retrovirus	120 nm	entry	alternative/cell type dependent	x		(Marechal et al., 2001)
			entry	main	x		(Liu et al., 2002)
			entry	dendritic cells	x		(Wang et al., 2008)
			entry	main		x	(Carter et al., 2011)
			entry	alternative		x	(Gobeil et al., 2013)
HPV-16	DNA	600 nm	entry	main, pseudovirus		x	(Schelhaas et al., 2012)
human rhinovirus 14	ssRNA +	30 nm	entry	main		x	(Khan et al., 2010)
Influenza	segmented RNA -	80-120 nm, filamentous ≤500 um	entry	alternative for influenza, main for filamentous influenza	x		(Rossman et al., 2012)
KSHV	DNA	100-150	entry	epithelial		x	(Raghu et al., 2009)

		nm		cells not fibroblasts			
LASV and Junin virus, LCMV	ssRNA, ambisense, ssRNA -	lassa: 120 nm junin: 50-300 nm	entry	main	x		(Iwasaki et al., 2014)
Nipah Virus	ssRNA -	40-600 nm	entry	direct fusion or MPC	x		(Pernet et al., 2009)
Porcine Parvovirus	ssDNA	20 nm	entry	clathrin and MPC (aggregate particles)	x		(Boisvert et al., 2010)
Vaccinia Virus	linear ds DNA	360 × 270 × 250 nm	entry	main	x		(Mercer and Helenius, 2008)
				filopodia (Cdc42) vs. blebbing (Rac1)	x		(Mercer et al., 2010)
				intracellular mature virus (MV) (alternative) and extracellular enveloped virus (EV) main	x		(Sandgren et al., 2010)
				EVs using MPC	x		(Schmidt et al., 2011)

Appendix A: CORONAVIRUS REPLICASE-REPORTER FUSIONS PROVIDE QUANTITATIVE ANALYSIS OF REPLICATION AND REPLICATION COMPLEX FORMATION

Articles of Significant Interest Selected from This Issue by the Editors

Adenovirus E1A Uses Paf1 and Bre1 To Stimulate Transcript Elongation by RNA Polymerase II

Adenovirus E1A is a potent transcriptional activator widely used to study control of transcriptional initiation. E1A functions through subversion and repurposing of cellular factors. Fonseca et al. (p. 5630–5637) describe a process by which E1A recruits the human Bre1 and Paf1 chromatin-modification complexes to viral genes to enhance transcriptional elongation by RNA polymerase II. This study reveals a new mechanism employed by E1A to stimulate viral transcription, which functions at the level of transcriptional elongation.

Coronavirus Replicase-Reporter Viruses Quantify Early Replication Events

Coronavirus replication occurs in association with virus-induced membrane structures, but the dynamics of replication complex formation are not well understood. Freeman et al. (p. 5319–5327) engineer murine hepatitis viruses to express green fluorescent protein or firefly luciferase as fusions with replicase nonstructural proteins 2 and 3, indicating that the coronavirus replicase gene can accommodate expansion and expression of reporters in viable viruses. These viruses can be used to quantify replication complex formation and virus replication in infected living cells.

A Nudivirus DNA Integrated into a Plant Sap-Sucking Insect Genome

Nudiviruses are a diverse group of double-stranded DNA viruses that preferentially infect insects and marine arthropods. Transmission usually occurs through feeding or mating. Cheng et al. (p. 5310–5318) report that a nudivirus can integrate its genome into chromosomes of the brown planthopper, a sap-sucking hemipteran insect. These results highlight an example of coevolution of an invertebrate virus and a plant sap-sucking insect and enhance an understanding of nudivirus evolution.

Assembly of an Icosahedral Virus Requires Only Weak Protein-Protein Interactions

Bacteriophage P22 serves as a model for assembly of double-stranded DNA viruses with icosahedral capsids. The P22 procapsid, an assembly intermediate, is generated when coat protein interacts with an internal scaffolding protein. A single basic amino acid in this scaffolding protein is required to direct procapsid assembly, although other residues modulate affinity. Cortines et al. (p. 5287–5297) identify the binding partners in coat protein and show that relatively weak electrostatic interactions between coat and scaffolding proteins power assembly of correctly sized and shaped procapsids. This work illustrates that simple interactions govern virus capsid assembly.

Oncolytic Parvovirus H-1PV Induces Immunogenic Cell Death

Oncolytic viruses show promise when used in combination with conventional chemotherapy. Successful lysis of cancer cells requires immunogenic cell death, commonly associated with release of ATP and high-mobility group box protein B1 (HMGB1). Angelova et al. (p. 5263–5276) demonstrate that while oncolytic parovirus H-1PV activates cell death pathways in pancreatic cancer cells, ATP is not released. Moreover, extracellular HMGB1 levels are elevated in all treated cells, whether or not the cells are dying. Treatment with gemcitabine, a chemotherapeutic agent, in combination with H-1PV infection leads to extracellular release of HMGB1. A concomitant increase in interleukin-1β secretion suggests that the consistent induction of HMGB1 serves as a danger signal and activates the inflammasome, thereby converting drug-induced apoptosis into immunogenic cell death.

doi:10.1128/JVI.00815-14

JVI
Journals.ASM.org

Coronavirus Replicase-Reporter Fusions Provide Quantitative Analysis of Replication and Replication Complex Formation

Megan Culler Freeman,[b,c] Rachel L. Graham,[d] Xiaotao Lu,[a,c] Christopher T. Peek,[a,c] Mark R. Denison[a,b,c]

Departments of Pediatrics[a] and Pathology, Microbiology, and Immunology,[b] and Elizabeth B. Lamb Center for Pediatric Research,[c] Vanderbilt University Medical Center, Nashville, Tennessee, USA; Department of Epidemiology, University of North Carolina, Chapel Hill, North Carolina, USA[d]

ABSTRACT

The replication of coronaviruses occurs in association with multiple virus-induced membrane structures that evolve during the course of infection; however, the dynamics of this process remain poorly understood. Previous studies of coronavirus replication complex organization and protein interactions have utilized protein overexpression studies and immunofluorescence of fixed cells. Additionally, live-imaging studies of coronavirus replicase proteins have used fluorescent reporter molecules fused to replicase proteins, but expressed from nonnative locations, mostly late-transcribed subgenomic mRNAs, in the presence or absence of the native protein. Thus, the timing and targeting of native replicase proteins expressed in real time from native locations in the genome remain unknown. In this study, we tested whether reporter molecules could be expressed from the replicase polyprotein of murine hepatitis virus as fusions with nonstructural protein 2 or 3 and whether such reporters could define the targeting and activity of replicase proteins during infection. We demonstrate that the fusion of green fluorescent protein and firefly luciferase with either nonstructural protein 2 or 3 is tolerated and that these reporter-replicase fusions can be used to quantitate replication complex formation and virus replication. The results show that the replicase gene has flexibility to accommodate a foreign gene addition and can be used directly to study replicase complex formation and evolution during infection as well as to provide highly sensitive and specific markers for protein translation and genome replication.

IMPORTANCE

Coronaviruses are a family of enveloped, positive-sense RNA viruses that are important agents of disease, including severe acute respiratory syndrome coronavirus and Middle East respiratory syndrome coronavirus. Replication is associated with multiple virus-induced membrane structures that evolve during infection; however, the dynamics of this process remain poorly understood. In this study, we tested whether reporter molecules expressed from native locations within the replicase polyprotein of murine hepatitis virus as fusions with nonstructural proteins could define the expression and targeting of replicase proteins during infection in live cells. We demonstrate that the replicase gene tolerates the introduction of green fluorescent protein or firefly luciferase as fusions with replicase proteins. These viruses allow early quantitation of virus replication as well as real-time measurement of replication complexes.

Coronaviruses (CoVs) are a family of RNA viruses that are important agents of human and animal diseases (1), including severe acute respiratory syndrome coronavirus (SARS-CoV) and the recently emerged Middle East respiratory syndrome coronavirus (MERS-CoV) (2–5). The genome of the CoV murine hepatitis virus (MHV) is one of the largest known replicating RNA molecules, at 31.3 kb (1). The 5′-most replicase gene is composed of two open reading frames (ORFs), ORF1a and ORF1b, and comprises approximately two-thirds of the genome. Translation begins upon entry into a host cell, first of replicase ORF1a and then of ORF1ab following a −1 ribosomal frameshift. The replicase polyproteins are proteolytically processed by papain-like protease 1 (PLP1) and PLP2 in nsp3 and by the nsp5 protease (3CLpro) to generate 16 nonstructural proteins (nsp1 to nsp16); functions include RNA-dependent RNA polymerase, helicase, primase, cap methylation, and a novel proofreading exonuclease (1). The replicase proteins nsp3, -4, and -6 have been demonstrated to be involved in membrane modifications leading to the formation of double-membrane vesicles (DMVs) (6). Each MHV nsp studied has been shown to localize to virus-induced DMVs and other modified host membranes, collectively referred to as replication complexes (RCs) (7–13). While much has been learned about virus-induced host cell modifications, little is known of the process of RC formation and how RCs change over time. It is known that nucleocapsid is associated with new sites of RNA synthesis but also sites of virus assembly in the endoplasmic reticulum-Golgi intermediate compartment (ERGIC) and in the Golgi compartment distinct from sites of replication (14). The mechanisms by which RCs form, RNA synthesis occurs, and nucleocapsids transit to sites of virion assembly, however, remain unknown.

To date, studies of CoV replication complex formation have involved immunofluorescence imaging of fixed cells using antibodies against native proteins (10, 12, 15, 16). For assessment of kinetics of replication, fluorescent and luminescent reporters have been expressed with either replicase proteins from expression

Received 6 January 2014 **Accepted** 3 March 2014
Published ahead of print 12 March 2014
Editor: S. Perlman
Address correspondence to Mark R. Denison, mark.denison@vanderbilt.edu.
Supplemental material for this article may be found at http://dx.doi.org/10.1128/JVI.00021-14.

doi:10.1128/JVI.00021-14

TABLE 1 Primers used for generation of reporter insertions

Primer	Sequence[a]	Amplification target	Sense	Description
MHV A	5′-AACGGCACTTCCTGCGTGTCCATG	MHV nsp1	+	Common MHV left nsp1 primer
MHV B	5′-CGTCTCCCTTAACACCCGCGATAGCCCTTAAGAAGAG	MHV nsp1	−	Common MHV right nsp1 primer
MHV-GFP C	5′-CGTCTCCTAAGATGGTGAGCAAGGGCGAGGAGCTGT	GFP	+	
MHV-GFP D	5′-CGTCTCGTGCCCTTGTACAGCTCGTCCATGCCGAGAGT	GFP	−	MHV-Δ2-GFP3
MHV-GFP D	5′-CGTCTCGTAACCTTGTACAGCTCGTCCATGCCGAGAGT	GFP	−	MHV-GFP2
MHV-FFL C	5′-CGTCTCCTAAGATGGAAGACGCCAAAAACATAAAGAAAG	FFL	+	
MHV-FFL D	5′-CGTCTCGTGCCCAATTTGGACTTTCCGCCCTTCTT	FFL	−	MHV-Δ2-FFL3
MHV-FFL D	5′-CGTCTCGTAACCAATTTGGACTTTCCGCCCTTCTT	FFL	−	MHV-FFL2
MHV E	5′-CGTCTCGTATCGCGGTGTTAAGAAAGTCGAGTTTAAC	MHV nsp3	+	Common MHV left nsp3 primer
MHV F	5′-ACTTGCACATATGAGACACAACGTCCCCA	MHV nsp3	−	Common MHV right nsp3 primer

[a] Underlining indicates residues added for cloning or mutagenesis purposes.

plasmids, reporter proteins replacing nonessential accessory ORFs, or replicase protein-reporter fusions expressed in place of accessory ORFs (17–20). Reporters have also been utilized within CoV replicon genomes (21). Studies with such constructs have provided insights into the function and interaction of replicase proteins during viral replication, and the constructs have also served as reporters for studies of CoV inhibitors (21–24). While these strategies have been useful for reports on overall virus replication, they were not designed to test the expression or localization of specific proteins, nor were they designed to report replicase gene expression. A replicase reporter virus has been constructed for equine arteritis virus, an arterivirus with a genome size less than half that of MHV, with the insertion of enhanced green fluorescent protein (EGFP) between nsp1 and nsp2 (25). The capacity of the CoV replicase gene to accept foreign genes, however, is not known, nor has foreign gene insertion within the replicase gene of any replicating CoV been tested without a compensatory deletion of viral genetic material. In this study, we describe the quantitative measurement of MHV replicase gene expression and the formation of replication complexes using engineered reporter viruses expressing green fluorescent protein (GFP) and firefly luciferase (FFL) as in-frame fusions with viral replicase proteins nsp2 and nsp3. nsp2 is a 65-kDa protein that has been shown to localize to CoV replication complexes but is dispensable for virus replication in culture (26). nsp3 is a 210-kDa protein that contains two essential proteases and other functional protein domains and is required for both virus-induced membrane modifications and virus replication (6). We demonstrate that GFP and FFL reporter fusions with nsp2 and nsp3 permit efficient virus replication, target replication complexes, provide the earliest indicators of MHV replication, and allow direct measurements of replication complex formation. These results also demonstrate the capacity of the MHV genome to tolerate expansion and identify sites for possible virus-mediated expression of foreign proteins within the replicase polyprotein.

MATERIALS AND METHODS

MHV and previously described mutant viruses, cells, and antibodies. Recombinant murine hepatitis virus strain A59 (GenBank accession number AY910861) was used as the wild type (WT) for all experiments (27, 28). MHV-Δnsp2, with an in-frame deletion of nsp2, and MHV-ΔCS2, with a deletion of the nsp2-3 cleavage site P1 Glu, were described previously (26). Delayed brain tumor (DBT) cells (29) and baby hamster kidney cells expressing the MHV receptor (BHK-MHVR) (30, 31) were grown in Dulbecco's modified Eagle medium (DMEM) that contained 10% fetal bovine serum (FBS), 1% 1 M HEPES, 100 units/ml of penicillin, 100 μg/ml streptomycin, and 0.23 μl/ml amphotericin B for all experiments. Medium for BHK-MHVR cells was supplemented with G418 (0.8 mg/ml) for selection of cells expressing the receptor. The polyclonal antibodies used in biochemical and imaging experiments were described previously. All polyclonal antibodies were raised in rabbits unless otherwise indicated. For MHV, these included antibodies specific for nsp1 (VU221) (16), nsp2 (VU154) (15), nsp3 (VU164) (26), and nsp8 (VU123) (11). Mouse monoclonal anti-firefly luciferase (FFL), clone LUC-1, was purchased from Sigma-Aldrich. Mouse monoclonal antibody specific for full-length GFP was purchased from SantaCruz Biotechnology. Mouse monoclonal antibody against the viral membrane protein (M) was generously provided by J. Fleming (University of Wisconsin, Madison).

Construction of mutant MHV cDNA plasmids. Insertions of reporter genes in place of the nsp2 coding sequences of MHV were engineered by using PCR with primers shown in Table 1. For ABCDEF primer sets, primers A and B generated an A/B PCR product, primers C and D generated a C/D PCR product, and primers E and F generated an E/F PCR product. AB, CD, and EF PCR amplicons were ligated into an ABCDEF product by using the class IIs restriction enzyme method, and ligation products were cloned into the appropriate fragment A vector by using unique sites: 5′-SacII and 3′-NdeI. Successful insertions of reporter gene sequences were confirmed by restriction digestion and sequencing. The infectious cDNA fragment A construct (pCR-XL-Topo-A), which consists of genome nucleotides (nt) 1 to 4882, was used as the template DNA (33). Reporter genes were cloned from pEGFP-C1 (GFP; Clontech) and pGEM-Luc (firefly luciferase; Promega).

Generation of MHV mutant viruses. Viruses containing PCR-generated insertions within the viral coding sequence were produced by using infectious cDNA assembly strategies for MHV as previously described, with modifications (27, 28, 33, 34). Plasmids containing the seven cDNA cassettes of the MHV genome were digested by using MluI, BsmBI, and SfiI for fragment A; BglI and BsmBI for fragments B and C; BsmBI and NciI for fragments D and E; BsmBI for fragment F; and BsmBI and SfiI for fragment G. Digested, gel-purified fragments were ligated together in a total reaction volume of ~100 μl overnight at 16°C. Following chloroform extraction and isopropanol precipitation of ligated DNA, capped, polyadenylated, full-length RNA transcripts of MHV infectious cDNA were generated *in vitro* by using the mMessage mMachine T7 transcription kit (Ambion) according to the manufacturer's protocol, with modifications. Twenty-microliter reaction mixtures were supplemented with 3 μl of 30 mM GTP, and transcription was performed at 40.5°C for 25 min, 37.5°C for 50 min, and 40.5°C for 25 min. In parallel, capped, polyadenylated RNA transcripts encoding the corresponding nucleocapsid (N) proteins were generated *in vitro* by using N cDNA generated by PCR (33, 34). N transcripts and mutant viral transcripts were then mixed and electroporated into BHK-MHVR cells. Cells were grown to subconfluence, trypsinized, and then washed twice with phosphate-buffered saline (PBS) and resuspended in PBS at a concentration of 10^7 cells/ml. Six hundred microliters of cells was then added to RNA transcripts in a 4-mm-gap

electroporation cuvette (BTX), and three electrical pulses of 850 V at 25 μF were delivered with a Bio-Rad Gene Pulser Xcell electroporator. Transfected cells were then seeded onto a layer of 10^6 uninfected DBT cells in a 75-cm^2 flask and incubated at 37°C for 30 to 90 h. Virus viability was determined by syncytium formation. RNA was recovered from infected cell monolayers by using TRIzol (Invitrogen) according to the manufacturer's instructions, and retention of the introduced mutations was verified by reverse transcription-PCR (RT-PCR) and sequencing.

Microscopy. DBT cells grown to 60% confluence on 12-mm glass coverslips were infected with reporter viruses. At 10 h postinfection (p.i.), medium was aspirated from cells, and cells were fixed and permeabilized in methanol at −20°C overnight. Cells were rehydrated in PBS for 20 min and blocked in PBS containing 5% bovine serum albumin (BSA). Blocking solution was aspirated, and cells were washed with immunofluorescence (IF) assay wash solution (PBS containing 1% BSA and 0.05% Nonidet P-40) at room temperature. Cells were incubated with primary antibodies where indicated (anti-nsp8 at a 1:250 dilution, anti-M at 1:1,000, or anti-FFL [Sigma-Aldrich] at 1:1,000) for 45 min. Cells were washed in IF wash solution 3 times for 5 min per wash. Cells were incubated in secondary antibodies (goat anti-rabbit Alexa Fluor 488 [1:1,000] or Alexa Fluor 546 [1:1,500]; Invitrogen Molecular Probes) for 30 min. Cells were washed 3 times for 5 min per wash, followed by a final wash in PBS, and then rinsed in distilled water. Coverslips were mounted with Aquapolymount (Polysciences) and visualized by confocal immunofluorescence microscopy on a Zeiss LSM 510 laser scanning confocal microscope at 488 and 543 nm with a 40× oil immersion lens. Images were processed and assembled by using Adobe Photoshop CS2 (9.0.2). For live-cell fluorescence microscopy, DBT cells were seeded onto 35-mm glass-bottom culture dishes (MatTek). Forty-eight hours later, cells were infected with MHV-GFP2 at a multiplicity of infection (MOI) of 1 PFU/cell. At 5 h p.i., plates were transferred to the live-cell incubator surrounding the objective stage of a Nikon Eclipse TE-2000S wide-field fluorescence microscope. Cells were imaged by using a 40× oil immersion lens through differential interference contrast (DIC) and fluorescein isothiocyanate (FITC) filters, with images being captured at 30-s intervals over the course of 4 h. Resulting images were merged and assembled by using Nikon Elements, ImageJ, and Adobe Photoshop CS2.

Protein immunoprecipitations. For protein labeling and immunoprecipitation experiments, cells were infected with MHV at an MOI of 10 and incubated at 37°C. At 4 h p.i., medium was aspirated and replaced with medium lacking methionine and cysteine and supplemented with actinomycin D (Sigma) at a final concentration of 20 μg/ml. At 5 h p.i., cells were labeled with [^{35}S]Met-Cys at a concentration of 0.08 mCi/ml. Radiolabeled cells were lysed in 1 ml no-SDS lysis buffer (1% NP-40, 0.5% sodium deoxycholate [DOC], 150 mM sodium chloride [NaCl], and 50 mM Tris [pH 8.0]) at 7 to 10 h p.i. Cellular debris and nuclei were pelleted by centrifugation at 14,000 × *g* for 3 min at room temperature (RT), and the supernatant was transferred into a fresh tube. One hundred microliters of cell lysate was subsequently used per 400 μl of immunoprecipitation reaction buffer. The lysate was combined with protein A-Sepharose beads and a 1:200 dilution of antibody in no-SDS lysis buffer supplemented with 1% SDS. After incubation at 4°C for 18 h, beads were pelleted and washed with low-salt lysis buffer (0.1% SDS lysis buffer with 150 mM NaCl), followed by high-salt lysis buffer (no-SDS lysis buffer with 1 M NaCl) and a final low-salt wash (0.5% SDS lysis buffer with 150 mM NaCl). After rinsing, proteins were eluted by the addition of 2× LDS (lithium dodecyl sulfate)–1× DTT (dithiothreitol) buffer (NuPage; Invitrogen) to the pelleted beads, which were heated at 70°C for 10 min prior to electrophoresis of the supernatant on 4 to 12% Bis-Tris or 3 to 8% Tris-acetate gels (NuPage; Invitrogen). A full-range rainbow ladder (GE Healthcare) and a ^{14}C ladder (PerkinElmer LAS) were used as molecular weight standards.

Viral replication assays. For viral replication analysis, DBT cells were infected in triplicate with WT MHV or mutant viruses at the MOIs indicated for each experiment. Following a 30-min adsorption with rocking at RT, medium was aspirated, and cells were washed 3 times with PBS and then incubated with prewarmed medium at 37°C. Aliquots of medium were collected from 0 to 24 h p.i., and virus titers were determined by plaque assays on DBT cells in duplicate, as described previously (35).

Competition assay. Confluent monolayers of DBT cells in T25 flasks were infected with WT MHV or MHV-GFP2 alone or at a 1:1, 1:10, or 10:1 ratio of WT MHV to MHV-GFP2 at a total MOI of 0.1 PFU/cell. Each flask was passaged 10 times, as described above for serial virus passages, and 1 ml supernatant was collected and stored at −80°C. DBT cells were seeded onto glass coverslips and infected at an MOI of 1 PFU/cell with passage 1 (P1), P3, and P10 of each combination of viruses. At 8 h p.i., slides were fixed with cold methanol (MeOH). Coverslips were immunostained with primary antibodies specific for nsp8 and a secondary antibody, goat anti-rabbit Alexa Fluor 546, as described above. Coverslips were mounted with Aquapolymount (Polysciences) and visualized by immunofluorescence microscopy on a Nikon Eclipse TE-2000S wide-field fluorescence microscope. Cells were imaged by using a 40× oil immersion lens through DIC, FITC, Cy3, and 4′,6-diamidino-2-phenylindole (DAPI) filters. The resulting images were merged and assembled by using Nikon Elements, ImageJ, and Adobe Photoshop CS2.

Luciferase activity versus viral replication assay. DBT cells in 6-well plates were infected with MHV-Δ2-FFL3 or MHV-FFL2 at an MOI of 1 PFU/cell and incubated at 37°C for 30 min. At 0.5 h p.i., medium was aspirated to remove the inoculum, and cells were washed three times with PBS and supplemented with prewarmed medium. At time points through 24 h p.i., the supernatant was harvested or cells were lysed in reporter lysis buffer (Promega) and subjected to one freeze-thaw cycle. Following freeze-thaw, lysates were vortexed and centrifuged briefly at top speed, and supernatants were transferred into new tubes. To measure luciferase activity, 20 μl of lysate was added to each well of an opaque 96-well plate. Plates were loaded onto a Chameleon luminometer, and an automatic injector was used to add 100 μl of reconstituted luciferase assay reagent (Promega) to each well as the samples were being read, for 5 s per well without delay. Viral replication was determined from harvested supernatants by a plaque assay, as described above.

RESULTS

Generation and recovery of MHV replicase reporter viruses. Since nsp2 is dispensable for replication (26), we first tested the tolerance for reporter expression in place of deleted nsp2. This approach was also used because the engineered genome length would not exceed that of WT MHV. We engineered constructs in which enhanced green fluorescent protein (EGFP) (0.71 kb/26.8 kDa) or firefly luciferase (FFL) (1.65 kb/60.7 kDa) (Fig. 1) replaced the nsp2 coding sequence. All constructs were initially designed with PLP1-specific cleavage sites at the N and C termini of the reporter, based on the hypothesis that processing of the reporter from nsp1 and nsp3 would be required for viability. Following electroporation of *in vitro*-transcribed genome RNA into BHK cells layered onto permissive DBT cells, cytopathic effect (CPE) of syncytia was detected by 24 h postelectroporation for both recombinant viruses. Medium supernatants from electroporated cultures were used to infect fresh DBT cells, and RNA was harvested and amplified by RT-PCR for sequencing of the entire genome. Viral genome sequencing demonstrated the retention of reporter genes without additional mutations in the genome. Passage of the P0 virus in culture demonstrated the stability of the inserted GFP and FFL sequences for >5 passages (data not shown). This confirmed the capacity of MHV to accept proteins of differing sizes and structures in place of deleted nsp2. These viruses are referred to as MHV-Δ2-GFP3 and MHV-Δ2-FFL3. We next determined the capacity of the MHV replicase to accept additional genetic material into its genome without deletion of the

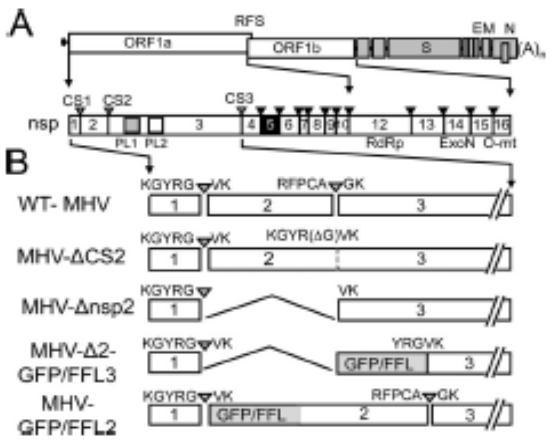

FIG 1 Generation and recovery of MHV replicase reporter viruses. (A) Schematic of MHV genome organization with ORF1a and ORF1b connected by a ribosomal frameshift (RFS) and downstream structural/accessory ORFs. S, spike; E, envelope; M, membrane; N, nucleocapsid. The ORF1ab polyprotein of MHV is shown with nonstructural protein domains 1 to 16 (nsp). Papain-like proteinase domains PL1 and PL2 are indicated by gray and white boxes, respectively, in nsp3. The nsp5 protease (3CLpro and Mpro) is indicated by the black box. Cleavages mediated by each domain are indicated by correspondingly colored arrowheads (CS1, cleavage site 1). Deletion is indicated by Δ. (B) Design of reporter fusion viruses. The top schematic shows WT MHV-A59 nsp1-nsp3 with cleavage site residues P5–P2′, with cleavage sites marked by carets. The next schematics show previously described MHV-ΔCS2 (lacking P1 Gly at the nsp2-3 cleavage site) and MHV-Δnsp2 with an in-frame deletion of nsp2 and a functional engineered nsp1-nsp3 cleavage site. GFP and FFL reporter gene insertions are indicated in gray. All confirmed functional cleavages are indicated by gray arrowheads. MHV-Δ2-GFP/FFL3, MHV with a deletion of nsp2 and fusion of GFP or FFL to nsp3; MHV-GFP/FFL2, MHV with the addition of GFP or FFL as a fusion to nsp2.

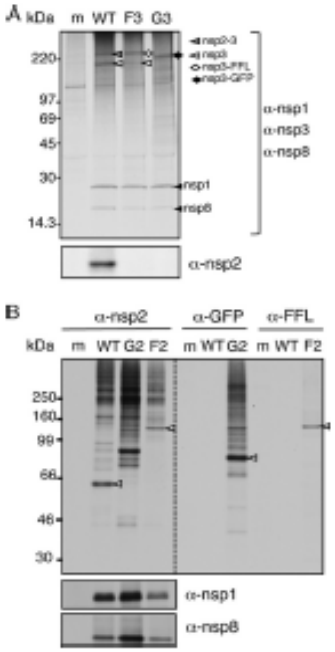

FIG 2 Polyprotein expression and processing in MHV replicase reporter viruses. (A) DBT cells were infected with WT MHV, MHV-Δ2-GFP3 (G3), and MHV-Δ2-FFL3 (F3). Radiolabeled proteins were immunoprecipitated by combined antibodies for nsp1, nsp3, and nsp8 and detected by fluorography. Molecular mass markers are indicated on the left. nsp3, nsp2-3, FFL-nsp3, and GFP-nsp3 are indicated. m, mock. (B) DBT cells were infected with WT MHV, MHV-GFP2 (G2), and MHV-FFL2 (F2), as indicated by the top labels, and radiolabeled proteins were harvested by immunoprecipitation and detected by fluorography. Antibodies used are indicated to the right or at the top. The dashed line represents the same gel with different exposure times: overnight on the left and 1 week on the right. Molecular mass markers are indicated on the left. nsp2, GFP-nsp2, and FFL-nsp2 are indicated by white arrowheads.

viral sequence. GFP and FFL were engineered between nsp1 and nsp2 while retaining all viral proteins. Since we sought to test whether reporter fusions with nsp2 could be recovered, we retained the cleavage site between nsp1 and the reporter but deleted the cleavage site between the reporter and the nsp2 amino terminus (Fig. 1B). Both recombinant viruses were recovered, their sequences were confirmed, and they were passaged for >5 passages, with retention of the introduced sequences (data not shown). These viruses are referred to as MHV-GFP2 and MHV-FFL2.

Polyprotein expression and processing in MHV replicase reporter viruses. MHV-Δ2-GFP3 and MHV-Δ2-FFL3 mutant viruses were engineered with predicted functional cleavage sites at the nsp1 and nsp3 junctions. To define the processing of nsp1-reporter-nsp3 from the replicase polyprotein, DBT cells were infected with WT MHV, MHV-Δ2-GFP3, or MHV-Δ2-FFL3 and radiolabeled, and proteins were immunoprecipitated from lysates of infected cells with antibodies specific for nsp1, -2, -3, and -8 (Fig. 2A). Immunoprecipitation of lysates from WT MHV-infected cells detected nsp1, -2, -3, -2-3, and -8. Immunoprecipitation of proteins from cell lysates of MHV-Δ2-FFL3- and MHV-Δ2-GFP3-infected cells detected both nsp1 and nsp8 but not nsp2, as expected. This indicated that processing was occurring at the junction between nsp1 and FFL/GFP and that expression and processing of downstream proteins from the replicase polyprotein were intact. Immunoprecipitation with anti-nsp3 in WT-infected cells detected the 210-kDa nsp3 as well as the known nsp2-nsp3 intermediate precursor (275 kDa). In contrast, a 210-kDa nsp3 protein was barely detectable following infection with MHV-Δ2-FFL3 and not detected from cells infected with MHV-Δ2-GFP3. Instead, anti-nsp3 antibodies detected a protein of ~271 kDa in MHV-Δ2-FFL3-infected cells (the predicted mobility of nsp3 plus FFL) and a protein of ~237 kDa in MHV-Δ2-GFP3-infected cells (the predicted mobility of nsp3 plus GFP). These results indicate that reporter molecules are efficiently processed at the nsp1-reporter junctions but minimally or not processed at the engineered cleavage sites between the reporter and nsp3. This suggested that while P1′ to P5′ residues are required for cleavage, the context of P5-P1 is also important. This result serendipitously demonstrated that viable recombinant MHV could be engineered with a reporter fusion with the 210-kDa nsp3 protein.

This outcome served as the rationale for the design of the "second-generation" reporters, with a retained cleavage site between nsp1 and the reporter and a deletion of the cleavage site between the reporter and nsp2. For MHV-GFP2 and MHV-FFL2, immu-

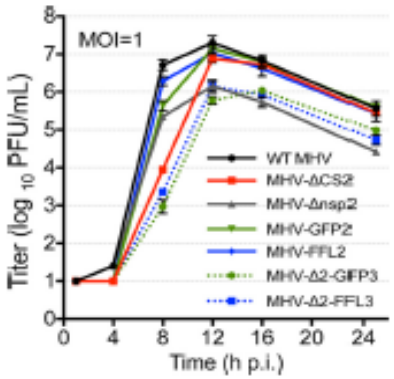

FIG 3 Replication of MHV reporter fusion viruses. DBT cells were infected with recombinant WT MHV, MHV-Δnsp2, MHV-ΔCS2, MHV-Δ2-GFP3, MHV-Δ2-FFL3, MHV-GFP2, and MHV-FFL2 at an MOI of 1 PFU/cell. The supernatant was sampled at the indicated times p.i., and titers were determined by plaque assays. Titers reported are the averages of three replicates ± standard deviations.

noprecipitation of infected cell lysates with anti-nsp1 and anti-nsp8 detected the respective proteins. Antibodies against nsp2 detected the 65-kDa nsp2 in WT-infected lysates but did not detect nsp2 in either reporter virus. Instead, anti-nsp2 immunoprecipitated proteins of 92 kDa or 126 kDa, consistent with the predicted sizes of the GFP-nsp2 and FFL-nsp2 fusion proteins, respectively (Fig. 2B). To confirm this, we immunoprecipitated lysates with anti-GFP and anti-FFL antibodies. Anti-FFL detected a protein from MHV-FFL2-infected cells with a mobility identical to that detected by anti-nsp2. The anti-GFP immunoprecipitation of MHV-GFP2-infected lysates detected a protein with a mobility differing slightly from that of anti-nsp2 but consistent with a fusion of nsp2-GFP. The reason for the difference in mobility is not clear but suggests different migrating forms of nsp2-GFP with different available epitopes recognized by anti-nsp2 and anti-GFP. The complete lack of nsp2 and the detection of new proteins consistent with nsp2-GFP and nsp2-FFL strongly supported the expression of stable fusion proteins that are not cleaved during infection. Overall, these results indicated that the recombinant viruses expressed the reporters as fusions with nsp3 or with nsp2.

Replication of MHV-Δ2-GFP3, MHV-Δ2-FFL3, MHV-GFP2, and MHV-FFL2. Previous work in our laboratory has shown that MHV-Δnsp2 replicates with kinetics similar to those of WT MHV but with a lower peak titer (26), while MHV mutants engineered to abolish cleavage site 2 between nsp2 and nsp3 (MHV-ΔCS2) demonstrated a prolonged eclipse phase but ultimately achieved WT-like peak titers (36). Finally, a loss of cleavage between nsp1 and nsp2 has been demonstrated to result in a decreased viral yield but WT-like timing of exponential replication (37). To test the effect of reporter fusions with nsp2 or nsp3, we infected murine DBT cells with MHV-Δ2-GFP3, MHV-Δ2-FFL3, MHV-GFP2, or MHV-FFL2 in direct comparison with WT MHV, MHV-Δnsp2, and MHV-ΔCS2, with measurement of supernatant virus titers by plaque assays at multiple time points postinfection (Fig. 3). MHV-Δnsp2 replicated with a 1-$\log_{10}$ impairment in viral titers but normal timing of exponential replication. MHV-ΔCS2 (nsp2-3 fusion) also replicated as previously reported, with delayed exponential replication but WT-like virus yield. MHV-Δ2-GFP3 and MHV-Δ2-FFL3 replication resulted in a cumulative phenotype: a 4-h delay in exponential replication similar to that of MHV-ΔCS2 and a decreased viral yield similar to that of MHV-Δnsp2. In contrast, both MHV-GFP2 and MHV-FFL2 demonstrated replication in culture with exponential replication and viral yields similar to those of WT MHV. This suggests that the replication phenotypes of MHV-Δ2-GFP3 and MHV-Δ2-FFL3 result from the deletion of nsp2 and the fusion of nsp2 with nsp3 and not from the insertion of foreign genes themselves. These results support our previous studies proposing that cleavage at the nsp3 N terminus is required for efficient onset of exponential replication (36). Similarly, the WT-like replication of MHV-GFP2 and MHV-FFL2 further shows that it is cleavage at the C terminus of nsp1 that is required for a WT-like yield. Finally, the results demonstrate that expansion of the replicase gene and polyprotein can still allow for WT-like replication.

Subcellular localization of nsp2 and nsp3 fusion reporters. We next tested the expression and localization of nsp2 and nsp3 reporter fusions in virus-infected cells. DBT cells on glass coverslips were infected with reporter-expressing MHV at an MOI of 1 PFU/cell, fixed at 10 h p.i., stained for replicase proteins, and examined by confocal microscopy (Fig. 4). DBT cells infected with WT MHV and stained with antibodies for nsp2, nsp3, nsp8, or membrane (M) protein demonstrated the established punctate cytoplasmic pattern of localization (Fig. 4A). Cells infected with MHV-Δ2-GFP3 or MHV-Δ2-FFL3 also exhibited a punctate, perinuclear cytoplasmic localization of reporter molecules by native fluorescence (GFP) or by IF with anti-FFL. Both GFP and FFL colocalized with nsp8 (Fig. 4B), a replicase protein known to localize to replication complexes, but were distinct from M, which localizes to sites of viral assembly in the ERGIC/Golgi compartment (Fig. 4A and data not shown for FFL). The punctate nature of the reporter localization suggests a mechanism for specific targeting to replication complexes. In addition, these results demonstrate that GFP fluorescence is intact when the reporter is fused to the N terminus of nsp3. DBT cells infected with MHV-GFP2 (Fig. 4C) also exhibited a punctate, perinuclear cytoplasmic localization and colocalized with nsp2 and nsp8, again demonstrating specific targeting to replication complexes and indicating that native fluorescence is intact in the nsp2-reporter fusion protein.

Competitive fitness of WT MHV versus MHV-GFP2. Since MHV-FFL2 and MHV-GFP2 demonstrated WT-like kinetics during replication in culture, we tested whether there was a fitness cost associated with the introduction of a foreign protein into the replicase polyprotein. Cells were infected with WT MHV or MHV-GFP2 alone or at a WT MHV/MHV-GFP2 ratio of 1:1, 1:10, or 10:1 at a combined MOI of 0.1 PFU/cell, followed by 10 passages of supernatant into fresh flasks of DBT cells. We then compared GFP expression with the expression of the replicase protein nsp8 to determine the relative competitiveness of MHV-GFP2. DBT cells seeded onto glass coverslips were infected with P1, P3, and P10 passages of each combination of viruses for 8 h. Following immunostaining for nsp8, coverslips were imaged and scored for nsp8 (indirect immunofluorescence [red]) and GFP (native green fluorescence). At all passages, WT MHV-infected cells exhibited only an nsp8 (red) signal, while MHV-GFP2-infected cells demonstrated colocalized nsp8 (red) and native GFP signals in all cells (Fig. 5). In competition experiments, at P1, MHV-GFP2-infected cells were detected but not at levels equiva-

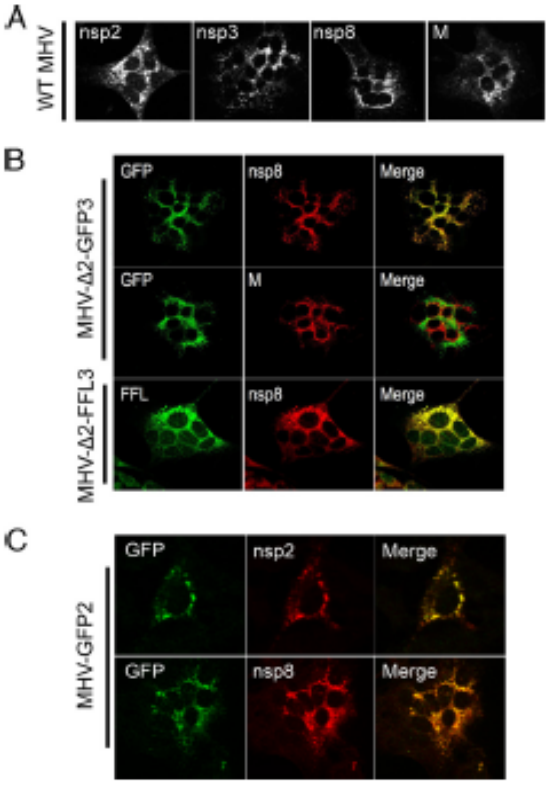

FIG 4 MHV nsp2 and nsp3 fusion reporters localize to replication complexes. DBT cells were infected with WT MHV (A), MHV-Δ2-GFP3 or MHV-Δ2-FFL3 (B), or MHV-GFP2 (C). At 10 h p.i., cells were fixed, stained with the indicated antibodies (anti-FFL, anti-nsp2, anti-nsp3, anti-nsp8, and anti-M), and imaged by confocal microscopy. GFP was detected by native fluorescence.

lent to the input ratios. By P3 to P10, even when a 10-fold advantage was given to MHV-GFP2, the recombinant virus could not compete with the WT. Thus, while GFP as a fusion with nsp2 had no effect on replication as measured by plaque assays, the insertion of the gene was associated with a fitness cost compared to the WT virus.

MHV-GFP2 allows quantitation of replication complex formation in live cells. We tested whether reporter-nsp fusions could be used to track the quantity and movement of these proteins within a single infected cell over time. DBT cells cultured in glass-bottomed dishes were infected with MHV-GFP2, and at 5 h p.i., they were imaged in a live-imaging chamber incubator at 37°C on a wide-field fluorescence microscope. Images were collected in the differential interference contrast (DIC) and green filter sets every 30 s for 2.5 h from the same field (Fig. 6; see also Fig. S1 in the supplemental material). Every 10th image was analyzed for corrected total cell fluorescence (CTCF) by selecting the cell as the region of interest (ROI) and correcting for the background within each individual image (38). Green fluorescence was evident from the first frame, and the CTCF value nearly tripled throughout infection, until it peaked at 6.75 h p.i. At the conclusion of imaging

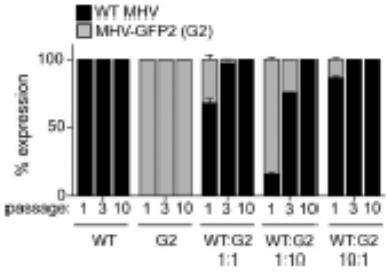

FIG 5 Competitive fitness of WT MHV and MHV-GFP2. DBT cells were infected with WT MHV or MHV-GFP2 alone or at a 1:1, 1:10, or 10:1 ratio of WT MHV to MHV-GFP2. DBT cells on glass coverslips were infected at an MOI of 1 PFU/cell with P1, P3, and P10 passages of each combination. At 8 h p.i., cells were fixed and imaged for nsp8 (red) and GFP (green). Cells containing green (MHV-GFP2) or red (WT MHV or MHV-GFP2) replication complexes were scored. Thirty images from two independent experiments were obtained and scored for cells infected only with WT MHV or only with MHV-GFP2, while for the samples infected with WT MHV and MHV-GFP2 at 1:1, 1:10, and 10:1 ratios, 50 images from two independent experiments were scored.

at 7.5 h p.i., the CTCF value decreased from the peak value by 30%. Throughout the collection of images, green fluorescence was localized perinuclearly, with increasing numbers and intensities of GFP foci from 5 to 7.5 h p.i. The increase in fluorescence intensity during infection indicates that more copies of GFP-nsp2 are being produced and accumulating, as each copy of nsp2 is fused to only

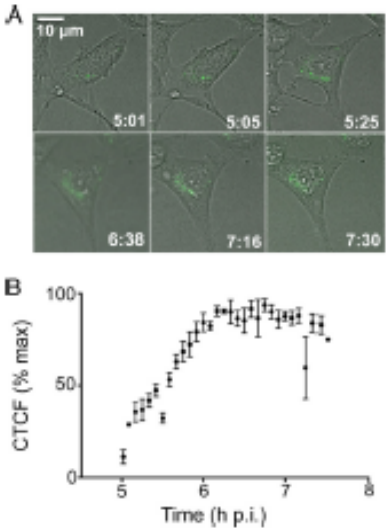

FIG 6 MHV-GFP2 quantitation of replication complex formation in live cells. (A) DBT cells on glass-bottom culture dishes were infected with MHV-GFP2 at an MOI of 1 PFU/cell. At 5 h p.i., dishes were transferred to a chamber incubator at 37°C, with imaging of DIC and GFP every 30 s for 2.5 h. Individual frames were used to generate this panel. The video sequence corresponding to this figure can be found in Fig. S1 in the supplemental material. (B) Corrected total cell fluorescence (CTCF) was measured for the cell by utilizing ImageJ. CTCF was calculated for every 10 frames and plotted over time. Data shown were calculated from three independent infected cells.

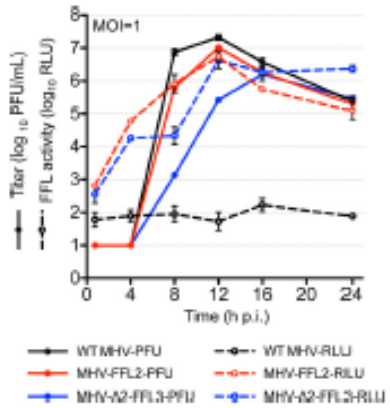

FIG 7 MHV-FFL2 and MHV-Δ2-FFL3 are quantitative measures of replication. DBT cells were infected with MHV-Δ2-FFL3 or MHV-FFL2 at an MOI of 1 PFU/cell in replicate wells. At the indicated times p.i., the supernatant was collected for measurement of virus titers by plaque assays, and cells were harvested for measurement of FFL activity. Titers (PFU) (solid lines) and luminescence (RLU) (dotted lines) are plotted. Data are represented as means ± standard deviations of three replicates.

one fluorescent molecule, in contrast to indirect fluorescence, where multiple fluorescent molecules have the capacity to bind to one viral protein. These results indicate that the reporter viruses MHV-GFP2 and MHV-Δ2-GFP3 can be used to directly measure the progression of RC formation in real time in single infected cells as well as to track the localization and movement of nsp2 and nsp3 over time.

Use of MHV-FFL2 and MHV-Δ2-FFL3 for quantitation of early virus replication. Translation of input genome RNA is the first step in virus replication, and ORF1a, encoding the nsp2 and nsp3 domains, is translated 100% of the time. We hypothesized that this would allow translation of luciferase to provide an earlier marker of viral replication. We inquired whether FFL expressed as fusions with nsp2 or nsp3 could be used to quantitatively measure replication and, if so, whether it was as sensitive as determination of virus titers. DBT cells were infected with MHV-FFL2 or MHV-Δ2-FFL3 at an MOI of 1 PFU/cell, supernatants were collected for plaque assays, and cells were harvested for luciferase assays at multiple times postinfection (Fig. 7). Both MHV-FFL2 and MHV-Δ2-FFL3 replicated as expected, with MHV-Δ2-FFL3 demonstrating delayed exponential replication and decreases in virus yield compared to MHV-FFL2. Luciferase activity (yield in relative light units [RLU]) for MHV-FFL2 showed a signal >3 $\log_{10}$ higher than the corresponding titer at 4 h p.i. while increasing in signal over time. At 8 h p.i., measurements of luciferase activity and titers were very similar. MHV-Δ2-FFL3-infected cells also demonstrated a >3-$\log_{10}$ increase in FFL signal compared to viral titers at 4 h p.i., but this increased signal was retained until 16 h p.i. Most importantly, for both viruses, FFL activity was detected earlier and was 100-fold higher than the virus titer during the eclipse phase. The amplification trend for MHV-FFL2 luminescence mirrors replication, as does the trend for MHV-Δ2-FFL3, suggesting that this assay can serve as a robust early surrogate for viral replication. Furthermore, the results demonstrate that replicase gene translation is occurring continuously and that the genome used as a translational template is being amplified, even in virus with a delayed exponential increase in virus titers. These results establish that the expression of the FFL reporter from the MHV replicase serves as a sensitive, quantitative marker of replicase polyprotein translation and as a discriminating indicator of viral replication. These results also suggest that it may be possible to uncouple measurements of genome translation and genome replication from measurements of infectious virus, which might act as a much earlier biological marker for studies of virus inhibition or studies or constitutive or conditional mutations.

DISCUSSION

In this study, we demonstrate that the CoV genome is capable of tolerating large substitutions or additions of foreign genetic material within the replicase protein as in-frame protein domains. Furthermore, we show that the fusion of reporters to replicase proteins is tolerated in efficiently replicating virus, allowing quantitative assessments of multiple stages of the virus life cycle. Specifically, these studies show that measurement of viral replication by using FFL can be a highly sensitive, early, and powerful surrogate for genome replication and that GFP fusions with nsp2 and nsp3 can allow quantitative assessments of replication complex formation and evolution during the course of infection. Finally, the results show that insertions of very different proteins are tolerated at each of these locations.

Most studies of CoV replication using the addition of reporters have involved the substitution of accessory ORFs. These ORFs have been used as general indicators of overall viral replication, mostly for testing of inhibitors or attenuation of replication (19–24, 39–41). However, these strategies are limited as direct indicators of genome replication, since they require subgenomic mRNA transcription for expression of the engineered reporters or are not contained within infectious virus. While reporters expressed from downstream ORFs are valuable as indicators of overall viral replication, they cannot distinguish genome replication from subgenomic mRNA transcription. Reporters have also been employed for analysis of coronavirus host interactions and cell biology. Specifically, the expression of nsp2-reporter or nsp4-reporter fusions as substitutions of MHV ORF4 or hemagglutinin esterase (HE) has been described and used to define the localization and movement of nsp's (42–44). While informative, these studies are limited in their interpretation by nsp expression from nonnative locations in the genome. We have shown that alternative expression of nsp2 can be detrimental to replication, even when expressed as a duplication with native nsp2 (44). Our results suggest that the context of the nsp2 location in the polyprotein is important for its interaction with adjacent replicase proteins. Although nsp2 is dispensable for replication (26), altering expression by a deletion or cleavage site alteration impacts replication and fitness.

The observation that GFP or FFL fusions with nsp2 had no detectable effect on the MHV replication cycle in culture was surprising and suggests significant flexibility in this region of the polyprotein for additional genetic information. A recent study of the evolution of the genomes of nidoviruses from the small arteriviruses (~15 kb) to the largest coronaviruses (up to 32 kb) proposed that proto-CoVs emerged due to the incorporation of a cassette of proteins, including the proofreading exonuclease in nsp14, which allowed more stability of larger genomes (45). It was also proposed that an increased genetic robustness to mutations

was also required for genome expansion and increased complexity. Our study supports that argument, with the incorporation of FFL expanding the MHV genome by ~5.3%. The virus can be recovered at P0 and P1 with high-titer stocks for use *in vitro* and *in vivo*, and the FFL coding sequence is maintained for at least 5 passages. However, the introduction of GFP as an nsp2 fusion results in a fitness cost during direct competition with MHV. It will be interesting to see if this fitness cost is similar for FFL or other foreign genes. It will also be of interest to see whether foreign genes are retained over a long passage in the absence of competition or if the subtle fitness cost results in selection against the foreign sequences in the long term.

The implications of stable replicase nsp-reporter fusions are significant for several reasons. It was not previously possible to directly quantitate the translation of the CoV replicase/transcriptase polyproteins in infected cells. CoV ORF1a expresses a ~495-kDa polyprotein (pp1a). Translation of ORF1b, which encodes critical replication enzymes, including nsp12–RNA-dependent RNA polymerase (RdRp) and nsp14-ExoN, requires a ribosomal frameshift between nsp10 and nsp12. Previous *in vitro* studies suggested that frameshift efficiencies range from 10 to 40% (46). Dual-luciferase systems have been used to examine structures and sequences in this region; however, this has never been tested by utilizing infectious virus (47, 48). Expression of different quantitative reporters from ORF1a and ORF1b could allow direct testing of the timing and stoichiometry of replicase polyprotein translation. We have recently recovered recombinant viruses expressing GFP as a fusion with nsp14 (our unpublished results), providing encouraging evidence that ORF1b reporter expression is possible. The early exponential signal from FFL-nsp2 is consistent with a rapid amplification of genome RNA prior to virus assembly and release and thus may be an early and sensitive reporter for studies of inhibitors of virus replication. Similarly, it was not previously possible to track the expression and localization of replicase proteins from their native locations in the genome. The native expression of fluorescent reporters fused to replicase proteins creates the opportunity to track replication complex formation in real time in a single cell, without potential artifacts due to cellular fixation for immunofluorescence or due to altered expression from subgenomic mRNAs or exogenous plasmids. Our results suggest that it may be possible to engineer reporter fusions with multiple replicase proteins for testing and visualization of protein-protein and protein-membrane interactions in live cells.

ACKNOWLEDGMENTS

We thank Michelle Becker, E. Clinton Smith, and Dia Beachboard for advice and critical reviews of the manuscript. We thank J. Fleming (University of Wisconsin, Madison) for the kind gift of the M antibody.

Experiments were performed in part through the use of the VUMC Cell Imaging Shared Resource, supported by NIH grants CA68485, DK20593, DK58404, HD15052, DK59637, and Ey008126. Support for this work was provided by National Institutes of Health grant R01 AI50083 (M.R.D.) from the National Institute of Allergy and Infectious Diseases. M.C.F. was supported by a Medical Scientist Training Program training grant through the Vanderbilt University School of Medicine (T32 GM07347). This work was also supported by the Elizabeth B. Lamb Center for Pediatric Research.

REFERENCES

1. Perlman S, Netland J. 2009. Coronaviruses post-SARS: update on replication and pathogenesis. Nat. Rev. Microbiol. 7:439–450. http://dx.doi.org/10.1038/nrmicro2147.
2. Ksiazek TG, Erdman D, Goldsmith CS, Zaki SR, Peret T, Emery S, Tong S, Urbani C, Comer JA, Lim W, Rollin PE, Dowell SF, Ling AE, Humphrey CD, Shieh WJ, Guarner J, Paddock CD, Rota P, Fields B, DeRisi J, Yang JY, Cox N, Hughes JM, LeDuc JW, Bellini WJ, Anderson LJ. 2003. A novel coronavirus associated with severe acute respiratory syndrome. N. Engl. J. Med. 348:1953–1966. http://dx.doi.org/10.1056/NEJMoa030781.
3. Peiris JS, Lai ST, Poon LL, Guan Y, Yam LY, Lim W, Nicholls J, Yee WK, Yan WW, Cheung MT, Cheng VC, Chan KH, Tsang DN, Yung RW, Ng TK, Yuen KY. 2003. Coronavirus as a possible cause of severe acute respiratory syndrome. Lancet 361:1319–1325. http://dx.doi.org/10.1016/S0140-6736(03)13077-2.
4. Rota PA, Oberste MS, Monroe SS, Nix WA, Campagnoli R, Icenogle JP, Penaranda S, Bankamp B, Maher K, Chen MH, Tong S, Tamin A, Lowe L, Frace M, DeRisi JL, Chen Q, Wang D, Erdman DD, Peret TC, Burns C, Ksiazek TG, Rollin PE, Sanchez A, Liffick S, Holloway B, Limor J, McCaustland K, Olsen-Rasmussen M, Fouchier R, Gunther S, Osterhaus AD, Drosten C, Pallansch MA, Anderson LJ, Bellini WJ. 2003. Characterization of a novel coronavirus associated with severe acute respiratory syndrome. Science 300:1394–1399. http://dx.doi.org/10.1126/science.1085952.
5. Zaki AM, van Boheemen S, Bestebroer TM, Osterhaus AD, Fouchier RA. 2012. Isolation of a novel coronavirus from a man with pneumonia in Saudi Arabia. N. Engl. J. Med. 367:1814–1820. http://dx.doi.org/10.1056/NEJMoa1211721.
6. Angelini MM, Akhlaghpour M, Neuman BW, Buchmeier MJ. 2013. Severe acute respiratory syndrome coronavirus nonstructural proteins 3, 4, and 6 induce double-membrane vesicles. mBio 4(4):pii=00524-13. http://dx.doi.org/10.1128/mBio.00524-13.
7. Gosert R, Kanjanahaluethai A, Egger D, Bienz K, Baker SC. 2002. RNA replication of mouse hepatitis virus takes place at double-membrane vesicles. J. Virol. 76:3697–3708. http://dx.doi.org/10.1128/JVI.76.8.3697-3708.2002.
8. Knoops K, Kikkert M, Worm SH, Zevenhoven-Dobbe JC, van der Meer Y, Koster AJ, Mommaas AM, Snijder EJ. 2008. SARS-coronavirus replication is supported by a reticulovesicular network of modified endoplasmic reticulum. PLoS Biol. 6:e226. http://dx.doi.org/10.1371/journal.pbio.0060226.
9. Ulasli M, Verheije MH, de Haan CA, Reggiori F. 2010. Qualitative and quantitative ultrastructural analysis of the membrane rearrangements induced by coronavirus. Cell. Microbiol. 12:844–861. http://dx.doi.org/10.1111/j.1462-5822.2010.01437.x.
10. Snijder EJ, van der Meer Y, Zevenhoven-Dobbe J, Onderwater JJ, van der Meulen J, Koerten HK, Mommaas AM. 2006. Ultrastructure and origin of membrane vesicles associated with the severe acute respiratory syndrome coronavirus replication complex. J. Virol. 80:5927–5940. http://dx.doi.org/10.1128/JVI.02501-05.
11. Bost AG, Carnahan RH, Lu XT, Denison MR. 2000. Four proteins processed from the replicase gene polyprotein of mouse hepatitis virus colocalize in the cell periphery and adjacent to sites of virion assembly. J. Virol. 74:3379–3387. http://dx.doi.org/10.1128/JVI.74.7.3379-3387.2000.
12. Brockway SM, Clay CT, Lu XT, Denison MR. 2003. Characterization of the expression, intracellular localization, and replication complex association of the putative mouse hepatitis virus RNA-dependent RNA polymerase. J. Virol. 77:10515–10527. http://dx.doi.org/10.1128/JVI.77.19.10515-10527.2003.
13. van der Meer Y, Snijder EJ, Dobbe JC, Schleich S, Denison MR, Spaan WJ, Locker JK. 1999. Localization of mouse hepatitis virus nonstructural proteins and RNA synthesis indicates a role for late endosomes in viral replication. J. Virol. 73:7641–7657.
14. Bost AG, Prentice E, Denison MR. 2001. Mouse hepatitis virus replicase protein complexes are translocated to sites of M protein accumulation in the ergic at late times of infection. Virology 285:21–29. http://dx.doi.org/10.1006/viro.2001.0932.
15. Sims AC, Ostermann J, Denison MR. 2000. Mouse hepatitis virus replicase proteins associate with two distinct populations of intracellular membranes. J. Virol. 74:5647–5654. http://dx.doi.org/10.1128/JVI.74.12.5647-5654.2000.
16. Brockway SM, Lu XT, Peters TR, Dermody TS, Denison MR. 2004. Intracellular localization and protein interactions of the gene 1 protein p28 during mouse hepatitis virus replication. J. Virol. 78:11551–11562. http://dx.doi.org/10.1128/JVI.78.21.11551-11562.2004.
17. Bosch BJ, de Haan CA, Rottier PJ. 2004. Coronavirus spike glycoprotein,

extended at the carboxy terminus with green fluorescent protein, is assembly competent. J. Virol. 78:7369–7378. http://dx.doi.org/10.1128/JVI.78.14.7369-7378.2004.
18. Das Sarma J, Scheen E, Seo SH, Koval M, Weiss SR. 2002. Enhanced green fluorescent protein expression may be used to monitor murine coronavirus spread in vitro and in the mouse central nervous system. J. Neurovirol. 8:381–391. http://dx.doi.org/10.1080/13550280260422686.
19. de Haan CA, van Genne L, Stoop JN, Volders H, Rottier PJ. 2003. Coronaviruses as vectors: position dependence of foreign gene expression. J. Virol. 77:11312–11323. http://dx.doi.org/10.1128/JVI.77.21.11312-11323.2003.
20. Fischer F, Stegen CF, Koetzner CA, Masters PS. 1998. Construction of a mouse hepatitis virus recombinant expressing a foreign gene. Adv. Exp. Med. Biol. 440:291–295.
21. Hertzig T, Scandella E, Schelle B, Ziebuhr J, Siddell SG, Ludewig B, Thiel V. 2004. Rapid identification of coronavirus replicase inhibitors using a selectable replicon RNA. J. Gen. Virol. 85:1717–1725. http://dx.doi.org/10.1099/vir.0.80044-0.
22. Ge F, Luo Y, Liew PX, Hung E. 2007. Derivation of a novel SARS-coronavirus replicon cell line and its application for anti-SARS drug screening. Virology 360:150–158. http://dx.doi.org/10.1016/j.virol.2006.10.016.
23. Roberts RS, Yount BL, Sims AC, Baker S, Baric RS. 2006. Renilla luciferase as a reporter to assess SARS-CoV mRNA transcription regulation and efficacy of anti-SARS-CoV agents. Adv. Exp. Med. Biol. 581:597–600. http://dx.doi.org/10.1007/978-0-387-33012-9_108.
24. Zhao G, Du L, Ma C, Li Y, Li L, Poon VK, Wang L, Yu F, Zheng BJ, Jiang S, Zhou Y. 2013. A safe and convenient pseudovirus-based inhibition assay to detect neutralizing antibodies and screen for viral entry inhibitors against the novel human coronavirus MERS-CoV. Virol. J. 10:266. http://dx.doi.org/10.1186/1743-422X-10-266.
25. van den Born E, Posthuma CC, Knoops K, Snijder EJ. 2007. An infectious recombinant equine arteritis virus expressing green fluorescent protein from its replicase gene. J. Gen. Virol. 88:1196–1205. http://dx.doi.org/10.1099/vir.0.82590-0.
26. Graham RL, Sims AC, Brockway SM, Baric RS, Denison MR. 2005. The nsp2 replicase proteins of murine hepatitis virus and severe acute respiratory syndrome coronavirus are dispensable for viral replication. J. Virol. 79:13399–13411. http://dx.doi.org/10.1128/JVI.79.21.13399-13411.2005.
27. Sperry SM, Kazi L, Graham RL, Baric RS, Weiss SR, Denison MR. 2005. Single-amino-acid substitutions in open reading frame (ORF) 1b-nsp14 and ORF 2a proteins of the coronavirus mouse hepatitis virus are attenuating in mice. J. Virol. 79:3391–3400. http://dx.doi.org/10.1128/JVI.79.6.3391-3400.2005.
28. Denison MR, Yount B, Brockway SM, Graham RL, Sims AC, Lu X, Baric RS. 2004. Cleavage between replicase proteins p28 and p65 of mouse hepatitis virus is not required for virus replication. J. Virol. 78:5957–5965. http://dx.doi.org/10.1128/JVI.78.11.5957-5965.2004.
29. Hirano N, Fujiwara K, Matumoto M. 1976. Mouse hepatitis virus (MHV-2). Plaque assay and propagation in mouse cell line DBT cells. Jpn. J. Microbiol. 20:219–225.
30. Lin HH, Kao JH, Chen PJ, Chen DS. 1996. Mechanism of vertical transmission of hepatitis G. Lancet 347:1116. http://dx.doi.org/10.1016/S0140-6736(96)90314-1.
31. Chen W, Madden VJ, Bagnell CR, Jr, Baric RS. 1997. Host-derived intracellular immunization against mouse hepatitis virus infection. Virology 228:318–332. http://dx.doi.org/10.1006/viro.1996.8402.
32. Reference deleted.
33. Yount B, Denison MR, Weiss SR, Baric RS. 2002. Systematic assembly of a full-length infectious cDNA of mouse hepatitis virus strain A59. J. Virol. 76:11065–11078. http://dx.doi.org/10.1128/JVI.76.21.11065-11078.2002.
34. Yount B, Curtis KM, Fritz EA, Hensley LE, Jahrling PB, Prentice E, Denison MR, Geisbert TW, Baric RS. 2003. Reverse genetics with a full-length infectious cDNA of severe acute respiratory syndrome coronavirus. Proc. Natl. Acad. Sci. U. S. A. 100:12995–13000. http://dx.doi.org/10.1073/pnas.1735582100.
35. Lavi E, Gilden DH, Wroblewska Z, Rorke LB, Weiss SR. 1984. Experimental demyelination produced by the A59 strain of mouse hepatitis virus. Neurology 34:597–603. http://dx.doi.org/10.1212/WNL.34.5.597.
36. Graham RL, Denison MR. 2006. Replication of murine hepatitis virus is regulated by papain-like proteinase 1 processing of nonstructural proteins 1, 2, and 3. J. Virol. 80:11610–11620. http://dx.doi.org/10.1128/JVI.01428-06.
37. Gadlage MJ, Denison MR. 2010. Exchange of the coronavirus replicase polyprotein cleavage sites alters protease specificity and processing. J. Virol. 84:6894–6898. http://dx.doi.org/10.1128/JVI.00752-10.
38. Burgess A, Vigneron S, Brioudes E, Labbe JC, Lorca T, Castro A. 2010. Loss of human greatwall results in G2 arrest and multiple mitotic defects due to deregulation of the cyclin B-Cdc2/PP2A balance. Proc. Natl. Acad. Sci. U. S. A. 107:12564–12569. http://dx.doi.org/10.1073/pnas.0914191107.
39. Curtis KM, Yount B, Baric RS. 2002. Heterologous gene expression from transmissible gastroenteritis virus replicon particles. J. Virol. 76:1422–1434. http://dx.doi.org/10.1128/JVI.76.3.1422-1434.2002.
40. Kilianski A, Mielech AM, Deng X, Baker SC. 2013. Assessing activity and inhibition of Middle East respiratory syndrome coronavirus papain-like and 3C-like proteases using luciferase-based biosensors. J. Virol. 87:11955–11962. http://dx.doi.org/10.1128/JVI.02105-13.
41. Pfefferle S, Schopf J, Kogl M, Friedel CC, Muller MA, Carbajo-Lozoya J, Stellberger T, von Dall'Armi E, Herzog P, Kallies S, Niemeyer D, Ditt V, Kuri T, Zust R, Pumpor K, Hilgenfeld R, Schwarz F, Zimmer R, Steffen I, Weber F, Thiel V, Herrler G, Thiel HJ, Schwegmann-Wessels C, Pohlmann S, Haas J, Drosten C, von Brunn A. 2011. The SARS-coronavirus-host interactome: identification of cyclophilins as target for pan-coronavirus inhibitors. PLoS Pathog. 7:e1002331. http://dx.doi.org/10.1371/journal.ppat.1002331.
42. Hagemeijer MC, Verheije MH, Ulasli M, Shaltiel IA, de Vries LA, Reggiori F, Rottier PJ, de Haan CA. 2010. Dynamics of coronavirus replication-transcription complexes. J. Virol. 84:2134–2149. http://dx.doi.org/10.1128/JVI.01716-09.
43. Hagemeijer MC, Ulasli M, Vonk AM, Reggiori F, Rottier PJ, de Haan CA. 2011. Mobility and interactions of coronavirus nonstructural protein 4. J. Virol. 85:4572–4577. http://dx.doi.org/10.1128/JVI.00042-11.
44. Gadlage MJ, Graham RL, Denison MR. 2008. Murine coronaviruses encoding nsp2 at different genomic loci have altered replication, protein expression, and localization. J. Virol. 82:11964–11969. http://dx.doi.org/10.1128/JVI.01126-07.
45. Lauber C, Goeman JJ, Parquet MC, Nga PT, Snijder EJ, Morita K, Gorbalenya AE. 2013. The footprint of genome architecture in the largest genome expansion in RNA viruses. PLoS Pathog. 9:e1003500. http://dx.doi.org/10.1371/journal.ppat.1003500.
46. Somogyi P, Jenner AJ, Brierley I, Inglis SC. 1993. Ribosomal pausing during translation of an RNA pseudoknot. Mol. Cell. Biol. 13:6931–6940.
47. Plant EP, Perez-Alvarado GC, Jacobs JL, Mukhopadhyay B, Hennig M, Dinman JD. 2005. A three-stemmed mRNA pseudoknot in the SARS coronavirus frameshift signal. PLoS Biol. 3:e172. http://dx.doi.org/10.1371/journal.pbio.0030172.
48. Plant EP, Sims AC, Baric RS, Dinman JD, Taylor DR. 2013. Altering SARS coronavirus frameshift efficiency affects genomic and subgenomic RNA production. Viruses 5:279–294. http://dx.doi.org/10.3390/v5010279.

Appendix B: PEDIATRICS CORONAVIRUS CHAPTER

I wrote the following text as a chapter for the 19th edition of the book *Pediatrics*.

Introduction

Coronaviruses are increasingly recognized as important human pathogens. They cause up to 15% of common colds and have been implicated in more serious diseases including croup, asthma exacerbations, bronchiolitis, and pneumonia. Evidence also suggests that coronaviruses may cause enteritis or colitis in neonates and infants and may be underappreciated as agents of meningitis or encephalitis. Four coronaviruses are endemic in humans: human coronaviruses (HCoV) 229E, OC43, NL63, and HKU1. In addition, two epidemics of previously unknown coronaviruses caused significant respiratory distress and high mortality rates among infected individuals. The discoveries of SARS-associated coronavirus (SARS-CoV), the cause of severe acute respiratory syndrome (SARS) in 2003, and of Middle East Respiratory Syndrome-CoV (MERS-COV) in 2012 support the potential for coronaviruses to emerge from animal hosts such as bats and become important human pathogens.

Etiology

Coronaviruses are enveloped viruses of medium to large size (80-220 nm) that possess the largest known single-stranded positive-sense RNA genomes. Recently, these viruses were shown to encode the protein nsp14-ExoN, which is the first known RNA proofreading enzyme and is likely responsible for the evolution of the large and complex

coronavirus genome (Denison et al., 2011). Coronaviruses derive their name from the characteristic surface projections of spike protein, which give a corona or crown-like appearance on negative-stain electron microscopy. Coronaviruses are organized taxonomically by a lettering system based on genomic phylogenetic relationships (van Boheemen et al., 2012). Alphacoronaviruses include human coronavirus 229E (HCoV-229E) and HCoV-NL63. Betacoronaviruses include four human pathogens and are commonly divided into four lineages, without formal taxonomic recognition. HCoV-OC43 and the HCoV-HKU1 are in lineage A, while SARS-CoV falls in lineage B. Lineages C and D were exclusively comprised of bat coronaviruses until the discovery of MERS-CoV, which aligns with lineage C. Gammacoronaviruses and deltacoronaviruses presently include exclusively non-human pathogens.

In 2002-2003, coronaviruses received international attention during the SARS outbreak, which was responsible for over 800 deaths in 30 countries. SARS-CoV, a novel coronavirus at the time of the epidemic, was found to be the causative agent of SARS. The detection of SARS-like coronaviruses in a live animal market in the Guangdong province in southern China, along with serologic evidence of exposure in food handlers in the same market, suggest that these markets may have facilitated the spread of SARS-CoV to humans from an animal reservoir. Subsequent studies identified SARS-like coronaviruses that are very closely related, but not direct precursors to, SARS-CoV in fecal specimens from asymptomatic Chinese horseshoe bats. Thus, although bats are thought to be a reservoir for SARS-like precursors, the precise antecedent to SARS-CoV remains to be identified.

In June 2012, another novel coronavirus, MERS-CoV was isolated from a man with acute pneumonia and renal failure in Saudi Arabia (Zaki et al., 2012). To date, an additional 827 cases have been confirmed in Saudi Arabia, UAE, Qatar, Jordan, Tunisia, France, Italy, and the United Kingdom. Two hundred and eighty seven of these patients died due to their infection. MERS-CoV differs from SARS in that seems to be less communicable, although human-to-human transmission has been confirmed (Perlman and Zhao, 2013). MERS-CoV has been shown to use dipeptidyl peptidase 4 (DPP4) as its cellular receptor, a difference between MERS-CoV and SARS-CoV which utilizes ACE-2, and is able to infect cells from several animal lineages, including human, pig, and bat, suggesting the possibility of movement between multiple species (Raj et al., 2013). Serologic studies in several domestic species in Saudi Arabia have demonstrated that nearly 100% of dromedary camels tested for antibodies to MERS-CoV were positive, and evidence of MERS-CoV antibodies were identified in samples from as long ago as 1992, while other herd animals tested in the region were negative for these antibodies as were dromedary camels tested in other regions of the world. A short MERS-CoV sequence was also discovered in a bat from the region. The way MERS-CoV is transmitted to humans, however, is still to be determined.

Epidemiology

Seroprevalence studies have demonstrated that antibodies against 229E and OC43 increase rapidly during early childhood, so that by adulthood 90-100% of persons are seropositive. Although less information is available for HKU1 and NL63, studies

demonstrate similar patterns of seroconversion to these viruses during early childhood. Although some degree of strain-specific protection may be afforded by recent infection, re-infections are common and occur despite the presence of strain-specific antibodies. Attack rates are similar in different age groups. Although infections occur throughout the year, there is a peak during the winter and early spring for each of these HCoVs (Dominguez et al., 2009). In the US, outbreaks of OC43 and 229E have occurred in 2- to 3-year alternating cycles. Independent studies of viral etiologies of upper and lower respiratory infections during the same period, but from different countries, have confirmed that all known human coronaviruses have a worldwide distribution. Studies using both viral culture and PCR multiplex assays have demonstrated that coronaviruses often occur as co-infections with other respiratory viruses, including respiratory syncytial virus (RSV), adenovirus, rhinovirus (RV), or human metapneumovirus (HMPV) (Stempel et al., 2009). Volunteer studies demonstrated that OC43 and 229E are transmitted predominantly through the respiratory route. Droplet spread appears to be most important, although aerosol transmission may also occur.

There have been no identified natural or laboratory-acquired cases of SARS-CoV since 2004, but the mechanisms of introduction, spread, and disease remain important for potential animal-to-human transmission and disease. The primary mode of SARS-CoV transmission occurred through direct or indirect contact of mucous membranes with infectious droplets or fomites. Aerosol transmission was less common, occurring primarily in the setting of endotracheal intubation, bronchoscopy, or treatment with aerosolized medications. Fecal-oral transmission did not appear to be an efficient mode

of transmission but may have occurred because of the profuse diarrhea observed in some patients. The seasonality of SARS-CoV remains unknown. SARS-CoV is not highly infectious, with generally only 2-4 secondary cases resulting from a single infected adult. During the SARS epidemic, a small number of infected individuals, “super-spreaders”, transmitted infection to a much larger number of persons, but the mechanism for this high degree of spread remains unknown. In contrast, persons with mild disease, such as children under twelve years of age, rarely transmitted the infection to others (Bitnun et al., 2009). Infectivity correlated with disease stage; transmission occurred almost exclusively during symptomatic disease. During the 2003 outbreak, most individuals with SARS-CoV infection were hospitalized within 3-4 days of symptom onset. Consequently, most subsequent infections occurred within hospitals and involved either health care workers or other hospitalized patients.

Pathogenesis

Coronaviruses have been reported to cause minimal cytopathology. Studies with SARS-CoV in human airway epithelial cell cultures indicate that ciliated cells are principal targets for infection and that infected ciliated cells may be directly extruded or lost from the infected monolayer. Thus, the cytopathology from other HCoVs may be due to direct cell infection and loss, though symptoms may also be due to the host immune response. Infection with OC43 and 229E is associated with the elaboration of cytokines, including interleukin-8 (IL-8) and interferon-γ (IFN-γ). In experimentally infected volunteers, serum-specific immunoglobulin (Ig) A and IgG antibody levels peak 12-14 days after infection but decline rapidly thereafter. At one year following experimental infection,

there is only partial protection against re-infection with the homologous strain, suggesting a challenge for the development of successful vaccines against HCoVs.

Clinical Manifestations

While all known human coronaviruses cause respiratory disease, the role of human coronaviruses in gastrointestinal and neurologic disease is less clear and remains to be proven. In addition to severe respiratory pathology, both SARS-CoV and MERS-CoV can cause renal failure, although this symptom is observed less frequently during SARS-CoV infections.

Respiratory Infections

Even though up to 50% of respiratory tract infections with OC43 and 229E are asymptomatic, coronaviruses are still responsible for up to 15% of common colds. Cold symptoms caused by human coronaviruses are indistinguishable from those caused by rhinoviruses and other respiratory viruses. The average incubation period is 2-4 days, with symptoms typically lasting 4-7 days (Lessler et al., 2009). Rhinorrhea, cough, sore throat, malaise, and headache are the most common symptoms. Fever occurs in up to 60% of cases. Coronavirus NL63 is a cause of croup in children under three years of age. Coronavirus infections have been linked to episodes of wheezing in asthmatic children, albeit at a lower frequency and severity than observed with rhinovirus and respiratory syncytial virus infections. Lower respiratory tract infections, including bronchiolitis and pneumonia, have also been reported in immunocompetent and immunocompromised, children and adults. As with RSV or RV, coronavirus detection in upper respiratory

infections is frequently associated with acute otitis media and can be isolated from middle ear fluid (Alper et al., 2009).

Non-Respiratory Sequelae

There is some evidence to support a role for coronaviruses in human gastrointestinal (GI) disease, particularly in young children. Coronavirus-like particles have been detected by electron microscopy in the stools of infants with nonbacterial gastroenteritis. In addition, several outbreaks in neonatal intensive care units of gastrointestinal disease characterized by diarrhea, bloody stools, abdominal distention, bilious gastric aspirates, and classic necrotizing enterocolitis have also been associated with the presence of coronavirus-like particles in stools. In older children and adults, coronavirus-like viruses have been observed with similar frequency in symptomatic and asymptomatic individuals, making it difficult to discern if they are pathogenic in the GI tract. Coronaviruses are well-known causes of neurologic disease in animals, including demyelinating encephalitis, but their role in causing human neurologic disease remains unclear. Coronaviruses have been detected by culture, *in situ* hybridization, and reverse transcriptase polymerase chain reaction (RT-PCR) in brain tissue from a few patients with multiple sclerosis. However, coronavirus RNA has also been recovered from the spinal fluid and brain tissue of adults without neurologic disease. HCoV-OC43 has been detected by RT-PCR in the spinal fluid and nasopharynx of one child with acute disseminated encephalomyelitis.

SARS-CoV

SARS-CoV infections in teenagers and adults included a viral replication phase and an immunologic phase. During the viral replication phase there was a progressive increase in viral load that reached its peak during the second week of illness. The appearance of specific antibodies coincided with peak viral replication. The clinical deterioration that typified the second and third week of illness was characterized by a decline in the viral load and evidence of tissue injury likely from cytokine-mediated immunity. The explanation for milder clinical disease in children less than 12 years of age has not been determined. Seroepidemiologic studies suggest that asymptomatic SARS-CoV infections were uncommon. The incubation period ranged from 1 to 14 days, with a median of 4-6 days. The clinical manifestations were nonspecific, most commonly consisting of fever, cough, malaise, coryza, chills or rigors, headache, and myalgia. Coryza was more common in children less than 12 years of age, whereas systemic symptoms were seen more often in teenagers. Some young children had no respiratory symptoms. Gastrointestinal symptoms, including diarrhea and nausea or vomiting, occurred in up to a third of cases. The clinical course of SARS-CoV infection varied with age. Adults were most severely affected, with initial onset of fever, cough, chills, myalgia, malaise, and headache. Following an initial improvement at the end of the first week, fever recurred and respiratory distress developed, with dyspnea, hypoxemia, and diarrhea. These symptoms progressed in 20% of patients to acute respiratory distress syndrome (ARDS) and respiratory failure. Acute renal failure with histological acute tubular necrosis was present in 6.9% of patients, likely due to hypoxic kidney damage. 28.8% of SARS patients had abnormal urinalysis, with viral genome detectable by qRT-PCR. In contrast,

children under 12 years of age had a relatively mild nonspecific illness, with only a minority experiencing significant lower respiratory tract disease and illness typically lasting less than five days. There were no deaths or ARDS in children under 12 years of age from SARS-CoV infection. Adolescents manifested increasing severity in direct correlation to increasing age; respiratory distress and hypoxemia were observed in 10-20% of patients, one third of which required ventilator support. The case fatality rate from SARS-CoV infection during the 2003 outbreak was 10-17%. No pediatric deaths were reported. The estimated case fatality rate according to age varied from <1% for those under 20 years of age to >50% for those over 65 years of age.

MERS-CoV

The incubation period of MERS-CoV is thought to be approximately ten days. Because of the relatively low rate of spread, it is considered to be less transmissible from person to person than SARS-CoV. Several clusters of patients have been diagnosed with confirmed cases, though it is difficult to determine if their infections were spread from person to person or if they shared a common environmental exposure. A cluster in the UK confirmed person-person transmission, as only one of the individuals had traveled to the Arabian Peninsula. Because the method of transmission is presently unknown, appropriate airborne and contact precautions are required when treating infected patients. Patients have presented with acute respiratory infection, a fever higher than 100.4 degrees F, cough, and pulmonary parenchymal disease such as pneumonia or ARDS. Lymphopenia, neutrophilia, and late thrombocytopenia occurred in the index-case patient. This patient also had progressive renal impairment, beginning on the ninth day of

symptoms which continued to progress until the patient's death at day 11. The case fatality rate is presently >35% for confirmed cases. A low percentage of pediatric cases have been discovered upon screening contacts of infected adults, though most have been asymptomatic (Memish et al., 2014).

Diagnosis

In the past, specific diagnostic tests for coronavirus infections were not available in most clinical settings. The use of conserved PCR primers for coronaviruses in multiplex RT-PCR viral diagnostic panels now allows widely available and sensitive detection of the viruses. Virus culture of primary clinical specimens remains a challenge for HCoVs HKU1, OC43, 229E and NL63, while both SARS-CoV and MERS-CoV can both successfully be grown in culture from respiratory samples. Serodiagnosis with complement fixation, neutralization, hemagglutination inhibition, enzyme immunoassay, or Western blots has been used in the research setting. The diagnosis of SARS-CoV infection can be confirmed by serologic testing, detection of viral RNA using RT-PCR, or isolation of the virus in cell culture. While serology for SARS-CoV has sensitivity and specificity approaching 100%, antibodies are not detectable until 10 days after the onset of symptoms, and IgG seroconversion may be delayed for up to 4 weeks. In addition, the SARS epidemic resulted in the inclusion of CoV conserved primers in many diagnostic PCR multiplex assays such that CoVs may be more readily detected. For emerging CoVs, such as MERS-CoV, highly conserved primers were used for initial detection, with confirmatory assays using specific primers. Thus, the mainstay of early diagnosis is RT-PCR. For all known endemic and emerging HCoVs, respiratory specimens

(nasopharyngeal swabs or aspirates) are most likely to be positive, but in a setting of a possible novel CoV, serum or stool may be positive. Two highly sensitive real-time RT-PCR assays are currently available for testing for MERS-CoV RNA in addition to utilizing immunofluorescence microscopy for the detection of antibody response.

Treatment and Prevention

Coronavirus infections of humans are acute and self-limited, although persistent infection and shedding may occur in multiple animal models in the setting of minimal or no symptomology. There are no available antiviral agents for clinical use against coronaviruses, although strategies targeting conserved coronavirus proteases have been shown to block replication of the virus in vitro. Challenges for development of effective vaccines targeted against OC43, 229E, HKU1, and NL63 include the fact that infections are rarely life threatening and re-infection is the rule, even in the presence of natural immunity from previous infections. Treatment of SARS-CoV and MERS-CoV infections is primarily supportive. The role of antiviral and immune-modulating agents remains inconclusive, largely because none of these therapies have been evaluated in properly conducted randomized controlled trials. Ribavirin was extensively used during the 2003 SARS-CoV outbreak, but is of questionable benefit given its poor *in vitro* activity against SARS-CoV at clinically relevant concentrations. The identification of the proofreading nsp14-exonuclease suggests that this activity may be important in resistance to antiviral nucleosides and RNA mutagens such as ribavirin. Systemic corticosteroid therapy was temporally associated with clinical improvement in some patients. In another small, open-label, nonrandomized pilot study, interferon-α was associated with more rapid

resolution of oxygen requirements and radiographic abnormalities. Human monoclonal antibodies derived from SARS patients demonstrate broad neutralization against early and late epidemic strains of SARS-CoV and could potentially be therapeutic.

Effective vaccines for SARS-CoV and MERS-CoV are highly desirable, but not yet available. A potential vaccine strategy would be to use the viral spike protein, which could be delivered as a recombinant protein or via viral or DNA vectors. This approach appears to be effective against closely related strains of SARS-CoV, but not necessarily early animal or human variants. A SARS-CoV vaccine approach that recently has shown success in animal models utilized a live-engineered SARS-CoV mutant with inactivated nsp14 exonuclease, demonstrating attenuation and protection in a variety of aged, immunocompromised mice (Graham et al., 2012). Approaches for rapid development of stably attenuated live viruses or broadly immunogenic and cross-protective protein immunogens continues to be a key area for future research. Although SARS-CoV demonstrated characteristics of symptomatic transmission that made it controllable by public health measures like quarantine, these characteristics cannot be assumed for future novel human coronaviruses. The recent outbreak of MERS-CoV serves as a reminder that coronavirus emergence is both likely and unpredictable, making it very important to continue studies of their replication, emergence, and transmission. Additionally, strategies for rapid recovery, testing, and development of vaccines and neutralizing human monoclonal antibodies may be essential to prevent the high morbidity and mortality associated with previous epidemics.

REFERENCES

Alagaili, A.N., Briese, T., Mishra, N., Kapoor, V., Sameroff, S.C., Burbelo, P.D., de Wit, E., Munster, V.J., Hensley, L.E., Zalmout, I.S., Kapoor, A., Epstein, J.H., Karesh, W.B., Daszak, P., Mohammed, O.B., Lipkin, W.I., 2014. Middle East respiratory syndrome coronavirus infection in dromedary camels in Saudi Arabia. mBio 5, e00884-00814.

Aleksandrowicz, P., Marzi, A., Biedenkopf, N., Beimforde, N., Becker, S., Hoenen, T., Feldmann, H., Schnittler, H.J., 2011. Ebola virus enters host cells by macropinocytosis and clathrin-mediated endocytosis. The Journal of infectious diseases 204 Suppl 3, S957-967.

Alper, C.M., Winther, B., Mandel, E.M., Hendley, J.O., Doyle, W.J., 2009. Rate of concurrent otitis media in upper respiratory tract infections with specific viruses. Archives of otolaryngology--head & neck surgery 135, 17-21.

Amstutz, B., Gastaldelli, M., Kalin, S., Imelli, N., Boucke, K., Wandeler, E., Mercer, J., Hemmi, S., Greber, U.F., 2008. Subversion of CtBP1-controlled macropinocytosis by human adenovirus serotype 3. The EMBO journal 27, 956-969.

Amyere, M., Mettlen, M., Van Der Smissen, P., Platek, A., Payrastre, B., Veithen, A., Courtoy, P.J., 2002. Origin, originality, functions, subversions and molecular signalling of macropinocytosis. International journal of medical microbiology : IJMM 291, 487-494.

Amyere, M., Payrastre, B., Krause, U., Van Der Smissen, P., Veithen, A., Courtoy, P.J., 2000. Constitutive macropinocytosis in oncogene-transformed fibroblasts depends on sequential permanent activation of phosphoinositide 3-kinase and phospholipase C. Molecular biology of the cell 11, 3453-3467.

Angelini, M.M., Akhlaghpour, M., Neuman, B.W., Buchmeier, M.J., 2013. Severe acute respiratory syndrome coronavirus nonstructural proteins 3, 4, and 6 induce double-membrane vesicles. mBio 4.

Annan, A., Baldwin, H.J., Corman, V.M., Klose, S.M., Owusu, M., Nkrumah, E.E., Badu, E.K., Anti, P., Agbenyega, O., Meyer, B., Oppong, S., Sarkodie, Y.A., Kalko, E.K., Lina, P.H., Godlevska, E.V., Reusken, C., Seebens, A., Gloza-Rausch, F., Vallo, P., Tschapka, M., Drosten, C., Drexler, J.F., 2013. Human betacoronavirus 2c EMC/2012-related viruses in bats, Ghana and Europe. Emerging infectious diseases 19, 456-459.

Araki, N., Johnson, M.T., Swanson, J.A., 1996. A role for phosphoinositide 3-kinase in the completion of macropinocytosis and phagocytosis by macrophages. The Journal of cell biology 135, 1249-1260.

Belouzard, S., Chu, V.C., Whittaker, G.R., 2009. Activation of the SARS coronavirus spike protein via sequential proteolytic cleavage at two distinct sites. Proceedings of the National Academy of Sciences of the United States of America 106, 5871-5876.

Belouzard, S., Millet, J.K., Licitra, B.N., Whittaker, G.R., 2012. Mechanisms of coronavirus cell entry mediated by the viral spike protein. Viruses 4, 1011-1033.

Bertram, S., Glowacka, I., Muller, M.A., Lavender, H., Gnirss, K., Nehlmeier, I., Niemeyer, D., He, Y., Simmons, G., Drosten, C., Soilleux, E.J., Jahn, O., Steffen, I., Pohlmann, S., 2011. Cleavage and activation of the severe acute respiratory syndrome coronavirus spike protein by human airway trypsin-like protease. Journal of virology 85, 13363-13372.

Bitnun, A., Read, S., Tellier, R., Petric, M., Richardson, S.E., 2009. Severe acute respiratory syndrome-associated coronavirus infection in Toronto children: a second look. Pediatrics 123, 97-101.

Boisvert, M., Fernandes, S., Tijssen, P., 2010. Multiple pathways involved in porcine parvovirus cellular entry and trafficking toward the nucleus. Journal of virology 84, 7782-7792.

Bosch, B.J., Bartelink, W., Rottier, P.J., 2008. Cathepsin L functionally cleaves the severe acute respiratory syndrome coronavirus class I fusion protein upstream of rather than adjacent to the fusion peptide. Journal of virology 82, 8887-8890.

Bosch, B.J., de Haan, C.A., Rottier, P.J., 2004. Coronavirus spike glycoprotein, extended at the carboxy terminus with green fluorescent protein, is assembly competent. Journal of virology 78, 7369-7378.

Bost, A.G., Carnahan, R.H., Lu, X.T., Denison, M.R., 2000. Four proteins processed from the replicase gene polyprotein of mouse hepatitis virus colocalize in the cell periphery and adjacent to sites of virion assembly. Journal of virology 74, 3379-3387.

Bost, A.G., Prentice, E., Denison, M.R., 2001. Mouse hepatitis virus replicase protein complexes are translocated to sites of M protein accumulation in the ERGIC at late times of infection. Virology 285, 21-29.

Bostwick, D.G., Ramnani, D., Qian, J., 2000. Prostatic intraepithelial neoplasia: animal models 2000. The Prostate 43, 286-294.

Brehmer, D., Greff, Z., Godl, K., Blencke, S., Kurtenbach, A., Weber, M., Muller, S., Klebl, B., Cotten, M., Keri, G., Wissing, J., Daub, H., 2005. Cellular targets of gefitinib. Cancer research 65, 379-382.

Brockway, S.M., Clay, C.T., Lu, X.T., Denison, M.R., 2003. Characterization of the expression, intracellular localization, and replication complex association of the putative mouse hepatitis virus RNA-dependent RNA polymerase. Journal of virology 77, 10515-10527.

Brockway, S.M., Lu, X.T., Peters, T.R., Dermody, T.S., Denison, M.R., 2004. Intracellular localization and protein interactions of the gene 1 protein p28 during mouse hepatitis virus replication. Journal of virology 78, 11551-11562.

Burgess, A., Vigneron, S., Brioudes, E., Labbe, J.C., Lorca, T., Castro, A., 2010. Loss of human Greatwall results in G2 arrest and multiple mitotic defects due to deregulation of the cyclin B-Cdc2/PP2A balance. Proceedings of the National Academy of Sciences of the United States of America 107, 12564-12569.

Carter, G.C., Bernstone, L., Baskaran, D., James, W., 2011. HIV-1 infects macrophages by exploiting an endocytic route dependent on dynamin, Rac1 and Pak1. Virology 409, 234-250.

Chen, W., Madden, V.J., Bagnell, C.R., Jr., Baric, R.S., 1997. Host-derived intracellular immunization against mouse hepatitis virus infection. Virology 228, 318-332.

Chumbler, N.M., Farrow, M.A., Lapierre, L.A., Franklin, J.L., Haslam, D.B., Goldenring, J.R., Lacy, D.B., 2012. Clostridium difficile Toxin B causes epithelial cell necrosis through an autoprocessing-independent mechanism. PLoS pathogens 8, e1003072.

Cudmore, S., Cossart, P., Griffiths, G., Way, M., 1995. Actin-based motility of vaccinia virus. Nature 378, 636-638.

Curtis, K.M., Yount, B., Baric, R.S., 2002. Heterologous gene expression from transmissible gastroenteritis virus replicon particles. Journal of virology 76, 1422-1434.

Das Sarma, J., Fu, L., Tsai, J.C., Weiss, S.R., Lavi, E., 2000. Demyelination determinants map to the spike glycoprotein gene of coronavirus mouse hepatitis virus. Journal of virology 74, 9206-9213.

Das Sarma, J., Scheen, E., Seo, S.H., Koval, M., Weiss, S.R., 2002. Enhanced green fluorescent protein expression may be used to monitor murine coronavirus spread in vitro and in the mouse central nervous system. Journal of neurovirology 8, 381-391.

de Haan, C.A., Stadler, K., Godeke, G.J., Bosch, B.J., Rottier, P.J., 2004. Cleavage inhibition of the murine coronavirus spike protein by a furin-like enzyme affects cell-cell but not virus-cell fusion. Journal of virology 78, 6048-6054.

de Haan, C.A., van Genne, L., Stoop, J.N., Volders, H., Rottier, P.J., 2003. Coronaviruses as vectors: position dependence of foreign gene expression. Journal of virology 77, 11312-11323.

Demory, M.L., Boerner, J.L., Davidson, R., Faust, W., Miyake, T., Lee, I., Huttemann, M., Douglas, R., Haddad, G., Parsons, S.J., 2009. Epidermal growth factor receptor translocation to the mitochondria: regulation and effect. The Journal of biological chemistry 284, 36592-36604.

Denison, M.R., 2011. Coronaviruses, Nelson textbook of pediatrics, 19 ed. Elsevier Saunders, Philadelphia, PA.

Denison, M.R., Graham, R.L., Donaldson, E.F., Eckerle, L.D., Baric, R.S., 2011. Coronaviruses: an RNA proofreading machine regulates replication fidelity and diversity. RNA biology 8, 270-279.

Denison, M.R., Perlman, S., 1986. Translation and processing of mouse hepatitis virus virion RNA in a cell-free system. Journal of virology 60, 12-18.

Denison, M.R., Yount, B., Brockway, S.M., Graham, R.L., Sims, A.C., Lu, X., Baric, R.S., 2004. Cleavage between replicase proteins p28 and p65 of mouse hepatitis virus is not required for virus replication. Journal of virology 78, 5957-5965.

Dharmawardhane, S., Schurmann, A., Sells, M.A., Chernoff, J., Schmid, S.L., Bokoch, G.M., 2000. Regulation of macropinocytosis by p21-activated kinase-1. Molecular biology of the cell 11, 3341-3352.

DiMaio, D., Petti, L.M., 2013. The E5 proteins. Virology 445, 99-114.

Doceul, V., Hollinshead, M., van der Linden, L., Smith, G.L., 2010. Repulsion of superinfecting virions: a mechanism for rapid virus spread. Science 327, 873-876.

Dominguez, S.R., Robinson, C.C., Holmes, K.V., 2009. Detection of four human coronaviruses in respiratory infections in children: a one-year study in Colorado. Journal of medical virology 81, 1597-1604.

Du, L., Kao, R.Y., Zhou, Y., He, Y., Zhao, G., Wong, C., Jiang, S., Yuen, K.Y., Jin, D.Y., Zheng, B.J., 2007. Cleavage of spike protein of SARS coronavirus by protease factor Xa is associated with viral infectivity. Biochemical and biophysical research communications 359, 174-179.

Earp, H.S., 3rd, Calvo, B.F., Sartor, C.I., 2003. The EGF receptor family--multiple roles in proliferation, differentiation, and neoplasia with an emphasis on HER4. Transactions of the American Clinical and Climatological Association 114, 315-333; discussion 333-314.

Eckerle, L.D., Lu, X., Sperry, S.M., Choi, L., Denison, M.R., 2007. High fidelity of murine hepatitis virus replication is decreased in nsp14 exoribonuclease mutants. Journal of virology 81, 12135-12144.

Fischer, F., Stegen, C.F., Koetzner, C.A., Masters, P.S., 1998. Construction of a mouse hepatitis virus recombinant expressing a foreign gene. Advances in experimental medicine and biology 440, 291-295.

Freeman, M.C., Graham, R.L., Lu, X., Peek, C.T., Denison, M.R., 2014. Coronavirus replicase-reporter fusions provide quantitative analysis of replication and replication complex formation. Journal of virology 88, 5319-5327.

Gadlage, M.J., Denison, M.R., 2010. Exchange of the coronavirus replicase polyprotein cleavage sites alters protease specificity and processing. Journal of virology 84, 6894-6898.

Gadlage, M.J., Graham, R.L., Denison, M.R., 2008. Murine coronaviruses encoding nsp2 at different genomic loci have altered replication, protein expression, and localization. Journal of virology 82, 11964-11969.

Ge, F., Luo, Y., Liew, P.X., Hung, E., 2007. Derivation of a novel SARS-coronavirus replicon cell line and its application for anti-SARS drug screening. Virology 360, 150-158.

Ge, X.Y., Li, J.L., Yang, X.L., Chmura, A.A., Zhu, G., Epstein, J.H., Mazet, J.K., Hu, B., Zhang, W., Peng, C., Zhang, Y.J., Luo, C.M., Tan, B., Wang, N., Zhu, Y., Crameri, G., Zhang, S.Y., Wang, L.F., Daszak, P., Shi, Z.L., 2013. Isolation and characterization of a bat SARS-like coronavirus that uses the ACE2 receptor. Nature 503, 535-538.

Glowacka, I., Bertram, S., Muller, M.A., Allen, P., Soilleux, E., Pfefferle, S., Steffen, I., Tsegaye, T.S., He, Y., Gnirss, K., Niemeyer, D., Schneider, H., Drosten, C., Pohlmann, S., 2011. Evidence that TMPRSS2 activates the severe acute respiratory syndrome coronavirus spike protein for membrane fusion and reduces viral control by the humoral immune response. Journal of virology 85, 4122-4134.

Gobeil, L.A., Lodge, R., Tremblay, M.J., 2013. Macropinocytosis-like HIV-1 internalization in macrophages is CCR5 dependent and leads to efficient but delayed degradation in endosomal compartments. Journal of virology 87, 735-745.

Gold, S., Monaghan, P., Mertens, P., Jackson, T., 2010. A clathrin independent macropinocytosis-like entry mechanism used by bluetongue virus-1 during infection of BHK cells. PloS one 5, e11360.

Gombold, J.L., Hingley, S.T., Weiss, S.R., 1993. Fusion-defective mutants of mouse hepatitis virus A59 contain a mutation in the spike protein cleavage signal. Journal of virology 67, 4504-4512.

Gosert, R., Kanjanahaluethai, A., Egger, D., Bienz, K., Baker, S.C., 2002. RNA replication of mouse hepatitis virus takes place at double-membrane vesicles. Journal of virology 76, 3697-3708.

Graham, R.L., Becker, M.M., Eckerle, L.D., Bolles, M., Denison, M.R., Baric, R.S., 2012. A live, impaired-fidelity coronavirus vaccine protects in an aged, immunocompromised mouse model of lethal disease. Nature medicine 18, 1820-1826.

Graham, R.L., Denison, M.R., 2006. Replication of murine hepatitis virus is regulated by papain-like proteinase 1 processing of nonstructural proteins 1, 2, and 3. Journal of virology 80, 11610-11620.

Graham, R.L., Donaldson, E.F., Baric, R.S., 2013. A decade after SARS: strategies for controlling emerging coronaviruses. Nature reviews. Microbiology 11, 836-848.

Graham, R.L., Sims, A.C., Brockway, S.M., Baric, R.S., Denison, M.R., 2005. The nsp2 replicase proteins of murine hepatitis virus and severe acute respiratory syndrome coronavirus are dispensable for viral replication. Journal of virology 79, 13399-13411.

Gu, Z., Noss, E.H., Hsu, V.W., Brenner, M.B., 2011. Integrins traffic rapidly via circular dorsal ruffles and macropinocytosis during stimulated cell migration. The Journal of cell biology 193, 61-70.

Haagmans, B.L., Al Dhahiry, S.H., Reusken, C.B., Raj, V.S., Galiano, M., Myers, R., Godeke, G.J., Jonges, M., Farag, E., Diab, A., Ghobashy, H., Alhajri, F., Al-Thani, M., Al-Marri, S.A., Al Romaihi, H.E., Al Khal, A., Bermingham, A., Osterhaus, A.D., AlHajri, M.M., Koopmans, M.P., 2014. Middle East respiratory syndrome coronavirus in dromedary camels: an outbreak investigation. The Lancet infectious diseases 14, 140-145.

Hagemeijer, M.C., Ulasli, M., Vonk, A.M., Reggiori, F., Rottier, P.J., de Haan, C.A., 2011. Mobility and interactions of coronavirus nonstructural protein 4. Journal of virology 85, 4572-4577.

Hagemeijer, M.C., Verheije, M.H., Ulasli, M., Shaltiel, I.A., de Vries, L.A., Reggiori, F., Rottier, P.J., de Haan, C.A., 2010. Dynamics of coronavirus replication-transcription complexes. Journal of virology 84, 2134-2149.

Haigler, H.T., McKanna, J.A., Cohen, S., 1979. Rapid stimulation of pinocytosis in human carcinoma cells A-431 by epidermal growth factor. The Journal of cell biology 83, 82-90.

Hansen, C.G., Nichols, B.J., 2009. Molecular mechanisms of clathrin-independent endocytosis. Journal of cell science 122, 1713-1721.

Haspot, F., Lavault, A., Sinzger, C., Laib Sampaio, K., Stierhof, Y.D., Pilet, P., Bressolette-Bodin, C., Halary, F., 2012. Human cytomegalovirus entry into dendritic cells occurs via a macropinocytosis-like pathway in a pH-independent and cholesterol-dependent manner. PloS one 7, e34795.

Henson, P.M., Bratton, D.L., Fadok, V.A., 2001. Apoptotic cell removal. Current biology : CB 11, R795-805.

Hertzig, T., Scandella, E., Schelle, B., Ziebuhr, J., Siddell, S.G., Ludewig, B., Thiel, V., 2004. Rapid identification of coronavirus replicase inhibitors using a selectable replicon RNA. The Journal of general virology 85, 1717-1725.

Hewlett, L.J., Prescott, A.R., Watts, C., 1994. The coated pit and macropinocytic pathways serve distinct endosome populations. The Journal of cell biology 124, 689-703.

Hingley, S.T., Gombold, J.L., Lavi, E., Weiss, S.R., 1994. MHV-A59 fusion mutants are attenuated and display altered hepatotropism. Virology 200, 1-10.

Hirano, N., Fujiwara, K., Matumoto, M., 1976. Mouse hepatitis virus (MHV-2). Plaque assay and propagation in mouse cell line DBT cells. Japanese journal of microbiology 20, 219-225.

Hui, D.S., Memish, Z.A., Zumla, A., 2014. Severe acute respiratory syndrome vs. the Middle East respiratory syndrome. Current opinion in pulmonary medicine.

Igakura, T., Stinchcombe, J.C., Goon, P.K., Taylor, G.P., Weber, J.N., Griffiths, G.M., Tanaka, Y., Osame, M., Bangham, C.R., 2003. Spread of HTLV-I between lymphocytes by virus-induced polarization of the cytoskeleton. Science 299, 1713-1716.

Iwasaki, M., Ngo, N., de la Torre, J.C., 2014. Sodium hydrogen exchangers contribute to arenavirus cell entry. Journal of virology 88, 643-654.

Just, I., Selzer, J., von Eichel-Streiber, C., Aktories, K., 1995. The low molecular mass GTP-binding protein Rho is affected by toxin A from Clostridium difficile. The Journal of clinical investigation 95, 1026-1031.

Kalin, S., Amstutz, B., Gastaldelli, M., Wolfrum, N., Boucke, K., Havenga, M., DiGennaro, F., Liska, N., Hemmi, S., Greber, U.F., 2010. Macropinocytotic uptake and infection of human epithelial cells with species B2 adenovirus type 35. Journal of virology 84, 5336-5350.

Kam, Y.W., Okumura, Y., Kido, H., Ng, L.F., Bruzzone, R., Altmeyer, R., 2009. Cleavage of the SARS coronavirus spike glycoprotein by airway proteases enhances virus entry into human bronchial epithelial cells in vitro. PloS one 4, e7870.

Kanjanahaluethai, A., Baker, S.C., 2000. Identification of mouse hepatitis virus papain-like proteinase 2 activity. Journal of virology 74, 7911-7921.

Kerr, M.C., Teasdale, R.D., 2009. Defining macropinocytosis. Traffic 10, 364-371.

Khan, A.G., Pickl-Herk, A., Gajdzik, L., Marlovits, T.C., Fuchs, R., Blaas, D., 2010. Human rhinovirus 14 enters rhabdomyosarcoma cells expressing icam-1 by a clathrin-, caveolin-, and flotillin-independent pathway. Journal of virology 84, 3984-3992.

Kilianski, A., Mielech, A.M., Deng, X., Baker, S.C., 2013. Assessing activity and inhibition of Middle East respiratory syndrome coronavirus papain-like and 3C-like proteases using luciferase-based biosensors. Journal of virology 87, 11955-11962.

Knoops, K., Kikkert, M., Worm, S.H., Zevenhoven-Dobbe, J.C., van der Meer, Y., Koster, A.J., Mommaas, A.M., Snijder, E.J., 2008. SARS-coronavirus replication is supported by a reticulovesicular network of modified endoplasmic reticulum. PLoS biology 6, e226.

Knoops, K., Swett-Tapia, C., van den Worm, S.H., Te Velthuis, A.J., Koster, A.J., Mommaas, A.M., Snijder, E.J., Kikkert, M., 2010. Integrity of the early secretory pathway promotes, but is not required for, severe acute respiratory syndrome coronavirus RNA synthesis and virus-induced remodeling of endoplasmic reticulum membranes. Journal of virology 84, 833-846.

Koivusalo, M., Welch, C., Hayashi, H., Scott, C.C., Kim, M., Alexander, T., Touret, N., Hahn, K.M., Grinstein, S., 2010. Amiloride inhibits macropinocytosis by lowering submembranous pH and preventing Rac1 and Cdc42 signaling. The Journal of cell biology 188, 547-563.

Krieger, S.E., Kim, C., Zhang, L., Marjomaki, V., Bergelson, J.M., 2013. Echovirus 1 entry into polarized Caco-2 cells depends on dynamin, cholesterol, and cellular factors associated with macropinocytosis. Journal of virology 87, 8884-8895.

Ksiazek, T.G., Erdman, D., Goldsmith, C.S., Zaki, S.R., Peret, T., Emery, S., Tong, S., Urbani, C., Comer, J.A., Lim, W., Rollin, P.E., Dowell, S.F., Ling, A.E., Humphrey, C.D., Shieh, W.J., Guarner, J., Paddock, C.D., Rota, P., Fields, B., DeRisi, J., Yang, J.Y., Cox, N., Hughes, J.M., LeDuc, J.W., Bellini, W.J., Anderson, L.J., 2003. A novel coronavirus associated with severe acute respiratory syndrome. The New England journal of medicine 348, 1953-1966.

Kuiken, T., Fouchier, R.A., Schutten, M., Rimmelzwaan, G.F., van Amerongen, G., van Riel, D., Laman, J.D., de Jong, T., van Doornum, G., Lim, W., Ling, A.E., Chan, P.K., Tam, J.S., Zambon, M.C., Gopal, R., Drosten, C., van der Werf, S., Escriou, N., Manuguerra, J.C., Stohr, K., Peiris, J.S., Osterhaus, A.D., 2003. Newly discovered coronavirus as the primary cause of severe acute respiratory syndrome. Lancet 362, 263-270.

Lau, S.K., Woo, P.C., Li, K.S., Huang, Y., Tsoi, H.W., Wong, B.H., Wong, S.S., Leung, S.Y., Chan, K.H., Yuen, K.Y., 2005. Severe acute respiratory syndrome coronavirus-like virus in Chinese horseshoe bats. Proceedings of the National Academy of Sciences of the United States of America 102, 14040-14045.

Lauber, C., Goeman, J.J., Parquet Mdel, C., Nga, P.T., Snijder, E.J., Morita, K., Gorbalenya, A.E., 2013. The footprint of genome architecture in the largest genome expansion in RNA viruses. PLoS pathogens 9, e1003500.

Lavi, E., Gilden, D.H., Wroblewska, Z., Rorke, L.B., Weiss, S.R., 1984. Experimental demyelination produced by the A59 strain of mouse hepatitis virus. Neurology 34, 597-603.

Leparc-Goffart, I., Hingley, S.T., Chua, M.M., Jiang, X., Lavi, E., Weiss, S.R., 1997. Altered pathogenesis of a mutant of the murine coronavirus MHV-A59 is associated with a Q159L amino acid substitution in the spike protein. Virology 239, 1-10.

Lessler, J., Reich, N.G., Brookmeyer, R., Perl, T.M., Nelson, K.E., Cummings, D.A., 2009. Incubation periods of acute respiratory viral infections: a systematic review. The Lancet infectious diseases 9, 291-300.

Li, W., Shi, Z., Yu, M., Ren, W., Smith, C., Epstein, J.H., Wang, H., Crameri, G., Hu, Z., Zhang, H., Zhang, J., McEachern, J., Field, H., Daszak, P., Eaton, B.T., Zhang, S., Wang, L.F., 2005. Bats are natural reservoirs of SARS-like coronaviruses. Science 310, 676-679.

Lin, H.H., Kao, J.H., Chen, P.J., Chen, D.S., 1996. Mechanism of vertical transmission of hepatitis G. Lancet 347, 1116.

Liu, N.Q., Lossinsky, A.S., Popik, W., Li, X., Gujuluva, C., Kriederman, B., Roberts, J., Pushkarsky, T., Bukrinsky, M., Witte, M., Weinand, M., Fiala, M., 2002. Human immunodeficiency virus type 1 enters brain microvascular endothelia by macropinocytosis dependent on lipid rafts and the mitogen-activated protein kinase signaling pathway. Journal of virology 76, 6689-6700.

Lu, Y., Lu, X., Denison, M.R., 1995. Identification and characterization of a serine-like proteinase of the murine coronavirus MHV-A59. Journal of virology 69, 3554-3559.

Marechal, V., Prevost, M.C., Petit, C., Perret, E., Heard, J.M., Schwartz, O., 2001. Human immunodeficiency virus type 1 entry into macrophages mediated by macropinocytosis. Journal of virology 75, 11166-11177.

Masters, P.S., 2006. The molecular biology of coronaviruses. Advances in virus research 66, 193-292.

Matsuyama, S., Ujike, M., Morikawa, S., Tashiro, M., Taguchi, F., 2005. Protease-mediated enhancement of severe acute respiratory syndrome coronavirus infection. Proceedings of the National Academy of Sciences of the United States of America 102, 12543-12547.

McDonald, D., Wu, L., Bohks, S.M., KewalRamani, V.N., Unutmaz, D., Hope, T.J., 2003. Recruitment of HIV and its receptors to dendritic cell-T cell junctions. Science 300, 1295-1297.

Meier, O., Boucke, K., Hammer, S.V., Keller, S., Stidwill, R.P., Hemmi, S., Greber, U.F., 2002. Adenovirus triggers macropinocytosis and endosomal leakage together with its clathrin-mediated uptake. The Journal of cell biology 158, 1119-1131.

Memish, Z.A., Al-Tawfiq, J.A., Assiri, A., Alrabiah, F.A., Hajjar, S.A., Albarrak, A., Flemban, H., Alhakeem, R.F., Makhdoom, H.Q., Alsubaie, S., Al-Rabeeah, A.A., 2014. Middle East Respiratory Syndrome Coronavirus Disease in Children. The Pediatric infectious disease journal.

Memish, Z.A., Mishra, N., Olival, K.J., Fagbo, S.F., Kapoor, V., Epstein, J.H., Alhakeem, R., Durosinloun, A., Al Asmari, M., Islam, A., Kapoor, A., Briese, T.,

Daszak, P., Al Rabeeah, A.A., Lipkin, W.I., 2013. Middle East respiratory syndrome coronavirus in bats, Saudi Arabia. Emerging infectious diseases 19, 1819-1823.

Mercer, J., Helenius, A., 2008. Vaccinia virus uses macropinocytosis and apoptotic mimicry to enter host cells. Science 320, 531-535.

Mercer, J., Helenius, A., 2009. Virus entry by macropinocytosis. Nature cell biology 11, 510-520.

Mercer, J., Helenius, A., 2012. Gulping rather than sipping: macropinocytosis as a way of virus entry. Current opinion in microbiology 15, 490-499.

Mercer, J., Knebel, S., Schmidt, F.I., Crouse, J., Burkard, C., Helenius, A., 2010. Vaccinia virus strains use distinct forms of macropinocytosis for host-cell entry. Proceedings of the National Academy of Sciences of the United States of America 107, 9346-9351.

Mettlen, M., Platek, A., Van Der Smissen, P., Carpentier, S., Amyere, M., Lanzetti, L., de Diesbach, P., Tyteca, D., Courtoy, P.J., 2006. Src triggers circular ruffling and macropinocytosis at the apical surface of polarized MDCK cells. Traffic 7, 589-603.

Meyer, B., Muller, M.A., Corman, V.M., Reusken, C.B., Ritz, D., Godeke, G.J., Lattwein, E., Kallies, S., Siemens, A., van Beek, J., Drexler, J.F., Muth, D., Bosch, B.J., Wernery, U., Koopmans, M.P., Wernery, R., Drosten, C., 2014. Antibodies against MERS Coronavirus in Dromedary Camels, United Arab Emirates, 2003 and 2013. Emerging infectious diseases 20, 552-559.

Moasser, M.M., Basso, A., Averbuch, S.D., Rosen, N., 2001. The tyrosine kinase inhibitor ZD1839 ("Iressa") inhibits HER2-driven signaling and suppresses the growth of HER2-overexpressing tumor cells. Cancer research 61, 7184-7188.

Mulherkar, N., Raaben, M., de la Torre, J.C., Whelan, S.P., Chandran, K., 2011. The Ebola virus glycoprotein mediates entry via a non-classical dynamin-dependent macropinocytic pathway. Virology 419, 72-83.

Nanbo, A., Imai, M., Watanabe, S., Noda, T., Takahashi, K., Neumann, G., Halfmann, P., Kawaoka, Y., 2010. Ebolavirus is internalized into host cells via macropinocytosis in a viral glycoprotein-dependent manner. PLoS pathogens 6, e1001121.

Navas, S., Seo, S.H., Chua, M.M., Das Sarma, J., Lavi, E., Hingley, S.T., Weiss, S.R., 2001. Murine coronavirus spike protein determines the ability of the virus to replicate in the liver and cause hepatitis. Journal of virology 75, 2452-2457.

Navas, S., Weiss, S.R., 2003. Murine coronavirus-induced hepatitis: JHM genetic background eliminates A59 spike-determined hepatotropism. Journal of virology 77, 4972-4978.

Nobes, C., Marsh, M., 2000. Dendritic cells: new roles for Cdc42 and Rac in antigen uptake? Current biology : CB 10, R739-741.

Nobes, C.D., Hall, A., 1995. Rho, rac and cdc42 GTPases: regulators of actin structures, cell adhesion and motility. Biochemical Society transactions 23, 456-459.

Orth, J.D., McNiven, M.A., 2006. Get off my back! Rapid receptor internalization through circular dorsal ruffles. Cancer research 66, 11094-11096.

Peiris, J.S., Lai, S.T., Poon, L.L., Guan, Y., Yam, L.Y., Lim, W., Nicholls, J., Yee, W.K., Yan, W.W., Cheung, M.T., Cheng, V.C., Chan, K.H., Tsang, D.N., Yung, R.W., Ng, T.K., Yuen, K.Y., 2003. Coronavirus as a possible cause of severe acute respiratory syndrome. Lancet 361, 1319-1325.

Perlman, S., Netland, J., 2009. Coronaviruses post-SARS: update on replication and pathogenesis. Nature reviews. Microbiology 7, 439-450.

Perlman, S., Zhao, J., 2013. Human coronavirus EMC is not the same as severe acute respiratory syndrome coronavirus. mBio 4.

Pernet, O., Pohl, C., Ainouze, M., Kweder, H., Buckland, R., 2009. Nipah virus entry can occur by macropinocytosis. Virology 395, 298-311.

Pfefferle, S., Schopf, J., Kogl, M., Friedel, C.C., Muller, M.A., Carbajo-Lozoya, J., Stellberger, T., von Dall'Armi, E., Herzog, P., Kallies, S., Niemeyer, D., Ditt, V., Kuri, T., Zust, R., Pumpor, K., Hilgenfeld, R., Schwarz, F., Zimmer, R., Steffen, I., Weber, F., Thiel, V., Herrler, G., Thiel, H.J., Schwegmann-Wessels, C., Pohlmann, S., Haas, J., Drosten, C., von Brunn, A., 2011. The SARS-coronavirus-host interactome: identification of cyclophilins as target for pan-coronavirus inhibitors. PLoS pathogens 7, e1002331.

Plant, E.P., Perez-Alvarado, G.C., Jacobs, J.L., Mukhopadhyay, B., Hennig, M., Dinman, J.D., 2005. A three-stemmed mRNA pseudoknot in the SARS coronavirus frameshift signal. PLoS biology 3, e172.

Plant, E.P., Sims, A.C., Baric, R.S., Dinman, J.D., Taylor, D.R., 2013. Altering SARS coronavirus frameshift efficiency affects genomic and subgenomic RNA production. Viruses 5, 279-294.

Prentice, E., Jerome, W.G., Yoshimori, T., Mizushima, N., Denison, M.R., 2004. Coronavirus replication complex formation utilizes components of cellular autophagy. The Journal of biological chemistry 279, 10136-10141.

Pu, Y., Zhang, X., 2008. Mouse hepatitis virus type 2 enters cells through a clathrin-mediated endocytic pathway independent of Eps15. Journal of virology 82, 8112-8123.

Qiu, Z., Hingley, S.T., Simmons, G., Yu, C., Das Sarma, J., Bates, P., Weiss, S.R., 2006. Endosomal proteolysis by cathepsins is necessary for murine coronavirus mouse hepatitis virus type 2 spike-mediated entry. Journal of virology 80, 5768-5776.

Raghu, H., Sharma-Walia, N., Veettil, M.V., Sadagopan, S., Chandran, B., 2009. Kaposi's sarcoma-associated herpesvirus utilizes an actin polymerization-dependent macropinocytic pathway to enter human dermal microvascular endothelial and human umbilical vein endothelial cells. Journal of virology 83, 4895-4911.

Raj, V.S., Mou, H., Smits, S.L., Dekkers, D.H., Muller, M.A., Dijkman, R., Muth, D., Demmers, J.A., Zaki, A., Fouchier, R.A., Thiel, V., Drosten, C., Rottier, P.J., Osterhaus, A.D., Bosch, B.J., Haagmans, B.L., 2013. Dipeptidyl peptidase 4 is a functional receptor for the emerging human coronavirus-EMC. Nature 495, 251-254.

Reusken, C.B., Haagmans, B.L., Muller, M.A., Gutierrez, C., Godeke, G.J., Meyer, B., Muth, D., Raj, V.S., Smits-De Vries, L., Corman, V.M., Drexler, J.F., Smits, S.L., El Tahir, Y.E., De Sousa, R., van Beek, J., Nowotny, N., van Maanen, K., Hidalgo-Hermoso, E., Bosch, B.J., Rottier, P., Osterhaus, A., Gortazar-Schmidt, C., Drosten, C., Koopmans, M.P., 2013. Middle East respiratory syndrome coronavirus neutralising serum antibodies in dromedary camels: a comparative serological study. The Lancet infectious diseases 13, 859-866.

Roberts, R.S., Yount, B.L., Sims, A.C., Baker, S., Baric, R.S., 2006. Renilla luciferase as a reporter to assess SARS-CoV mRNA transcription regulation and efficacy of anti-SARS-CoV agents. Advances in experimental medicine and biology 581, 597-600.

Robison, C.S., Whitt, M.A., 2000. The membrane-proximal stem region of vesicular stomatitis virus G protein confers efficient virus assembly. Journal of virology 74, 2239-2246.

Rossman, J.S., Leser, G.P., Lamb, R.A., 2012. Filamentous influenza virus enters cells via macropinocytosis. Journal of virology 86, 10950-10960.

Saeed, M.F., Kolokoltsov, A.A., Albrecht, T., Davey, R.A., 2010. Cellular entry of ebola virus involves uptake by a macropinocytosis-like mechanism and subsequent trafficking through early and late endosomes. PLoS pathogens 6, e1001110.

Salonen, A., Ahola, T., Kaariainen, L., 2005. Viral RNA replication in association with cellular membranes. Current topics in microbiology and immunology 285, 139-173.

Sanchez, E.G., Quintas, A., Perez-Nunez, D., Nogal, M., Barroso, S., Carrascosa, A.L., Revilla, Y., 2012. African swine fever virus uses macropinocytosis to enter host cells. PLoS pathogens 8, e1002754.

Sandgren, K.J., Wilkinson, J., Miranda-Saksena, M., McInerney, G.M., Byth-Wilson, K., Robinson, P.J., Cunningham, A.L., 2010. A differential role for macropinocytosis in mediating entry of the two forms of vaccinia virus into dendritic cells. PLoS pathogens 6, e1000866.

Schelhaas, M., Shah, B., Holzer, M., Blattmann, P., Kuhling, L., Day, P.M., Schiller, J.T., Helenius, A., 2012. Entry of human papillomavirus type 16 by actin-dependent, clathrin- and lipid raft-independent endocytosis. PLoS pathogens 8, e1002657.

Schmidt, F.I., Bleck, C.K., Helenius, A., Mercer, J., 2011. Vaccinia extracellular virions enter cells by macropinocytosis and acid-activated membrane rupture. The EMBO journal 30, 3647-3661.

Scobey, T., Yount, B.L., Sims, A.C., Donaldson, E.F., Agnihothram, S.S., Menachery, V.D., Graham, R.L., Swanstrom, J., Bove, P.F., Kim, J.D., Grego, S., Randell, S.H., Baric, R.S., 2013. Reverse genetics with a full-length infectious cDNA of the Middle East respiratory syndrome coronavirus. Proceedings of the National Academy of Sciences of the United States of America 110, 16157-16162.

Sheahan, T., Rockx, B., Donaldson, E., Corti, D., Baric, R., 2008. Pathways of cross-species transmission of synthetically reconstructed zoonotic severe acute respiratory syndrome coronavirus. Journal of virology 82, 8721-8732.

Shulla, A., Heald-Sargent, T., Subramanya, G., Zhao, J., Perlman, S., Gallagher, T., 2011. A transmembrane serine protease is linked to the severe acute respiratory syndrome coronavirus receptor and activates virus entry. Journal of virology 85, 873-882.

Simmons, G., Gosalia, D.N., Rennekamp, A.J., Reeves, J.D., Diamond, S.L., Bates, P., 2005. Inhibitors of cathepsin L prevent severe acute respiratory syndrome coronavirus entry. Proceedings of the National Academy of Sciences of the United States of America 102, 11876-11881.

Simmons, G., Reeves, J.D., Rennekamp, A.J., Amberg, S.M., Piefer, A.J., Bates, P., 2004. Characterization of severe acute respiratory syndrome-associated coronavirus (SARS-CoV) spike glycoprotein-mediated viral entry. Proceedings of the National Academy of Sciences of the United States of America 101, 4240-4245.

Sims, A.C., Ostermann, J., Denison, M.R., 2000. Mouse hepatitis virus replicase proteins associate with two distinct populations of intracellular membranes. Journal of virology 74, 5647-5654.

Snijder, E.J., van der Meer, Y., Zevenhoven-Dobbe, J., Onderwater, J.J., van der Meulen, J., Koerten, H.K., Mommaas, A.M., 2006. Ultrastructure and origin of membrane vesicles associated with the severe acute respiratory syndrome coronavirus replication complex. Journal of virology 80, 5927-5940.

Somogyi, P., Jenner, A.J., Brierley, I., Inglis, S.C., 1993. Ribosomal pausing during translation of an RNA pseudoknot. Molecular and cellular biology 13, 6931-6940.

Sperry, S.M., Kazi, L., Graham, R.L., Baric, R.S., Weiss, S.R., Denison, M.R., 2005. Single-amino-acid substitutions in open reading frame (ORF) 1b-nsp14 and ORF 2a proteins of the coronavirus mouse hepatitis virus are attenuating in mice. Journal of virology 79, 3391-3400.

Stempel, H.E., Martin, E.T., Kuypers, J., Englund, J.A., Zerr, D.M., 2009. Multiple viral respiratory pathogens in children with bronchiolitis. Acta Paediatr 98, 123-126.

Suksanpaisan, L., Susantad, T., Smith, D.R., 2009. Characterization of dengue virus entry into HepG2 cells. Journal of biomedical science 16, 17.

Swanson, J.A., 2008. Shaping cups into phagosomes and macropinosomes. Nature reviews. Molecular cell biology 9, 639-649.

Swanson, J.A., Watts, C., 1995. Macropinocytosis. Trends in cell biology 5, 424-428.

Thorp, E.B., Gallagher, T.M., 2004. Requirements for CEACAMs and cholesterol during murine coronavirus cell entry. Journal of virology 78, 2682-2692.

Tooze, J., Tooze, S., Warren, G., 1984. Replication of coronavirus MHV-A59 in sac- cells: determination of the first site of budding of progeny virions. European journal of cell biology 33, 281-293.

Tooze, J., Tooze, S.A., Fuller, S.D., 1987. Sorting of progeny coronavirus from condensed secretory proteins at the exit from the trans-Golgi network of AtT20 cells. The Journal of cell biology 105, 1215-1226.

Tseng, C.T., Sbrana, E., Iwata-Yoshikawa, N., Newman, P.C., Garron, T., Atmar, R.L., Peters, C.J., Couch, R.B., 2012. Immunization with SARS coronavirus vaccines leads to pulmonary immunopathology on challenge with the SARS virus. PloS one 7, e35421.

Tugizov, S.M., Herrera, R., Palefsky, J.M., 2013. Epstein-Barr virus transcytosis through polarized oral epithelial cells. Journal of virology 87, 8179-8194.

van Boheemen, S., de Graaf, M., Lauber, C., Bestebroer, T.M., Raj, V.S., Zaki, A.M., Osterhaus, A.D., Haagmans, B.L., Gorbalenya, A.E., Snijder, E.J., Fouchier, R.A., 2012. Genomic characterization of a newly discovered coronavirus associated with acute respiratory distress syndrome in humans. mBio 3.

van den Born, E., Posthuma, C.C., Knoops, K., Snijder, E.J., 2007. An infectious recombinant equine arteritis virus expressing green fluorescent protein from its replicase gene. The Journal of general virology 88, 1196-1205.

van der Meer, Y., Snijder, E.J., Dobbe, J.C., Schleich, S., Denison, M.R., Spaan, W.J., Locker, J.K., 1999. Localization of mouse hepatitis virus nonstructural proteins and RNA synthesis indicates a role for late endosomes in viral replication. Journal of virology 73, 7641-7657.

Veithen, A., Cupers, P., Baudhuin, P., Courtoy, P.J., 1996. v-Src induces constitutive macropinocytosis in rat fibroblasts. Journal of cell science 109 (Pt 8), 2005-2012.

Verheije, M.H., Raaben, M., Mari, M., Te Lintelo, E.G., Reggiori, F., van Kuppeveld, F.J., Rottier, P.J., de Haan, C.A., 2008. Mouse hepatitis coronavirus RNA replication depends on GBF1-mediated ARF1 activation. PLoS pathogens 4, e1000088.

Wang, J.H., Wells, C., Wu, L., 2008. Macropinocytosis and cytoskeleton contribute to dendritic cell-mediated HIV-1 transmission to CD4+ T cells. Virology 381, 143-154.

Wen, Z., Zhao, B., Song, K., Hu, X., Chen, W., Kong, D., Ge, J., Bu, Z., 2013. Recombinant lentogenic Newcastle disease virus expressing Ebola virus GP infects cells independently of exogenous trypsin and uses macropinocytosis as the major pathway for cell entry. Virology journal 10, 331.

West, M.A., Bretscher, M.S., Watts, C., 1989. Distinct endocytotic pathways in epidermal growth factor-stimulated human carcinoma A431 cells. The Journal of cell biology 109, 2731-2739.

West, M.A., Prescott, A.R., Eskelinen, E.L., Ridley, A.J., Watts, C., 2000. Rac is required for constitutive macropinocytosis by dendritic cells but does not control its downregulation. Current biology : CB 10, 839-848.

Yamada, Y., Liu, X.B., Fang, S.G., Tay, F.P., Liu, D.X., 2009. Acquisition of cell-cell fusion activity by amino acid substitutions in spike protein determines the infectivity of a coronavirus in cultured cells. PloS one 4, e6130.

Yount, B., Curtis, K.M., Fritz, E.A., Hensley, L.E., Jahrling, P.B., Prentice, E., Denison, M.R., Geisbert, T.W., Baric, R.S., 2003. Reverse genetics with a full-length infectious cDNA of severe acute respiratory syndrome coronavirus. Proceedings of the National Academy of Sciences of the United States of America 100, 12995-13000.

Yount, B., Denison, M.R., Weiss, S.R., Baric, R.S., 2002. Systematic assembly of a full-length infectious cDNA of mouse hepatitis virus strain A59. Journal of virology 76, 11065-11078.

Zaki, A.M., van Boheemen, S., Bestebroer, T.M., Osterhaus, A.D., Fouchier, R.A., 2012. Isolation of a novel coronavirus from a man with pneumonia in Saudi Arabia. The New England journal of medicine 367, 1814-1820.

Zhao, G., Du, L., Ma, C., Li, Y., Li, L., Poon, V.K., Wang, L., Yu, F., Zheng, B.J., Jiang, S., Zhou, Y., 2013. A safe and convenient pseudovirus-based inhibition assay to detect neutralizing antibodies and screen for viral entry inhibitors against the novel human coronavirus MERS-CoV. Virology journal 10, 266.

Zumla, A.I., Memish, Z.A., 2014. Middle East respiratory syndrome coronavirus: epidemic potential or a storm in a teacup? The European respiratory journal.